International Journal of Solids and Structures 155 (2018) 160–184

Contents lists available at ScienceDirect

International Journal of Solids and Structures

journal homepage: www.elsevier.com/locate/ijsolstr

An energetic formulation of a gradient damage model for concrete and its numerical implementation

Mariela Luege[a,*], Antonio Orlando[b], Martin E. Almenar[a], Elvio A. Pilotta[c]

[a] CONICET, Instituto de Estructuras, FACET, Universidad Nacional de Tucumán, Argentina
[b] CONICET, Departamento de Bioingeniería, FACET, Universidad Nacional de Tucumán, Argentina
[c] CIEM-CONICET, FAMAF, Universidad Nacional de Córdoba, Argentina

ARTICLE INFO

Article history:
Received 4 March 2018
Revised 7 June 2018
Available online 29 July 2018

Keywords:
Concrete material behavior
Gradient damage model
Rate-independent processes
Energetic formulation
Two-sided energetic inequality
Dissipation based continuation Newton's method

ABSTRACT

The energetic formulation of a rate-independent system assumes that the evolution of the system is driven by two scalar-valued functions: the storage energy functional and the dissipation pseudo-potential. The evolution of the material system is then characterized by two energetic principles: the global stability condition and the energy balance between stored and dissipated energies with the work of external loading. Rate-independent generalized standard materials are endowed with such structure, whereas the existence of such energetic structure is not so apparent in materials with non-associated flow rule. In this paper, we consider a rate-independent gradient damage model for concrete where the evolution of the damage does not follow the normality rule. We will show that such model can be nevertheless derived by a dissipation potential at the expense of having a state variable-dependent potential, and therefore the energetic formulation can be obtained also in this case. After introducing the incremental minimization problem consistent with such formulation, we obtain a discrete version of the stability condition and establish lower and upper *a-priori* energy bounds met by the energetic solution. These are fundamental results for the analysis of the formulation.

The actual numerical solution of the incremental minimization problem is realized by considering first a variable splitting in order to treat the gradient of the damage field as an independent variable, and then by applying the augmented Lagrangian method to tackle with the resulting constrained optimization problem. We solve the first order stationarity conditions of the augmented Lagrangian functional by a path-following Newton's method based on the energy dissipation rate control.

We show that we are able to describe highly non-linear responses of the material, such as softening branches and snap-back responses. Several numerical tests are performed to verify the objectivity of the formulation and of the proposed numerical method. Details of the numerical implementation are also given.

1. Introduction

Concrete failure as result of propagation and coalescence of microcracks can be modeled by continuum damage mechanics using the framework of thermodynamic of irreversible processes (Besson et al., 2010; Krajcinovic, 1996; Lemaitre, 1996). Within such setting, the material is characterized by state and internal variables and its behavior can be described by constitutive equations and thermodynamic potentials, so to meet the fundamental principles of thermodynamics and classical continuum mechanics. Though useful in many cases of practical interest (Krajcinovic, 1996; Lemaitre, 1996), it was soon recognized that both from a physical (Bazant, 1976; 1991) and a mathematical point of view (Pijaudier-Cabot and Bazant, 1987; Belytschko et al., 1986; Benallal et al., 1993), the locality assumption of the classical continuum mechanics was not satisfactory. Such assumption does not account for length scales and long-range effects of the material microstructure, thus the resulting continuum constitutive theory is, for instance, not able to capture size effects on structural strength (Bazant and Planas, 1997) and produces unrealistic concentration phenomena, such as strain and damage localization, on bands of infinitesimal width with null energy dissipation (Belytschko et al., 1986), leading to ill-posed problems. From the numerical point of view, this would produce spurious mesh sensitivity of the numerical results. Still remaining in the field of the continuum description of the behavior

* Corresponding author.
E-mail addresses: mluege@herrera.unt.edu.ar (M. Luege), aorlando@herrera.unt.edu.ar (A. Orlando), malmenar@herrera.unt.edu.ar (M.E. Almenar), pilotta@famaf.unc.edu.ar (E.A. Pilotta).

https://doi.org/10.1016/j.ijsolstr.2018.07.017
0020-7683/

of the concrete, a common remedy has been to resort to different theories of generalized continuum mechanics. Of particular interest are those which replace the constitutive assumption of the local action (Besson et al., 2010; Peric and Owen, 2008) with one describing the nonlocal interaction between the material points (Maugin, 2017).

In this paper, we will consider a nonlocal rate-independent damage model for concrete, where the nonlocality is introduced by taking the gradient of the damage as internal variable and the time-scale invariance results from the absence of all rate-dependent processes, such as viscosity in the material modeling and inertial forces in the balance equations. Furthermore, we consider damage evolution that accounts for the non-symmetric behavior in tension and compression, and damage threshold that is adjusted with respect to the loading direction. The use of the damage gradient as an internal variable is usually motivated by micromechanics considerations and is a concept that was suggested in Frémond and Nedjar (1995) and Frémond and Nedjar (1996). It has also been justified from the mathematical viewpoint by the boundedness of the damage field for the control of the localization band width (Mielke and Roubíček, 2006).

For the derivation of the evolution equations, different approaches have been however suggested. For instance, Lorentz and Andrieux (1999), Lorentz and Andrieux (2003), and Lorentz and Godard (2011) use the standard principle of virtual power to derive the balance equations of momentum, but they then apply the methods of continuum thermodynamics (Halphen and Nguyen, 1975; Germain et al., 1983) through the definition of a global potential energy and a global dissipation potential which produce a formulation of the constitutive laws at the structure scale. This is done because of the constraint between the damage variable and its gradient (Lorentz and Andrieux, 1999; 2003), which would not allow the damage gradient to be considered as an independent variable. Despite the integral formulation of these equations, it is shown that such relations can however be expressed in a pointwise manner. In the pointwise formulation, the constitutive equations retain the same algebraic structure as in the local constitutive theory, except for the consistency condition that contains now the Laplacian of the damage variable. While such dependence was also put forward by Comi (1999) as a constitutive assumption, in Lorentz and Andrieux (1999), Lorentz and Andrieux (2003), and Lorentz and Godard (2011) it appears as a consequence of the constitutive theory. In the approach proposed by Frémond and Nedjar (1995) and Frémond and Nedjar (1996), on the other hand, the starting point is an extended version of the principle of virtual work where both the power of the external and internal forces present additional terms associated with the microscopic movements which produce damage (Frémond, 2002). By this approach, the field equations of momentum balance are coupled to additional ones which express the balance of the forces dual to the kinematic variables used to describe the microscopic movements. This system of field equations is then completed by the constitutive equations which are also here derived by the methods of continuum thermodynamics (Halphen and Nguyen, 1975; Germain et al., 1983) through the definition of the free Helmholtz energy and the dissipation pseudo-potential, originating a first order gradient type dissipative theory in the full thermodynamic context. The two previous constitutive theories, which assume the gradient damage as an internal variable, have been related to each other in Nguyen (2010, 2014) and shown to be substantially equivalent.

The energetic formulation proposed by Mielke and coworkers in Mielke et al. (2002), Mielke (2005), Mielke and Roubíček (2006), Mielke et al. (2010), and Mielke and Roubíček (2015), on the other hand, unifies the different point of views, is of clear mechanical interpretation, and offers at once a framework for the modeling, analysis and numerical simulation of rate-independent processes that can experience discontinuity jumps in time and space and concentration of deformations and damage. This is possible because of the minimal regularity assumptions needed for its setting up and for a shift of the viewpoint, from a local to a global one. In the energetic formulation the evolution of the material deformation and damage is the result of an energy balance condition and of a stability condition. The main ingredients of the theory are therefore the definition of the total stored energy, which can be non convex, and of the dissipation distance, which is well defined also for discontinuous damage evolutions. Furthermore, given the type of formulation, a suitable concept of weak solvability for the differential model is introduced which yields to the notion of energetic solution.

Despite the large class of applications that have been addressed by the energetic theory, especially in the field of mechanics (Bourdin et al., 2000; Mielke et al., 2002; Mielke and Roubíček, 2006; Francfort and Garroni, 2006; Bouchitté et al., 2009; Mielke and Roubíček, 2009), the theory has therein been applied to generalized standard materials where the material mechanisms responsible for the energy dissipation are independent on the current state of the material itself. This has streamlined the mathematical analysis of the formulation given that the objective of those works was essentially the study of existence of solutions of the energetic formulation. The associativity of the flow rule, which in the context of damage modeling means the use of the thermodynamic force dual of the damage variable as damage driving force that enters the damage evolution criterion, and the independence of the dissipation on the current state of the material are simplifying assumptions which do not hold generally for materials such as concrete, soils and rocks (Vermeer and de Borst, 1984). On the other hand, while the definition of the main ingredients of the energetic formulation, that is, the storage energy functional and the dissipation potential, appear quite natural for generalized standard materials, or for model materials meeting the Drucker–Ilyushin inequality (Marigo, 2002), this seems not to be the case when the latter assumptions are not met, which would thus preclude the existence of an energetic structure. We will show that this is not always true. On the contrary, for our gradient damage model which presents the damage activated in terms of a damage surface different from the thermodynamic force dual of the damage variable, it is possible to derive the energetic formulation at the expense of introducing a state variable-dependent dissipation potential. The description of non-associativity in terms of a state variable-dependent dissipation potential, or equivalently, a state-dependent loading function, is, however, not new (Germain et al., 1983, Section IV 3) and it has been revitalized by Francfort (2018) to describe, for instance, the non-associated model of nonlinear kinematic hardening of Armstrong-Frederick, and the Drucker–Prager cap model.

The realization of the variational structure for our gradient damage model is a fundamental result, for it can be used to establish the link between the gradient damage model and a discrete crack model, and justifies the former as approximation of the latter (Pham et al., 2011; Marigo et al., 2016), typically by $\Gamma-$convergence arguments (Conti et al., 2016a). Furthermore, it has also been recognized that the existence of a variational structure allows the prediction of crack nucleation and crack propagation without requiring the introduction of *ad-hoc* criteria (Alessi et al., 2014; Marigo et al., 2016; Tamé et al., 2018).

The purpose of the present study is, therefore, (*i*) to derive the energetic formulation of a gradient damage model for concrete where the damage evolution criterion is defined in terms of a stress-based damage surface built upon the failure criterion for concrete by Lubliner et al. (1989) and Oller et al. (1990); (*ii*) to find fundamental properties met by the incremental energetic so-

lutions; and (*iii*) to propose a computational procedure for the numerical simulation of the energetic formulation.

We will find that the energetic formulation of this model is also defined by a stored energy which depends on the gradient of the damage variable, in addition to the strain and the damage variable, whereas the energy dissipation is modeled by a dissipation pseudo-potential which depends on the evolution of the damage and on the current state of the material system. By applying a semi-implicit scheme, the incremental problems corresponding to our continuous formulation have the form of minimization problems and can be thus used for the consistent numerical simulation of the theory itself. Using the optimality property of the discrete energetic solution, we prove, in particular, also for the case of state-dependent dissipation, a discrete version of the stability condition which ensures the stability of the discrete energetic solution, and a two-sided energy estimate which, compared to the one in Mielke et al. (2010), presents now the upper bound with an additional term that accounts for the variation of dissipation between the instant t_{n-1} and t_n due to the different state of the system. Both results are fundamental ingredients for the proof of existence of energetic solutions in the analysis of Mielke et al. (2002), Mielke and Roubíček (2015), and Mielke et al. (2008), for the design of the numerical strategies implemented in Bourdin et al. (2008), Bourdin (2007), Mielke et al. (2010), Benesova (2011), and Conti et al. (2016b) and for the stability analysis of the numerical scheme (Mielke and Roubíček, 2009).

After this introduction, in Section 2 we develop our rate-independent gradient damage model for concrete with a state-dependent dissipation pseudo-potential and derive the corresponding energetic formulation. We then recall the relationship between such formulation and the gradient damage constitutive theories of Lorentz and Andrieux (1999), Lorentz and Andrieux (2003), Lorentz and Godard (2011), Frémond and Nedjar (1995), and Frémond and Nedjar (1996). The energetic formulation is then used in Section 3 to justify our incremental minimization problem. In this Section we also derive the discrete stability condition and the two-sided energy inequality, and describe the numerical strategy that has been adopted to solve the incremental minimization problem. Section 4 contains numerical examples showing the performance of the formulation and of the proposed numerical method whereas Section 5 reports some concluding remarks about the formulation and the numerical method. An appendix with the detailed expressions of the terms of the Jacobian concludes the paper.

2. Energetic formulation of a gradient damage model

In this section we first introduce a rate-independent gradient damage model, following the approach proposed by Frémond (2002) and Frémond and Nedjar (1996). We then develop a variational characterization of the resulting initial boundary value problem, based on the energetic formulation proposed by Francfort and Mielke (2006), Mielke (2005), Mielke and Roubíček (2006), and Mielke and Roubíček (2015). Finally, we will discuss the relation between the energetic formulation and other constitutive theories of gradient damage model.

2.1. Notations, main assumptions and field equations

We consider the quasi-static evolution of an homogeneous isotropic body made of brittle damaging material with reference configuration $\Omega \in \mathbb{R}^n$, $n = 1, 2, 3$, and boundary $\partial\Omega$, with outward normal $\boldsymbol{n}$, split into a Dirichlet boundary $\partial\Omega_D$ and the remaining Neumann boundary $\partial\Omega_N := \partial\Omega \backslash \partial\Omega_D$ where displacements $\boldsymbol{w}$ and surface tractions $\boldsymbol{t}$ are prescribed, respectively. We assume the displacement field $\boldsymbol{u}$ to be small and the system to undergo isothermal processes with uniform temperature in Ω. The state of the system is then characterized by the linearized strain $\boldsymbol{\varepsilon}(\boldsymbol{u}) = \nabla^{sym}\boldsymbol{u} := (\nabla\boldsymbol{u} + \nabla\boldsymbol{u}^T)/2$, where ∇ denotes the gradient operator, and additional variables which are introduced to capture the effects of microfractures at the material point on its macroscopic properties. As such additional variables we consider the damage variable field β and its gradient $\nabla\beta$. The field variable β can take values in $[0, 1]$ with $\beta = 0$ when the material is undamaged and $\beta = 1$ for completed damaged material, i.e. when the material is not able to sustain any stress. Its gradient $\nabla\beta$ is introduced to account for the influence of the damage at a point on damage of its neighborhood. Following the method of virtual power, we assume as in Frémond (2002) that damage is produced by microscopic motions which break bonds among particles and such motion is described on the macroscopic level by the rate quantities $\dot{\beta} := d\beta/dt$ and $\nabla\dot{\beta} := \nabla(d\beta/dt)$. The underlying assumption of the theory is that the power of these motions must be taken into account in the power of the internal forces.

Let $\mathcal{V}$ denote the space of all continuous displacement fields that generate compatible strain fields and $\mathcal{V}_{D,0} \subset \mathcal{V}$ the linear space of the kinematically admissible virtual displacement fields, that is, the space of the continuous displacement fields $\boldsymbol{u}_{D,0}$ meeting the homogeneous kinematic boundary conditions on $\partial\Omega_D$, i.e. $\boldsymbol{u}_{D,0} = \boldsymbol{0}$ on $\partial\Omega_D$. We furthermore denote by $\mathcal{V}_D \subset \mathcal{V}$ the affine space of kinematically admissible fields, i.e. $\boldsymbol{u} \in \mathcal{V}$ such that $\boldsymbol{u} = \boldsymbol{w}$ on $\partial\Omega_D$. Let $\boldsymbol{u}_{D,\boldsymbol{w}} \in \mathcal{V}_D$ be a given (fixed) extension of $\boldsymbol{w}$ onto $\bar{\Omega}$, the closure of Ω with $\bar{\Omega} = \Omega \cup \partial\Omega_D \cup \partial\Omega_N$. Such extension is generally referred to as lifting of the Dirichlet boundary data (Quarteroni, 2017) and can be obtained, for instance, by taking an interpolation of $\boldsymbol{w}$ onto $\bar{\Omega}$ by finite element shape functions. Then, for any $\boldsymbol{u} \in \mathcal{V}_D$, there exists a $\boldsymbol{u}_{D,0} \in \mathcal{V}_{D,0}$ such that $\boldsymbol{u} = \boldsymbol{u}_{D,0} + \boldsymbol{u}_{D,\boldsymbol{w}}$ and we express this by writing that $\mathcal{V}_D = \boldsymbol{u}_{D,\boldsymbol{w}} + \mathcal{V}_{D,0}$.

We use the notation $\boldsymbol{\varepsilon}_{D,0} = \nabla^{sym}\boldsymbol{u}_{D,0}$ to refer to the linearized strain of virtual admissible displacement fields, and use the symbol $\mathcal{B}$ for the linear space of the admissible damage fields, which are here required to be scalar fields $0 \le \beta \le 1$ such that $\nabla\beta$ is bounded so to make sense the integrals we write.

By applying the extended virtual work principle (Frémond, 2002; Maugin, 2017), we obtain the following two field equations: the standard balance equations of linear momentum between the stress field $\boldsymbol{\sigma}$ and the external forces $\boldsymbol{f}$ and $\boldsymbol{t}$,

$$\begin{array}{ll} \text{div}\,\boldsymbol{\sigma} + \boldsymbol{f} = \boldsymbol{0} & \text{in } \Omega \\ \boldsymbol{\sigma}\boldsymbol{n} = \boldsymbol{t} & \text{on } \partial\Omega_N \end{array} \tag{2.1}$$

with the corresponding Neumann boundary conditions, and the microforce balance equations between the internal forces $\boldsymbol{H}$ and V dual of the kinematic variables $\nabla\dot{\beta}$ and $\dot{\beta}$, respectively

$$\begin{array}{ll} \text{div}\,\boldsymbol{H} - V = 0 & \text{in } \Omega \\ \boldsymbol{H}\cdot\boldsymbol{n} = 0 & \text{on } \partial\Omega \end{array} \tag{2.2}$$

with the corresponding boundary values.

2.2. Constitutive equations

The field balance equations of the previous section must be completed by the constitutive equations which are hereafter derived within the framework of continuum thermomechanics and for the class of generalized standard models (Besson et al., 2010; Frémond, 2002). We start thus from the Clausius–Duhem inequality which, for isothermal processes and uniform temperature, states that the part of the total internal power which is not reversible must be non-negative, that is

$$-\dot{\psi} + \boldsymbol{\sigma} : \dot{\boldsymbol{\varepsilon}} + V\dot{\beta} + \boldsymbol{H}\cdot\nabla\dot{\beta} \ge 0 \tag{2.3}$$

where ψ is the free Helmholtz energy per unit volume defined in terms of the state variables, i.e, $\psi = \psi(\boldsymbol{\varepsilon}, \beta, \nabla\beta)$, and $\boldsymbol{\sigma} : \dot{\boldsymbol{\varepsilon}} + V\dot{\beta} + \boldsymbol{H} \cdot \nabla\dot{\beta}$ is the total internal power as defined in the previous section. We assume then, as part of our modeling assumptions, that the internal forces, $\boldsymbol{\sigma}$, V and $\boldsymbol{H}$ can be additively split into a non-dissipative and dissipative component as follows

$$\boldsymbol{\sigma} = \boldsymbol{\sigma}^{nd} + \boldsymbol{\sigma}^{d}, \quad V = V^{nd} + V^{d}, \quad \boldsymbol{H} = \boldsymbol{H}^{nd} + \boldsymbol{H}^{d}, \tag{2.4}$$

where the non-dissipative components are those which produce reversible power. As a result, they are defined in terms of the free Helmholtz energy $\psi = \psi(\boldsymbol{\varepsilon}, \beta, \nabla\beta)$ as follows

$$\boldsymbol{\sigma}^{nd} = \frac{\partial\psi}{\partial\boldsymbol{\varepsilon}}, \quad V^{nd} = \frac{\partial\psi}{\partial\beta}, \quad \boldsymbol{H}^{nd} = \frac{\partial\psi}{\partial\nabla\beta}. \tag{2.5}$$

By accounting for (2.5) into (2.3) and noting (2.4), the Clausius–Duhem inequality reduces to the following condition

$$\boldsymbol{\sigma}^{d} : \dot{\boldsymbol{\varepsilon}} + V^{d}\dot{\beta} + \boldsymbol{H}^{d} \cdot \nabla\dot{\beta} \geq 0. \tag{2.6}$$

The material model is thus completely determined if, in addition to (2.5), we define $\boldsymbol{\sigma}^d$, V^d and $\boldsymbol{H}^d$ such that (2.6) is satisfied. The specific definition of $\boldsymbol{\sigma}^d$, V^d and $\boldsymbol{H}^d$ depends in turn on the mechanisms inside the material responsible for the irreversibility of the process. For the generalized standard models, $\boldsymbol{\sigma}^d$, V^d and $\boldsymbol{H}^d$ are defined in terms of a function ϕ, referred to as dissipation pseudo-potential, which is assumed: (*i*) to depend on $(\dot{\boldsymbol{\varepsilon}}, \dot{\beta}, \nabla\dot{\beta})$; (*ii*) to be parametrized by the state variables $(\boldsymbol{\varepsilon}, \beta, \nabla\beta)$ and (*iii*) to have structural properties which ensure the validity of (2.6), such as ϕ convex with respect to the rate variables, subdifferentiable, non-negative and such that $\phi(\boldsymbol{0}, 0, \boldsymbol{0}; (\boldsymbol{\varepsilon}, \beta, \nabla\beta)) = 0$ for any $(\boldsymbol{\varepsilon}, \beta, \nabla\beta)$. In this case, if we assume

$$(\boldsymbol{\sigma}^d, V^d, \boldsymbol{H}^d) \in \partial_{(\dot{\boldsymbol{\varepsilon}}, \dot{\beta}, \nabla\dot{\beta})}\phi(\dot{\boldsymbol{\varepsilon}}, \dot{\beta}, \nabla\dot{\beta}; (\boldsymbol{\varepsilon}, \beta, \nabla\beta)) \tag{2.7}$$

where $\partial\phi(x; y)$ denotes the subdifferential of ϕ with respect to x by treating y as parameter, i.e. $\alpha \in \partial\phi(x; y) \Leftrightarrow \phi(z; y) - \phi(x; y) \geq \alpha \cdot (z - x)\ \forall z$, we can easily check that condition (2.6) is met. If in addition ϕ is a positively homogeneous function of degree *one* with respect to the rate variables, i.e. $\phi(tx; y) = t\phi(x; y)\ \forall t > 0$, then the evolution laws defined by (2.7) are rate-independent, i.e., invariant with respect to time scaling. Within such framework, the model is thus completely specified by the two functions: $\psi = \psi(\boldsymbol{\varepsilon}, \beta, \nabla\beta)$ and $\phi = \phi(\dot{\boldsymbol{\varepsilon}}, \dot{\beta}, \nabla\dot{\beta}; (\boldsymbol{\varepsilon}, \beta, \nabla\beta))$.

Let $X \subset \mathbb{R}$ and denote by $I_X : \mathbb{R} \to \mathbb{R} \cup \{+\infty\}$ the indicator function of X, i.e. $I_X(x) = 0$ if $x \in X$ and $I_X(x) = +\infty$ otherwise. For the definition of our model, we assume:

(i) the free Helmhotz energy given by

$$\psi(\boldsymbol{\varepsilon}, \beta, \nabla\beta) = \frac{1}{2}R(\beta)\mathbb{E}\boldsymbol{\varepsilon} : \boldsymbol{\varepsilon} + \frac{c}{2}|\nabla\beta|^2 + I_{[0,1]}(\beta) \tag{2.8}$$

where $\mathbb{E}$ is the Hooke elastic material tensor, $R(\beta)$ is a decreasing function in $[0, 1]$ such that $R(0) = 1$ and $R(1) = 0$ which we refer to as softening function and is described in Section 2.3, c is a regularizing parameter which introduces a size-dependent scale effect in the model and accounts for the influence of the damage at a material point on its neighborhood, and $I_{[0,1]}(\beta)$ is the indicator function of the interval $[0, 1]$ which enforces the constraint $\beta \in [0, 1]$;

(ii) the dissipation pseudo-potential given by

$$\phi(\dot{\boldsymbol{\varepsilon}}, \dot{\beta}, \nabla\dot{\beta}; (\boldsymbol{\varepsilon}, \beta, \nabla\beta)) = (k + V^* - V^{nd})\dot{\beta} + I_{\mathbb{R}^+}(\dot{\beta}) \tag{2.9}$$

where V^{nd} is obtained by $(2.5)_2$, V^* is related to the damage criterion as it will be discussed below in Section 2.4, k is the initial damage threshold that determines the activation of the damage, and $I_{\mathbb{R}^+}(\dot{\beta})$ is introduced to enforce the constraint $\dot{\beta} \geq 0$ corresponding to the assumption of irreversibility of the damage, i.e. no healing.

Remark 2.1.

(a) The choice of ϕ dependent only on $\dot{\beta}$ means that we are assuming that at the material point the only internal dissipation mechanisms are those associated with $\dot{\beta}$. Such dissipation is furthermore assumed to depend on the current state of the system through the dependence of ϕ on $(\epsilon, \beta, \nabla\beta)$. Equivalently, we will see below (see Remark 2.3) that such choice for the dissipation potential corresponds to assume a loading function f with the threshold dependent on the state of the system.

(b) The function ϕ defined by (2.9) is linear with respect to $\dot{\beta}$ and is non-negative provided that $(k + V^*(\boldsymbol{\varepsilon}, \beta, \nabla\beta) - V^{nd}(\boldsymbol{\varepsilon}, \beta, \nabla\beta)) \geq 0$ for any $(\boldsymbol{\varepsilon}, \beta, \nabla\beta)$. By realizing such condition, we satisfy (2.6) and the evolution is rate-independent. We refer to Section 2.4 for a discussion of the condition $k + V^* - V^{nd} \geq 0$ which depends clearly on the choice of the damage criterion V^*.

If we let $R'(\beta) := dR/d\beta$, from (2.5) by accounting of (2.8) we get

$$\boldsymbol{\sigma}^{nd} = R(\beta)\mathbb{E}\boldsymbol{\varepsilon}, \quad V^{nd} = \frac{1}{2}R'(\beta)\mathbb{E}\boldsymbol{\varepsilon} : \boldsymbol{\varepsilon} + \partial_\beta I_{[0,1]}(\beta)$$
$$\boldsymbol{H}^{nd} = c\nabla\beta, \tag{2.10}$$

and from (2.7) using (2.9), where ϕ depends only on $\dot{\beta}$, we obtain

$$\boldsymbol{\sigma}^{d} = \boldsymbol{0}, \quad V^{d} \in \partial_{\dot{\beta}}\phi = k + V^* - V^{nd} + \partial_{\dot{\beta}} I_{\mathbb{R}_0^+}(\dot{\beta}), \quad \boldsymbol{H}^{d} = \boldsymbol{0}. \tag{2.11}$$

Remark 2.2. If in (2.11) we assume $V^* = V^{nd}$ and consider the local version of the model ($c = 0$), we find the evolution law of the standard local damage model, with $-V^{nd} \in k + \partial_{\dot{\beta}} I_{\mathbb{R}_0^+}(\dot{\beta})$.

The balance Eqs. (2.1) and (2.2) along with the constitutive Eqs. (2.4), (2.10) and (2.11), complemented by the predefined value of the damage profile at the time $t = 0$, for instance $\beta(\boldsymbol{x}, 0) = 0$, describe the full evolution of the system. For our subsequent developments, it is, however, convenient to rewrite the evolution law (2.11) into an equivalent manner. By substituting $\boldsymbol{H} = c\nabla\beta$ into (2.2) and assuming $c(\boldsymbol{x}) = c$ in Ω, we obtain $V = c\Delta\beta$ which, replaced into (2.11) after noting $(2.4)_2$, gives

$$c\Delta\beta - k - V^* \in \partial_{\dot{\beta}} I_{\mathbb{R}_0^+}(\dot{\beta}). \tag{2.12}$$

Thus, if we let $f = c\Delta\beta - k - V^*$ and recall the definition of $\partial_{\dot{\beta}} I_{\mathbb{R}_0^+}(\dot{\beta})$ (Hiriart-Urruty and Lemaréchal, 2001), (2.12) represents the following set of conditions

$$\begin{aligned} f &= 0 \quad \text{if } \dot{\beta} > 0 \\ f &< 0 \quad \text{if } \dot{\beta} = 0 \end{aligned} \tag{2.13}$$

which can in turn be succinctly expressed in the following manner

$$f \leq 0, \quad f\dot{\beta} = 0, \quad \dot{\beta} \geq 0. \tag{2.14}$$

Remark 2.3. At variance of the classical model of damage coupled with elasticity referred to in Krajcinovic (1996) as brittle damage, here the damage threshold is dependent also on the state $(\boldsymbol{\varepsilon}, \beta, \nabla\beta)$ of the system and is non-local.

Box 1 summarizes the classical formulation of the evolution problem with $R(\beta)$ and V^* to be defined, for instance, as in Section 2.3 and Section 2.4, respectively.

2.3. Softening function

One of the influence of damage on the macroscopic behavior of the material is a decreasing unloading-reloading stiffness which is accounted for by the function $R(\beta)$. Whenever β is defined such

Balance Equations

$$\operatorname{div}\boldsymbol{\sigma} + \boldsymbol{f} = \boldsymbol{0} \quad \text{in } \Omega$$
$$\operatorname{div}\boldsymbol{H} - V = 0 \quad \text{in } \Omega$$

Constitutive Equations

State Equations

$$\boldsymbol{\sigma} = R(\beta)\mathbb{E}\boldsymbol{\varepsilon}$$
$$\boldsymbol{H} = c\nabla\beta$$
$$V = V^{nd} + V^{d}$$
$$V^{nd} = R'(\beta)\frac{1}{2}\mathbb{E}\boldsymbol{\varepsilon} : \boldsymbol{\varepsilon} + \partial_\beta I_{[0,\,1]}(\beta)$$
$$V = c\Delta\beta$$

Evolution Equations

$$f = c\Delta\beta - k - V^*\,,$$
$$f \le 0\,, \quad f\dot{\beta} = 0\,, \quad \dot{\beta} \ge 0\,,$$
$$V^* = R'(\beta)\frac{(\sigma_{eq}(\varepsilon))^2}{2E}\,,$$

with $R(\beta)$ and σ_{eq} defined by (2.15) and (2.16), respectively.

Initial and Boundary Values

$$\beta(\boldsymbol{x}, 0) = 0 \quad \text{in } \Omega$$
$$\boldsymbol{\sigma}\boldsymbol{n} = \boldsymbol{t} \quad \text{on } \partial\Omega_N$$
$$\boldsymbol{u}(x,t) = \boldsymbol{w}(\boldsymbol{x},t) \quad \text{on } \partial\Omega_D$$
$$\boldsymbol{H}\cdot\boldsymbol{n} = 0 \quad \text{on } \partial\Omega\,.$$

Kinematic Conditions and Constraints

$$\boldsymbol{\varepsilon} = \frac{1}{2}(\nabla\boldsymbol{u} + \nabla\boldsymbol{u}^T)$$
$$\beta \in [0,\,1]$$

Box. 1. Differential formulation of the evolution of the gradient damage model.

that $\beta = 0$ corresponds to the elastic, undamaged state and $\beta = 1$ to material failure, $R(\beta)$ must be a decreasing function with β. The classical assumption for $R(\beta)$ due to Kachanov (1958) is a linear interpolation of the two states $\beta = 0$ and $\beta = 1$ by taking simply $R(\beta) = 1 - \beta$. Still, even other expressions have been suggested for $R(\beta)$ and justified by analyzing the asymptotic behavior of the resulting model in the case of uniaxial tension (Pham and Marigo, 2010a; 2010b; Lorentz and Andrieux, 1999; Lorentz et al., 2011). In order to retrieve the response of a cohesive zone model as the length scale goes to zero while keeping the other macroscopic parameters constant, Lorentz et al. (2011) and Lorentz (2017) suggest the following expression for $R(\beta)$, which will also be adopted in this work,

$$R(\beta) = \frac{(1-\beta)^2}{(1-\beta)^2 + \frac{3E_0G_f}{2f_{t0}^2D}\beta(1 + p\beta\exp(q\beta^2))} \tag{2.15}$$

with G_f the fracture energy, E_0 the initial Young's modulus, f_{t0} the uniaxial tensile strength, p a shape parameter related to the opening displacement at failure, q a positive dimensionless parameter that controls the curvature of the cohesive response, and D the half band width given in Lorentz et al. (2011) by $D = \sqrt{2c/k}$ with c and k the parameters that enter (2.8) and (2.9), respectively. We refer to Lorentz et al. (2011) and Lorentz (2017) for the details of the derivation of (2.15) and the asymptotic analysis of the model.

Remark 2.4. For uniaxial traction, due to the expression of the damage surface given below, our model coincides with the one given in Lorentz et al. (2011, 2012) and Lorentz (2017), i.e. we find that $\phi = k\dot{\beta}$ (see Remark 2.5(a)), which is shown to converge to a cohesive zone model.

2.4. Damage surface

An important ingredient of the model formulation in Box 1 is the selection of V^*. The choice of V^* defines the conditions that determine the occurrence of damage and regulates its evolution. In the brittle damage models proposed in Lorentz and Godard (2011) and Lorentz et al. (2012), for instance, it is assumed $V^* = V^{nd}$ corresponding to a strain-based damage criterion which does not differentiate between the energy accumulated in tension and compression that activates the damage. On the other hand, to account for the non-symmetric behavior in traction and compression, one can either modify the free energy ψ, thus V^{nd} that enters the expression of ϕ or define directly V^*. Examples of damage criteria of the first type are given in Amor et al. (2009) and Freddi and Royer-Carfagni (2010) which can be obtained within the current framework by simply taking $V^* = V^{nd}$ with V^{nd} defined in terms of the free energy therein considered, whereas instances of the second approach are the damage criteria suggested by Frémond and Nedjar (1995) and Nedjar (2001) which can be obtained by taking

$$V^* = -\frac{1}{2}\left[\left(\frac{\beta(1-M)}{1-M\beta}(2\mu\boldsymbol{\varepsilon}^+ : \boldsymbol{\varepsilon}^+ + \lambda(\mathrm{tr}^+(\boldsymbol{\varepsilon}))^2\right)\right]$$

where the part positive $\boldsymbol{\varepsilon}^+$ of the strain tensor is obtained after the diagonalization of $\boldsymbol{\varepsilon}$, $\mathbf{tr}^+(\boldsymbol{\varepsilon}) = \max\{0,\, \mathbf{tr}(\boldsymbol{\varepsilon})\}$ and M is a dimensionless factor that ensures the pseudo-potential to be positive, or also the damage criteria given in Comi (1999), Eq. (3). By these approaches one relates the damage criteria to the strain energy or to some part of it. For brittle elastic material, such as the concrete, on the other hand, stress-based criteria are more reliable (Krajcinovic, 1996). This means that one assumes damage evolution to be driven by an equivalent strain that quantifies the local deformation state in the material. Among the several definitions

(Lorentz, 2017; Giry et al., 2011), here we consider

$$V^* = R'(\beta)\frac{(\sigma_{eq})^2}{2E} \tag{2.16}$$

with σ_{eq} the equivalent stress of the stress-based failure criterion for the concrete proposed by Lubliner et al. (1989) and Oller et al. (1990) which has proved successful in simulating concrete behavior under different type of loadings. This criterion is expressed in the undamaged configuration in terms of the undamaged stress $\boldsymbol{\sigma}_0 = \mathbb{E}\boldsymbol{\varepsilon}$ as follows

$$\sigma_{eq} = \frac{1}{\ell_1(1-\ell_2)}\left(\sqrt{3J_2} + \ell_2 I_1 + \ell_3\langle\sigma_{0,max}\rangle - \ell_4\langle-\sigma_{0,max}\rangle\right) \tag{2.17}$$

where $I_1 = \mathbf{tr}(\boldsymbol{\sigma}_0)$, $J_2 = 1/2[\mathbf{tr}(\boldsymbol{\sigma}_0^2) - 1/3(\mathbf{tr}(\boldsymbol{\sigma}_0))^2]$, $\sigma_{0,\,max}$ the maximum principal stress of $\boldsymbol{\sigma}_0$ and $\langle\cdot\rangle$ the Macaulay bracket defined as $\langle x\rangle = 1/2(x+|x|)$. In (2.17), the parameters ℓ_1, ℓ_2, ℓ_3 and ℓ_4 are dimensionless constants which are derived from (2.17) for special stress states paths, and are obtained in Lubliner et al. (1989), Oller et al. (1990), and Zhang and Li (2012) as follows

$$\ell_1 = \frac{f_{c0}}{f_{t0}}, \quad \ell_2 = \frac{(f_{b0}/f_{c0})-1}{2(f_{b0}/f_{c0})-1}$$
$$\ell_3 = (1-\ell_2)(f_{c0}/f_{t0}) - (1+\ell_2), \quad \ell_4 = \frac{3(1-K_c)}{2K_c-1} \tag{2.18}$$

where f_{b0}, f_{c0} and f_{t0} are the initial equibiaxial, uniaxial compressive and uniaxial tensile strength, respectively, and K_c is the ratio of $\sqrt{J_2}$ on the tensile meridian to that on the compressive meridian (Zhang and Li, 2012). For details on their derivation in elementary tests, we refer to Lubliner et al. (1989), Oller et al. (1990), and Zhang and Li (2012).

Remark 2.5.

(a) Under uniaxial traction stress σ, $\sigma_{0,max} = \sigma > 0$, and taking into account for (2.18), we find that (2.17) yields $\sigma_{eq} = \sigma$. In biaxial compression, $\sigma_{0,max} = 0$ and (2.17) reduces to the Drucker–Prager criterion, whereas in triaxial stress states, if tensile stresses components are present, i.e. $\sigma_{0,\,max} > 0$, (2.17) is a combination of the Drucker–Prager criterion and of the Rankine criterion. For $\sigma_{0,\,max} < 0$, on the other hand, we have a modified Drucker–Prager criterion.

(b) As a result of the choice (2.16) for V^*, and by accounting for (2.10), we can now verify that there holds

$$k + V^* - V^{nd} = k - \frac{1}{2}R'(\beta)\left(\mathbb{E}\boldsymbol{\varepsilon}:\boldsymbol{\varepsilon} - \frac{(\sigma_{eq})^2}{E}\right) \geq 0\,,$$

which ensures the pseudo-potential of dissipation to be non negative. In absence of damage, $\Delta\beta = 0$, and from the condition $f < 0$, we get $k + V^* > 0$, and so is, 'a fortiori', $k + V^* - 1/2R'(\beta)\mathbb{E}\boldsymbol{\varepsilon}:\boldsymbol{\varepsilon} > 0$, given that $R'(\beta) < 0$. When damage occurs, $1/2\mathbb{E}\boldsymbol{\varepsilon}:\boldsymbol{\varepsilon}$ represents the elastic energy that would be stored in the material if it were undamaged, which must thus be greater than $(\sigma_{eq})^2/(2E)$, related somehow to the energy of the damaged state.

2.5. Energetic formulation

We present now the energetic formulation corresponding to the differential model given in Box 1 as an application of the theory described in Mielke and Roubíček (2015). Such formulation generalizes the differential model in the sense that it allows for solutions $q(\boldsymbol{x},t) = (\boldsymbol{u}(\boldsymbol{x},t), \boldsymbol{\varepsilon}(\boldsymbol{x},t), \beta(\boldsymbol{x},t), \nabla\beta(\boldsymbol{x},t))$ with jumps with respect to time and space, and for free energies ψ that are not convex, permitting in this manner the modeling of a larger class of phenomena. We will see, however, that this generalization will be at the cost of enforcing the evolution law (2.7) only in an integral form, such as in the gradient damage models advanced, for instance, in Lorentz and Benallal (2005) and Lorentz and Godard (2011).

We assume that the variables $(\boldsymbol{u}, \boldsymbol{\varepsilon}, \beta, \boldsymbol{z})$ (with then $\boldsymbol{\varepsilon} = \nabla^{sym}\boldsymbol{u}$ and $\boldsymbol{z} = \nabla\beta$) that describe the evolution process of the system, belong to a Banach space $\mathcal{Q} = \mathcal{V}_D \times \mathcal{W} \times \mathcal{B} \times \mathcal{X}$ which serves as a state space and is assumed for now with the minimal regularity assumptions necessary for the formulation to make sense. In the above notation, $\mathcal{W}$ is the space of the compatible strain fields whereas $\mathcal{X}$ is the space of the gradient fields. Furthermore, in the following, in order to streamline notations, we will use indifferently the symbol q to denote either $(\boldsymbol{u}, \boldsymbol{\varepsilon}, \beta, \nabla\beta)$ or $(\boldsymbol{\varepsilon}, \beta, \nabla\beta)$ or $(\boldsymbol{u}, \beta)$ and the symbol $\mathcal{Q}$ to denote the corresponding space, being always clear from the context what the right formulation should be. If necessary, the notation will then be made rigorous.

The space $\mathcal{Q}$ is independent of the time, in the sense that if $[0,T]$ is our time interval of interest, we require that for all $t \in [0,T]$, $q(\cdot,t) \in \mathcal{Q}$. In the following, we will also be using the notation $q(t) \in \mathcal{Q}$ to denote the $\boldsymbol{x}$–dependent fields for any value of t. We consider then the stored energy functional $\mathcal{E} : [0,T] \times \mathcal{Q} \to \mathbb{R} \cup \{\infty\}$ defined by

$$\mathcal{E}(t, q(t)) = \int_\Omega \psi(\boldsymbol{\varepsilon}(\boldsymbol{x},t), \beta(\boldsymbol{x},t), \nabla\beta(\boldsymbol{x},t))\,d\boldsymbol{x} - \langle\ell(t), \boldsymbol{u}\rangle \tag{2.19}$$

with $\langle\cdot,\cdot\rangle$ the linear form modeling the work of the external time-dependent loading, which in the case of the model of Box 1 is given by

$$\langle\ell(t), \boldsymbol{u}\rangle = \int_\Omega \boldsymbol{f}(\boldsymbol{x},t)\cdot\boldsymbol{u}(\boldsymbol{x},t)\,d\boldsymbol{x} + \int_{\partial\Omega_N} \boldsymbol{t}(s,t)\cdot\boldsymbol{u}(s,t)\,ds\,, \tag{2.20}$$

and the dissipation functional $\mathcal{R} : \mathcal{W} \times \mathcal{B} \to \mathbb{R} \cup \{\infty\}$ given by

$$\mathcal{R}(\dot\beta;\ (\boldsymbol{\varepsilon},\ \beta)) = \int_\Omega \phi(\dot\beta(\boldsymbol{x},t);\ (\boldsymbol{\varepsilon}(\boldsymbol{x},t), \beta(\boldsymbol{x},t))\,d\boldsymbol{x}\,, \tag{2.21}$$

in the case of smooth evolutions. Likewise Mielke and Roubíček (2015), we refer to the triple $(\mathcal{Q}, \mathcal{E}, \mathcal{R})$ as Energetic Rate-Independent System given that its specification defines completely the evolution of the model.

Definition 1. We say that $q(\boldsymbol{x},t) = \big(\boldsymbol{u}(\boldsymbol{x},t), \boldsymbol{\varepsilon}(\boldsymbol{x},t), \beta(\boldsymbol{x},t), \nabla\beta(\boldsymbol{x},t)\big)$ is an energetic solution of the system $(\mathcal{Q}, \mathcal{E}, \mathcal{R})$ if for all $t \in [0,T]$, the following two conditions are met,

$$\mathcal{E}(t, q(t)) + \int_0^t \mathcal{R}(\dot\beta;\ (\boldsymbol{\varepsilon},\ \beta))\,d\tau = \mathcal{E}(0, q(0)) + \int_0^t \frac{\partial\mathcal{E}}{\partial\tau}(\tau,\ q(\tau))\,d\tau\,, \tag{E}$$

$$\forall\tilde q = (\tilde{\boldsymbol{u}}, \tilde{\boldsymbol{\varepsilon}}, \tilde\beta, \nabla\tilde\beta) \in \mathcal{Q},\quad \mathcal{E}(t, q(t)) \leq \mathcal{E}(t,\tilde q) + \mathcal{R}(\tilde\beta - \beta;\ (\boldsymbol{\varepsilon}, \beta)). \tag{S}$$

Both in (E) and in (S), the Dirichlet boundary conditions are automatically accounted for and we refer to it by saying that $\tilde q \in \mathcal{Q}$ is an admissible state.

Remark 2.6. The term $\partial\mathcal{E}/\partial t$ which occurs in (E) represents the variation of the total stored energy $\mathcal{E}$ for the explicit dependence of $\mathcal{E}$ on t. This results from time dependent loadings $\ell(t)$ and prescribed displacements $\boldsymbol{w} = \boldsymbol{w}(\boldsymbol{x},t)$ on $\partial\Omega_D$. Given the expression (2.19) of $\mathcal{E}$, it is not difficult to show (compare also with Francfort and Mielke, 2006, page 60) that if for any $\boldsymbol{u} \in \mathcal{V}_D$, we write $\boldsymbol{u} = \boldsymbol{u}_{D,0} + \boldsymbol{u}_{D,\boldsymbol{w}}$ with $\boldsymbol{u}_{D,0} \in \mathcal{V}_{D,0}$ (see Section 2.1), there holds

$$\frac{\partial}{\partial t}\mathcal{E}(t, q(t)) = \int_\Omega \frac{\partial\psi}{\partial\boldsymbol{\varepsilon}} : \boldsymbol{\varepsilon}(\dot{\boldsymbol{u}}_{D,\boldsymbol{w}})\,d\boldsymbol{x} - \langle\dot\ell(t), \boldsymbol{u}\rangle - \langle\ell(t), \dot{\boldsymbol{u}}_{D,\boldsymbol{w}}\rangle\,, \tag{2.22}$$

i.e. $\partial\mathcal{E}/\partial t$ is equal to the work done by the external actions, where also the work associated with the lift function $\boldsymbol{u}_{D,\,\boldsymbol{w}}$ of the Dirichlet boundary data $\boldsymbol{w}$ and the free stored energy associated with

$\boldsymbol{\varepsilon}(\dot{\boldsymbol{u}}_{D,\boldsymbol{w}})$ must be taken into account. We recall that by definition (2.20), it is

$$\langle \dot{\ell}(t), \boldsymbol{u}\rangle = \int_\Omega \dot{\boldsymbol{f}}(\boldsymbol{x},t)\cdot\boldsymbol{u}(\boldsymbol{x},t)\,d\boldsymbol{x} + \int_{\partial\Omega_N} \dot{\boldsymbol{t}}(s,t)\cdot\boldsymbol{u}(s,t)\,ds$$

$$\text{and}\quad \langle \ell(t), \dot{\boldsymbol{u}}_{D,\boldsymbol{w}}\rangle = \int_\Omega \boldsymbol{f}(\boldsymbol{x},t)\cdot\dot{\boldsymbol{u}}_{D,\boldsymbol{w}}(\boldsymbol{x},t)\,d\boldsymbol{x} + \int_{\partial\Omega_N} \boldsymbol{t}(s,t)\cdot\dot{\boldsymbol{u}}_{D,\boldsymbol{w}}(s,t)\,ds\,. \tag{2.23}$$

Condition (E) represents therefore an energy balance equation which enforces that during the evolution $q=q(t)$ of the system, the work $\int_0^t \partial\mathcal{E}/\partial\tau\,d\tau$ of the external actions during the time interval $[0,t]$ for any $t\in[0,T]$, is equal to the sum of the variation of the total stored energy in the time interval $[0,t]$ and the energy dissipated by damage during the same time interval $[0,t]$. Condition (S), on the other hand, enforces a stability property of the process $q=q(t)$ by requiring that the gain of the total stored energy $\mathcal{E}(t,q(t))-\mathcal{E}(t,\tilde{q})$ at any other admissible state $\tilde{q}$ is not greater than the dissipation associated with such variation of state.

Compared to the differential model, for the energetic formulation to make sense, we need the regularity with respect to time of the loading so that $\partial\mathcal{E}/\partial t$ be defined. Furthermore, the occurrence of condition (E) implies that along a process $q=q(t)$ the total energy $\mathcal{E}$ is continuous with respect to time, even though the response of the system can experience discontinuity jumps in time.

Remark 2.7. The field $\beta(\boldsymbol{x},0)$, which appears in (E) through $q(0)$, is the initial condition associated with the evolution of the damage variable β, and is indeed a data, whereas $\boldsymbol{u}(\boldsymbol{x},0)$ is obtained by solving the equilibrium elastic equation at $t=0$.

For sake of completeness and reader's convenience, next we illustrate the relationship between an energetic solution and a solution of the differential model given in Box 1. However, it must be remarked that the following relationships have been also established in Pham and Marigo (2010a,b), Pham et al. (2011), Marigo et al. (2016), where they have been obtained using the variational formulation of Pham and Marigo (2010a,b) which is derived by the Drucker-Ilyushin inequality (Marigo, 2002) and a unilateral local minimization of the total energy. This variational formulation coincides with the energetic formulation of Mielke in the case of local stability.

Let us assume $q(t)=(\boldsymbol{u},\beta)\in\mathcal{V}_D\times\mathcal{B}$ be a solution of (E) and (S) for any $t\in[0,T]$, and consider the following variations

$$\tilde{\boldsymbol{u}}=\boldsymbol{u}+\alpha\boldsymbol{v},\quad \tilde{\boldsymbol{\varepsilon}}=\boldsymbol{\varepsilon}(\boldsymbol{u})+\alpha\boldsymbol{\varepsilon}(\boldsymbol{v}),$$
$$\tilde{\beta}=\beta+\alpha\gamma,\quad \nabla\tilde{\beta}=\nabla\beta+\alpha\nabla\gamma\,, \tag{2.24}$$

for any $(\boldsymbol{v},\gamma)\in\mathcal{V}_{D,0}\times\mathcal{B}$ and $\alpha>0$. The corresponding expansion of $\mathcal{E}$ reads then as

$$\mathcal{E}(t,\tilde{\boldsymbol{u}},\tilde{\boldsymbol{\varepsilon}},\tilde{\beta},\nabla\tilde{\beta}) = \mathcal{E}(t,\boldsymbol{u},\boldsymbol{\varepsilon},\beta,\nabla\beta) + \alpha\int_\Omega\left(\frac{\partial\psi(q(t))}{\partial\boldsymbol{\varepsilon}}:\boldsymbol{\varepsilon}(\boldsymbol{v}) + \frac{\partial\psi(q(t))}{\partial\beta}\gamma + \frac{\partial\psi(q(t))}{\partial\nabla\beta}\cdot\nabla\gamma\right)d\boldsymbol{x} - \alpha\langle\ell(t),\boldsymbol{v}\rangle + o(\alpha)$$
$$\text{for all } (\boldsymbol{v},\gamma)\in\mathcal{V}_{D,0}\times\mathcal{B},\quad \alpha>0\,, \tag{2.25}$$

where $o(\alpha)$ is the o-little symbol of Landau such that $\lim_{\alpha\to0} o(\alpha)/\alpha=0$. By replacing (2.25) into the stability condition (S) and taking into account the definitions (2.5) along with the assumptions that $\boldsymbol{\sigma}^d=\boldsymbol{0}$ and $\boldsymbol{H}^d=\boldsymbol{0}$, corresponding to having the dissipation pseudo-potential ϕ dependent only on $\dot{\beta}$, we have

$$\mathcal{E}(t,q(t)) \le \mathcal{E}(t,q(t)) + \alpha\int_\Omega\left(\boldsymbol{\sigma}:\boldsymbol{\varepsilon}(\boldsymbol{v}) + V^{nd}\gamma + \boldsymbol{H}\cdot\nabla\gamma\right)d\boldsymbol{x} - \alpha\langle\ell(t),\boldsymbol{v}\rangle + o(\alpha) + \alpha\int_\Omega\phi(\gamma;(\boldsymbol{\varepsilon},\beta))\,d\boldsymbol{x}$$
$$\text{for all } (\boldsymbol{v},\gamma)\in\mathcal{V}_{D,0}\times\mathcal{B},\quad \alpha>0\,, \tag{2.26}$$

where we have used the definition (2.21) of $\mathcal{R}(\dot{\beta};q)$ and the fact that $\phi(\cdot\,;(\boldsymbol{\varepsilon},\beta))$ is positively homogeneous of degree one. The application then of Green theorem to the term $\int_\Omega \boldsymbol{H}\cdot\nabla\gamma\,d\boldsymbol{x}$ and letting $\alpha\to0$ give

$$0 \le \int_\Omega\left(\boldsymbol{\sigma}:\boldsymbol{\varepsilon}(\boldsymbol{v}) + (V^{nd}-\mathbf{div}\boldsymbol{H})\gamma\right)d\boldsymbol{x} - \langle\ell(t),\boldsymbol{v}\rangle + \int_\Omega\phi(\gamma;(\boldsymbol{\varepsilon},\beta))\,d\boldsymbol{x} \qquad \text{for all } (\boldsymbol{v},\gamma)\in\mathcal{V}_{D,0}\times\mathcal{B}\,, \tag{2.27}$$

which is equivalent to the following two conditions

$$\int_\Omega\boldsymbol{\sigma}:\boldsymbol{\varepsilon}(\boldsymbol{v})\,d\boldsymbol{x} - \langle\ell(t),\boldsymbol{v}\rangle = 0 \quad \text{for all } \boldsymbol{v}\in\mathcal{V}_{D,0}\,, \tag{2.28}$$

$$\int_\Omega\left((V^{nd}-\mathbf{div}\boldsymbol{H})\gamma + \phi(\gamma;(\boldsymbol{\varepsilon},\beta))\right)d\boldsymbol{x}\ge0 \quad \text{for all } \gamma\in\mathcal{B}\,, \tag{2.29}$$

where (2.28) represents the weak form of the balance equation of the linear momentum whereas (2.29) will be used to retrieve the integral form of the evolution law. With this aim, we first take the total time derivative of condition (E) which gives

$$\frac{d}{dt}\mathcal{E}(t,q(t)) + \mathcal{R}(\dot{\beta};(\boldsymbol{\varepsilon},\beta)) = \frac{\partial}{\partial t}\mathcal{E}(t,q(t))\,. \tag{2.30}$$

Given the expression (2.19) of $\mathcal{E}$, we then apply the chain rule and account for the lifting of the boundary data $\boldsymbol{u}=\boldsymbol{u}_{D,0}+\boldsymbol{u}_{D,\boldsymbol{w}}$ to obtain

$$\begin{aligned}
\frac{d}{dt}\mathcal{E}(t,q(t)) &= \int_\Omega\frac{d\psi}{dt}\,d\boldsymbol{x} - \langle\ell(t),\dot{\boldsymbol{u}}\rangle - \langle\dot{\ell}(t),\boldsymbol{u}\rangle\\
&= \int_\Omega\left(\frac{\partial\psi}{\partial\boldsymbol{\varepsilon}}:\dot{\boldsymbol{\varepsilon}} + \frac{\partial\psi}{\partial\beta}\dot{\beta} + \frac{\partial\psi}{\partial\nabla\beta}\cdot\nabla\dot{\beta}\right)d\boldsymbol{x}\\
&\quad -\langle\ell(t),\dot{\boldsymbol{u}}\rangle - \langle\dot{\ell}(t),\boldsymbol{u}\rangle\,,\\
&= \int_\Omega\left(\frac{\partial\psi}{\partial\boldsymbol{\varepsilon}}:\dot{\boldsymbol{\varepsilon}}_{D,0} + \frac{\partial\psi}{\partial\beta}\dot{\beta} + \frac{\partial\psi}{\partial\nabla\beta}\cdot\nabla\dot{\beta}\right)d\boldsymbol{x}\\
&\quad -\langle\ell(t),\dot{\boldsymbol{u}}_{D,0}\rangle\\
&\quad +\int_\Omega\frac{\partial\psi}{\partial\boldsymbol{\varepsilon}}:\dot{\boldsymbol{\varepsilon}}_{D,\boldsymbol{w}}\,d\boldsymbol{x} - \langle\ell(t),\dot{\boldsymbol{u}}_{D,\boldsymbol{w}}\rangle - \langle\dot{\ell}(t),\boldsymbol{u}\rangle\,,\\
&= \int_\Omega\left(\frac{\partial\psi}{\partial\boldsymbol{\varepsilon}}:\dot{\boldsymbol{\varepsilon}}_{D,0} + \frac{\partial\psi}{\partial\beta}\dot{\beta} + \frac{\partial\psi}{\partial\nabla\beta}\cdot\nabla\dot{\beta}\right)d\boldsymbol{x}\\
&\quad -\langle\ell(t),\dot{\boldsymbol{u}}_{D,0}\rangle\\
&\quad +\frac{\partial}{\partial t}\mathcal{E}(t,q(t))\,,
\end{aligned} \tag{2.31}$$

where we have used (2.22) and let $\dot{\boldsymbol{\varepsilon}}=\nabla^{sym}(\dot{\boldsymbol{u}})$, $\dot{\boldsymbol{\varepsilon}}_{D,0}=\nabla^{sym}(\dot{\boldsymbol{u}}_{D,0})$ and $\dot{\boldsymbol{\varepsilon}}_{D,\boldsymbol{w}}=\nabla^{sym}(\dot{\boldsymbol{u}}_{D,\boldsymbol{w}})$.

By comparing now (2.31) and (2.30), and using (2.5) and (2.21), we find

$$\int_\Omega\left(\boldsymbol{\sigma}:\dot{\boldsymbol{\varepsilon}}_{D,0} + V^{nd}\dot{\beta} + \boldsymbol{H}\cdot\nabla\dot{\beta}\right)d\boldsymbol{x} - \langle\ell(t),\dot{\boldsymbol{u}}_{D,0}\rangle + \int_\Omega\phi(\dot{\beta};(\boldsymbol{\varepsilon},\beta))\,d\boldsymbol{x} = 0\,. \tag{2.32}$$

Since by (2.28) it is

$$\int_\Omega\boldsymbol{\sigma}:\dot{\boldsymbol{\varepsilon}}_{D,0}\,d\boldsymbol{x} - \langle\ell(t),\dot{\boldsymbol{u}}_{D,0}\rangle = 0\,, \tag{2.33}$$

given that $\boldsymbol{u}_{D,0} \in \mathcal{V}_{D,0}$, the application of Green theorem to the term $\int_\Omega \boldsymbol{H} \cdot \nabla\dot{\beta}\, d\boldsymbol{x}$ in (2.32) yields

$$\int_\Omega \left((V^{nd} - \text{div}\boldsymbol{H})\dot{\beta} + \phi(\dot{\beta}; (\boldsymbol{\varepsilon}, \beta))\right) d\boldsymbol{x} = 0\,. \tag{2.34}$$

Thus, by subtracting (2.34) to (2.29) and letting $V^d = \mathbf{div}\boldsymbol{H} - V^{nd}$, we finally have

$$\int_\Omega \phi(\gamma; (\boldsymbol{\varepsilon}, \beta))\, d\boldsymbol{x} \geq \int_\Omega \phi(\dot{\beta}; (\boldsymbol{\varepsilon}, \beta))\, d\boldsymbol{x} + \int_\Omega V^d(\gamma - \dot{\beta})\, d\boldsymbol{x} \quad \text{for all } \gamma \in \mathcal{B}\,, \tag{2.35}$$

which is the integral form of the evolution law

$$V^d \in \partial\phi(\dot{\beta}; (\boldsymbol{\varepsilon}, \beta))\,. \tag{2.36}$$

Remark 2.8. While we have obtained (2.35) as a consequence of the energetic formulation, condition (2.35) is in fact a constitutive assumption in the gradient damage models developed in Lorentz and Andrieux (1999, 2003), which are, therefore, in this respect, consistent with the present energetic formulation.

As for the inverse implication, given $q = q(t)$ solution of the differential model, while for general ψ we can still conclude that q verifies the energy balance condition (E), as will it be shown below, the stability condition (S) does not hold in general. A condition for this to occur is the convexity of ψ. However, this is not our case, given that ψ is not convex but it is separately convex. In such a case, the solution $q = q(t)$ of the differential model meets a weaker condition than (S) which is referred to as local stability condition (Mielke, 2005; Mielke and Roubíček, 2015; Pham and Marigo, 2010b) that reads as

$$\forall(\boldsymbol{v}, \gamma) \in \mathcal{V}_{D,0} \times \mathcal{B}, \quad \langle D_q\mathcal{E}(t, (\boldsymbol{\varepsilon}, \beta, \nabla\beta)), (\boldsymbol{v}, \gamma)\rangle + \mathcal{R}(\gamma; (\boldsymbol{\varepsilon}, \beta)) \geq 0 \tag{LS}$$

where $D_q\mathcal{E}$ denotes the Gateaux derivative of $\mathcal{E}$ defined by the linear form

$$\langle D_q\mathcal{E}, (\boldsymbol{v}, \gamma)\rangle = \int_\Omega \left[\boldsymbol{\sigma} : \boldsymbol{\varepsilon}(\boldsymbol{v}) + V^{nd}\gamma + \boldsymbol{H} \cdot \nabla\gamma\right] d\boldsymbol{x} - \langle \ell, \boldsymbol{v}\rangle \quad \text{for all}(\boldsymbol{v}, \gamma) \in \mathcal{V}_{D,0} \times \mathcal{B}\,, \tag{2.37}$$

with $\boldsymbol{\sigma} = \boldsymbol{\sigma}(\boldsymbol{\varepsilon}(\boldsymbol{u}))$ and $V^{nd} = V^{nd}(\boldsymbol{u}, \beta)$.

Remark 2.9. If we compare (2.27) with (2.37) and we recall the definition (2.21) of $\mathcal{R}$, we conclude that (2.27) is nothing other than condition (LS). As a result, condition (S) implies condition (LS). The inverse implication holds if, for instance, $\mathcal{E} = \mathcal{E}(t, \cdot)$ is convex. In such a case, it is

$$\forall\tilde{q} \in \mathcal{Q}, \quad \mathcal{E}(t, \tilde{q}) - \mathcal{E}(t, q) \geq \langle D_q\mathcal{E}(t, q), \tilde{q} - q\rangle\,, \tag{2.38}$$

and noting that $\forall\tilde{q} \in \mathcal{Q}$, $\tilde{q} - q \in \mathcal{V}_{D,0} \times \mathcal{B}$, (LS) gives

$$\forall\tilde{q} \in \mathcal{Q}, \quad \langle D_q\mathcal{E}(t, q), \tilde{q} - q\rangle + \mathcal{R}(\tilde{\beta} - \beta; q) \geq 0\,, \tag{2.39}$$

which together with (2.38) yields (S).

To derive the energy balance condition (E) from the differential model, let us start from the balance equations of linear momentum (2.1) tested by $\dot{\boldsymbol{u}}_{D,0}$ and the microforce balance Eq. (2.2) tested by $\dot{\beta}$. After integrating each of them over Ω and applying Green theorem, we obtain

$$\int_\Omega \boldsymbol{\sigma} : \dot{\boldsymbol{\varepsilon}}_{D,0}\, d\boldsymbol{x} - \langle \ell(t), \dot{\boldsymbol{u}}_{D,0}\rangle = 0 \tag{2.40}$$

$$\int_\Omega \boldsymbol{H} \cdot \nabla\dot{\beta}\, d\boldsymbol{x} + \int_\Omega V^{nd}\dot{\beta}\, dx + \int_\Omega V^d\dot{\beta}\, d\boldsymbol{x} = 0\,. \tag{2.41}$$

where we have accounted for $(2.4)_2$ in deriving (2.41). Now, by adding and subtracting the terms $\int_\Omega \boldsymbol{\sigma} : \dot{\boldsymbol{\varepsilon}}_{D,\boldsymbol{w}}\, d\boldsymbol{x}$ and $\langle \ell(t), \dot{\boldsymbol{u}}_{D,\boldsymbol{w}}\rangle$, (2.40) can also be written as

$$\int_\Omega \boldsymbol{\sigma} : \dot{\boldsymbol{\varepsilon}}\, d\boldsymbol{x} - \int_\Omega \boldsymbol{\sigma} : \dot{\boldsymbol{\varepsilon}}_{D,\boldsymbol{w}}\, d\boldsymbol{x} - \langle \ell(t), \dot{\boldsymbol{u}}\rangle + \langle \ell(t), \dot{\boldsymbol{u}}_{D,\boldsymbol{w}}\rangle = 0\,, \tag{2.42}$$

where $\dot{\boldsymbol{u}} = \dot{\boldsymbol{u}}_{D,0} + \dot{\boldsymbol{u}}_{D,\boldsymbol{w}}$ and $\dot{\boldsymbol{\varepsilon}} = \dot{\boldsymbol{\varepsilon}}_{D,0} + \dot{\boldsymbol{\varepsilon}}_{D,\boldsymbol{w}}$. By summing up (2.42) to (2.41) and after rearranging the terms, it is also

$$\int_\Omega \left(\boldsymbol{\sigma} : \dot{\boldsymbol{\varepsilon}} + V^{nd}\dot{\beta} + \boldsymbol{H} \cdot \nabla\dot{\beta}\right) d\boldsymbol{x} - \langle \ell(t), \dot{\boldsymbol{u}}\rangle - \int_\Omega \boldsymbol{\sigma} : \dot{\boldsymbol{\varepsilon}}_{D,\boldsymbol{w}}\, d\boldsymbol{x} + \langle \ell(t), \dot{\boldsymbol{u}}_{D,\boldsymbol{w}}\rangle + \int_\Omega V^d\dot{\beta}\, d\boldsymbol{x} = 0\,. \tag{2.43}$$

Given that

$$\int_\Omega \left(\boldsymbol{\sigma} : \dot{\boldsymbol{\varepsilon}} + V^{nd}\dot{\beta} + \boldsymbol{H} \cdot \nabla\dot{\beta}\right) d\boldsymbol{x} = \int_\Omega \frac{d\psi}{dt}\, d\boldsymbol{x}, \tag{2.44}$$

then (2.43) is also equal to

$$\int_\Omega \frac{d\psi}{dt}\, d\boldsymbol{x} - \langle \ell(t), \dot{\boldsymbol{u}}\rangle - \int_\Omega \boldsymbol{\sigma} : \dot{\boldsymbol{\varepsilon}}_{D,\boldsymbol{w}}\, d\boldsymbol{x} + \langle \ell(t), \dot{\boldsymbol{u}}_{D,\boldsymbol{w}}\rangle + \int_\Omega V^d\dot{\beta}\, d\boldsymbol{x} = 0\,, \tag{2.45}$$

which is convenient to express as

$$\frac{d\mathcal{E}}{dt} + \langle \dot{\ell}(t), \boldsymbol{u}\rangle - \int_\Omega \boldsymbol{\sigma} : \dot{\boldsymbol{\varepsilon}}_{D,\boldsymbol{w}}\, d\boldsymbol{x} + \langle \ell(t), \dot{\boldsymbol{u}}_{D,\boldsymbol{w}}\rangle + \int_\Omega V^d\dot{\beta}\, d\boldsymbol{x} = 0\,, \tag{2.46}$$

after comparing (2.45) with (2.31). By using now (2.22), and noting that $\partial\psi/\partial\boldsymbol{\varepsilon} = \boldsymbol{\sigma}$, we have that (2.46) can also be written as

$$\frac{d\mathcal{E}}{dt} - \frac{\partial\mathcal{E}}{\partial t} + \int_\Omega V^d\dot{\beta}\, d\boldsymbol{x} = 0\,. \tag{2.47}$$

Since $\phi(\cdot\,; (\boldsymbol{\varepsilon}, \beta))$ is convex and positively homogeneous of degree one, and

$$V^d \in \partial_{\dot{\beta}}\phi\left(\dot{\beta}; (\boldsymbol{\varepsilon}, \beta)\right), \tag{2.48}$$

the following representation holds

$$\phi\left(\dot{\beta}; (\boldsymbol{\varepsilon}, \beta)\right) = V^d\dot{\beta}\,, \tag{2.49}$$

which replaced into (2.47), integrating over $[0, t]$ and using (2.21) yields finally (E).

To derive now the stability condition (LS) from the differential model, let us observe that since

$$V^d \in \partial_{\dot{\beta}}\phi(\dot{\beta}; (\boldsymbol{\varepsilon}, \beta))\,, \tag{2.50}$$

then it is also

$$V^d \in \partial\phi(0; (\boldsymbol{\varepsilon}, \beta))\,, \tag{2.51}$$

and by the definition of subdifferential, we have

$$\forall\gamma \in \mathcal{B}, \quad \phi(\gamma; (\boldsymbol{\varepsilon}, \beta)) \geq \phi(0; (\boldsymbol{\varepsilon}, \beta)) + V^d\gamma\,, \tag{2.52}$$

which is the same as

$$\forall\gamma \in \mathcal{B}, \quad \phi(\gamma; (\boldsymbol{\varepsilon}, \beta)) \geq (div\ \boldsymbol{H} - V^{nd})\gamma\,, \tag{2.53}$$

where we have taken into account $(2.4)_2$ and used the fact that $\phi(0; (\boldsymbol{\varepsilon}, \beta)) = 0$. Integrating over Ω and applying Green theorem to the term $\int_\Omega \text{div}H\gamma\, d\boldsymbol{x}$, we find

$$\forall\gamma \in \mathcal{B}, \quad \int_\Omega \left(V^{nd}\gamma + \boldsymbol{H} \cdot \nabla\gamma\right) d\boldsymbol{x} + \int_\Omega \phi(\gamma; (\boldsymbol{\varepsilon}, \beta))\, d\boldsymbol{x} \geq 0\,, \tag{2.54}$$

which summed up to the weak form of the equilibrium equation yields

$$\forall(\boldsymbol{v}, \gamma) \in \mathcal{V}_{D,0} \times \mathcal{B}, \quad \int_\Omega \left[\boldsymbol{\sigma} : \boldsymbol{\varepsilon}(\boldsymbol{v}) + V^{nd}\gamma + \boldsymbol{H} \cdot \nabla\gamma\right] - \langle \ell, \gamma\rangle + \int_\Omega \phi(\gamma; (\boldsymbol{\varepsilon}, \beta))\, d\boldsymbol{x} \geq 0\,, \tag{2.55}$$

which is (LS) and concludes the proof.

For the continuous gradient damage model, Fig. 1 compares the relationship between the energetic formulation as developed in

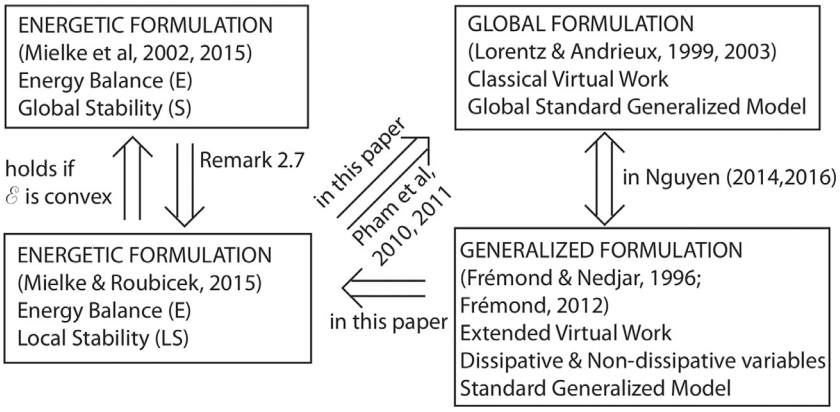

Fig. 1. Relationship between different continuous gradient damage model formulations. If $q \in \mathcal{Q}$ is solution of the energetic formulation (E)+(S), then q is also solution of (E)+(LS), and of the global formulation of Lorentz and Andrieux (1999, 2003). If $q \in \mathcal{Q}$ is solution of the generalized formulation of Frémond and Nedjar (1996) and Frémond (2002), then q is also solution of (E)+(LS). The equivalence between the global formulation and the generalized formulation is established in Nguyen (2014, 2016). The relationship between the formulation (E)+(LS) and the global formulation of Lorentz and Andrieux (1999, 2003) was also established in Pham and Marigo (2010b), and Pham et al. (2011).

Mielke et al. (2010) and in Section 2, the generalized formulation based on the extended virtual work as developed by Frémond and Nedjar (1996) and Frémond (2002) and recalled in Section 2, and the generalized formulation based on global expressions of the energy and dissipation potentials due to Lorentz and Andrieux (1999, 2003). As for the equivalence between the last two formulations, we refer to Nguyen (2014, 2016).

3. The fully discrete scheme

In this section we derive the fully discrete finite element approximations of the energetic formulation. These approximations are obtained by deriving a time incremental problem in the form of a global minimization of the sum of the total and dissipated energy over each time step, using a semi-implicit Euler method for the time discretization. Given the structure of the objective function, we apply then a variable splitting to obtain an equivalent constrained optimization problem which is then transformed into a saddle-point problem of an augmented Lagrangian function. We finally use the finite element method for the spatial discretization.

3.1. The time-incremental two-field minimization problem

Given the time interval $[0,T]$, let $\mathcal{P} = \{0 = t_0, \ldots, t_N = T\}$ where $0 = t_0 < t_1 < \ldots < t_N = T$ and consider a partition of $[0,T]$ into the subintervals $[t_n, t_{n+1}]$ for $n = 0, \ldots, N-1$, with the time instants t_n not necessarily equidistant. Denote by $q_n^{\mathcal{P}} = (u_n^{\mathcal{P}}, \boldsymbol{\varepsilon}_n^{\mathcal{P}}, \beta_n^{\mathcal{P}}, \nabla\beta_n^{\mathcal{P}})$ an approximation of $q = q(t)$ at t_n corresponding to the partition $\mathcal{P}$ and by $q^{\mathcal{P}}(t)$ the piecewise constant interpolant defined as $q^{\mathcal{P}}(t) = q_{n-1}^{\mathcal{P}}$ for $t \in [t_{n-1}, t_n[$, $n = 1, \ldots, N$ and $q^{\mathcal{P}}(T) = q_N^{\mathcal{P}}$. When we refer to a fixed partition, the superscript $\mathcal{P}$ will be omitted. We consider then the following time incremental minimization problems.

Let $\mathcal{P} = \{0 = t_0, \ldots, t_N = T\}$, $N \in \mathbb{N}$
For $n = 0, \ldots, N-1$
Given External loading: $\ell(t_{n+1})$ Neumann b.c.
$\boldsymbol{w}(x, t_{n+1})$ on $\partial\Omega_D$ Dirichlet b.c.
State of the system at t_n : $q_n = (\boldsymbol{u}_n, \beta_n) \in \mathcal{V}_D \times \mathcal{B}$
Find $q_{n+1} = (\boldsymbol{u}_{n+1}, \beta_{n+1}) \in \mathcal{Q} = \mathcal{V}_D \times \mathcal{B}$ such that minimize over $\mathcal{Q}$ the function

$$\mathcal{F}(\tilde{q}) = \mathcal{E}(t_{n+1}, \tilde{q}) + \mathcal{R}(\tilde{\beta} - \beta_n; q_n) \tag{3.1}$$

subject to

$$\begin{aligned} &0 \le \beta_{n+1} \le 1, \\ &\beta_n \le \beta_{n+1}\,. \end{aligned} \tag{3.2}$$

In (3.1) we let

$$\begin{aligned} \mathcal{E}(t_{n+1}, \tilde{q}) &= \int_\Omega \psi(\tilde{\boldsymbol{\varepsilon}}, \tilde{\beta}, \nabla\tilde{\beta})\, d\boldsymbol{x} - \langle \ell(t_{n+1}), \tilde{\boldsymbol{u}} \rangle \\ \mathcal{R}(\tilde{\beta} - \beta_n; q_n) &= \int_\Omega \phi\big(\tilde{\beta} - \beta_n;\ (\boldsymbol{\varepsilon}_n, \beta_n)\big)\, d\boldsymbol{x}\,, \end{aligned} \tag{3.3}$$

with $\tilde{\boldsymbol{u}} = \tilde{\boldsymbol{u}}_{D,0} + \boldsymbol{u}_{D,\boldsymbol{w}}$ and $\tilde{\boldsymbol{\varepsilon}} = \tilde{\boldsymbol{\varepsilon}}_{D,0} + \boldsymbol{\varepsilon}_{D,\boldsymbol{w}}$, whereas for $n = 0$ the initial data q_0 is given by $\beta(\boldsymbol{x}, 0)$ and $\boldsymbol{u}(\boldsymbol{x}, 0)$ (see Remark 2.7).

Remark 3.1.

(a) The side conditions on the variable β correspond to the constitutive assumptions on β and $\dot{\beta}$, which were enforced by introducing the indicator functions $I_{[0,1]}(\beta)$ and $I_{\mathbb{R}^+}(\dot{\beta})$ in the definition of the free energy ψ (2.8) and of the dissipation pseudo-potential ϕ (2.9), respectively. It follows that by taking into account now explicitly such conditions in (3.1), the expressions of ψ and ϕ that enter the definitions (3.3) of $\mathcal{E}$ and $\mathcal{R}$, respectively, are thus given as follows

$$\begin{aligned} \psi(\boldsymbol{\varepsilon}_{n+1}, \beta_{n+1}, \nabla\beta_{n+1}) &= \frac{1}{2} R(\beta_{n+1}) \mathbb{E}\boldsymbol{\varepsilon}_{n+1} : \boldsymbol{\varepsilon}_{n+1} + \frac{c}{2} |\nabla\beta_{n+1}|^2 \\ \phi(\beta_{n+1} - \beta_n;\ (\boldsymbol{\varepsilon}_n, \beta_n)) &= \Big(k + V^*(\boldsymbol{\varepsilon}_n, \beta_n) - V^{nd}(\boldsymbol{\varepsilon}_n, \beta_n)\Big) \\ &\qquad (\beta_{n+1} - \beta_n)\,, \end{aligned} \tag{3.4}$$

with V^* and V^{nd} defined by (2.16) and $(2.10)_2$, respectively.

(b) The time discrete problem expresses the minimization of the sum of the total energy at the current time t_{n+1} and the dissipated energy in the given time step, with the size of the time step that does not appear. This is a characteristic of rate-independent systems which is inherited from ϕ being

positively homogeneous of degree one and can be seen as follows. Over each time step $[t_n, t_{n+1}]$, we can take

$$\int_{t_n}^{t_{n+1}} \phi\big(\dot\beta(\boldsymbol{x},\tau);\ (\boldsymbol{\varepsilon},\beta)\big)\,d\tau \approx \phi\big(\dot\beta(\boldsymbol{x},\xi_n);\ (\boldsymbol{\varepsilon}(\boldsymbol{x},\xi_n),\beta(\boldsymbol{x},\xi_n))\big)\Delta t_n$$

with $\xi_n \in [t_n, t_{n+1}]$ and $\Delta t_n = t_{n+1} - t_n$. Here, using the fact that ϕ is positively homogeneous of degree one and the Lagrange mean value theorem, we conclude that

$$\int_{t_n}^{t_{n+1}} \phi\big(\dot\beta;\ (\boldsymbol{\varepsilon},\beta)\big)\,d\tau \approx \phi\big(\beta_{n+1}(\boldsymbol{x})-\beta_n(\boldsymbol{x});\ (\boldsymbol{\varepsilon}_n(\boldsymbol{x}),\beta_n(\boldsymbol{x}))\big)$$

The evolutionary character of (3.1) derives from the constraint $\beta_n \le \beta_{n+1}$ and, in our case of state-dependent dissipation pseudo-potential, by the occurrence of $(\boldsymbol{\varepsilon}_n, \beta_n)$ in the expression of ϕ.

(*c*) Solutions of (3.1) takes on the form $\boldsymbol{u}_{n+1}(\boldsymbol{x}) = \boldsymbol{u}_{n+1,D,0}(\boldsymbol{x}) + \boldsymbol{u}_{D,\boldsymbol{w}}(\boldsymbol{x}, t_{n+1})$ with $\boldsymbol{u}_{D,\boldsymbol{w}}(\boldsymbol{x},t)$ known function (see Section 2.1).

In the case of dissipation pseudo-potential independent on the state of the system, that is, for $\mathcal{R}(\dot\beta; q) = \mathcal{R}(\dot\beta)$, the theoretical justification of (3.1) as time discrete scheme of the energetic formulation (E) and (S) relies on two results. The first is that the solutions of (3.1) satisfy the following properties

$$\mathcal{E}(t_{n+1}, q_{n+1}) \le \mathcal{E}(t_{n+1}, \tilde q) + \mathcal{R}(\tilde\beta - \beta_{n+1}) \quad \text{for all } \tilde q \in \mathcal{Q}\,, \tag{3.5}$$

$$\int_{t_n}^{t_{n+1}} \frac{\partial}{\partial\tau}\mathcal{E}(\tau, q_{n+1})\,d\tau \le \mathcal{E}(t_{n+1}, q_{n+1}) - \mathcal{E}(t_n, q_n) + \mathcal{R}(\beta_{n+1}-\beta_n) \le \int_{t_n}^{t_{n+1}} \frac{\partial}{\partial\tau}\mathcal{E}(\tau, q_n)\,d\tau \tag{3.6}$$

which are, somehow, closely related to (S) and (E), respectively. The second mostly important result is the validity of *a-priori* estimates of the energy and dissipation potential (Mielke et al., 2008). Using such estimates and structural properties of the functionals, such as the lower-semicontinuity of $\mathcal{E}$ and $\mathcal{R}$, Mielke et al. (2008) and Mielke and Roubíček (2015) prove by Γ-convergence the existence of an energetic solution.

In our case, where ϕ depends also on the state of the system, if $q_{n+1} = (\boldsymbol{u}_{n+1}, \beta_{n+1})$ denotes a solution of (3.1), we are able to verify the following results:

(*i*) A stability condition met by q_{n+1} that reads as follows

$$\boxed{\mathcal{E}(t_{n+1}, q_{n+1}) \le \mathcal{E}(t_{n+1}, \tilde q) + \mathcal{R}(\tilde\beta - \beta_{n+1};\ q_n) \quad \text{for all } \tilde q \in \mathcal{Q}}\,. \tag{3.7}$$

(*ii*) The upper bound to $\mathcal{E}(t_{n+1}, q_{n+1}) - \mathcal{E}(t_n, q_n) + \mathcal{R}(\beta_{n+1}-\beta_n)$ given by

$$\boxed{\mathcal{E}(t_{n+1}, q_{n+1}) - \mathcal{E}(t_n, q_n) + \mathcal{R}(\beta_{n+1}-\beta_n; q_n) \le \int_{t_n}^{t_{n+1}} \frac{\partial}{\partial\tau}\mathcal{E}(\tau, q_n)\,d\tau,} \tag{3.8}$$

which is the same as the one that occurs in (3.6) for state-independent dissipation pseudo-potential.

(*iii*) The lower bound to $\mathcal{E}(t_{n+1}, q_{n+1}) - \mathcal{E}(t_n, q_n) + \mathcal{R}(\beta_{n+1}-\beta_n)$ given by

$$\boxed{\mathcal{E}(t_{n+1}, q_{n+1}) - \mathcal{E}(t_n, q_n) + \mathcal{R}(\beta_{n+1}-\beta_n; q_n) \ge \int_{t_n}^{t_{n+1}} \frac{\partial}{\partial\tau}\mathcal{E}(\tau, q_{n+1})\,d\tau + \mathcal{R}(\beta_{n+1}-\beta_n; q_n) - \mathcal{R}(\beta_{n+1}-\beta_n; q_{n-1})} \tag{3.9}$$

which would recover the left side inequality in (3.6) if $\mathcal{R}$ does not depend on the state of the system.

Furthermore, the same a-priori estimates as in Mielke et al. (2008), Eqs. (3.10) and (3.11) and given by

$$\mathcal{E}(t, q^{\mathcal{P}}(t)) + c_0 \le c_2 \exp(c_1 t) \quad \text{for any } t \in [0, T],$$
$$\sum_{n=1}^{N-1} \mathcal{R}(\beta_{n+1}-\beta_n; q_n) \le c_2 \exp(c_1 T)\,, \tag{3.10}$$

with $c_0, c_1, c_2 > 0$, are still valid.

The proofs of the previous results adapt fundamentally the arguments of Mielke and Roubíček (2015), page 52 and Mielke et al. (2008), where we need to take into account that according to Remark 3.1(*b*), if the constraints (3.3) are violated, then the function (3.1) takes on infinity value.

For any admissible $\tilde q = (\tilde{\boldsymbol{u}}, \tilde\beta) \in \mathcal{Q} = \mathcal{V}_D \times \mathcal{B}$, we have

$$\begin{aligned}\mathcal{E}(t_{n+1}, \tilde q) + \mathcal{R}(\tilde\beta - \beta_{n+1}; q_n) = \mathcal{E}(t_{n+1}, \tilde q) &+ \mathcal{R}(\tilde\beta - \beta_n; q_n)\\ &+\mathcal{R}(\tilde\beta - \beta_{n+1}; q_n)\\ &-\mathcal{R}(\tilde\beta - \beta_n; q_n)\,.\end{aligned} \tag{3.11}$$

Using that q_{n+1} solves (3.1), we obtain

$$\begin{aligned}\mathcal{E}(t_{n+1}, \tilde q) + \mathcal{R}(\tilde\beta - \beta_{n+1}; q_n) \ge \mathcal{E}(t_{n+1}, q_{n+1}) &+ \mathcal{R}(\beta_{n+1} - \beta_n; q_n)\\ &+\mathcal{R}(\tilde\beta - \beta_{n+1}; q_n) - \mathcal{R}(\tilde\beta - \beta_n; q_n)\,.\end{aligned} \tag{3.12}$$

Since from the definition of $\mathcal{R}(\dot\beta; q_n)$, there holds

$$\mathcal{R}(\beta_{n+1}-\beta_n; q_n) + \mathcal{R}(\beta-\beta_{n+1}; q_n) - \mathcal{R}(\beta-\beta_n; q_n) \ge 0 \tag{3.13}$$

which is the triangle inequality with respect to the first variable, by comparing (3.13) with (3.12) we conclude (3.7).

For the proof of (3.8), we first observe that for all admissible $\tilde q = (\tilde{\boldsymbol{u}}, \tilde\beta) \in \mathcal{Q} = \mathcal{V}_D \times \mathcal{B}$, there holds

$$\begin{aligned}&\mathcal{E}(t_{n+1}, q_{n+1}) - \mathcal{E}(t_n, q_n) + \mathcal{R}(\beta_{n+1}-\beta_n; q_n)\\ &\le \mathcal{E}(t_{n+1}, \tilde q) + \mathcal{R}(\tilde\beta - \beta_n; q_n) - \mathcal{E}(t_n, q_n)\,,\end{aligned} \tag{3.14}$$

which is obtained from the definition of q_{n+1} as solution of (3.1). By specializing (3.14) for $\tilde q = q_n = (\boldsymbol{u}_n, \beta_n)$ we then find (3.8).

For the proof of (3.9), we start from

$$\begin{aligned}&\mathcal{E}(t_{n+1}, q_{n+1}) - \mathcal{E}(t_n, q_n) + \mathcal{R}(\beta_{n+1}-\beta_n;\ q_n)\\ &= \mathcal{E}(t_{n+1}, q_{n+1}) - \mathcal{E}(t_n, q_{n+1}) + \mathcal{E}(t_n, q_{n+1}) - \mathcal{E}(t_n, q_n)\\ &+\mathcal{R}(\beta_{n+1}-\beta_n;\ q_{n-1}) + \mathcal{R}(\beta_{n+1}-\beta_n;\ q_n) - \mathcal{R}(\beta_{n+1}-\beta_n;\ q_{n-1})\,,\end{aligned} \tag{3.15}$$

and use the stability (3.7) of q_n with $\tilde q = q_{n+1}$ so that

$$\mathcal{E}(t_n, q_{n+1}) - \mathcal{E}(t_n, q_n) + \mathcal{R}(\beta_{n+1}-\beta_n;\ q_{n-1}) \ge 0\,, \tag{3.16}$$

which replaced into (3.15) yields (3.9).

For the proof of (3.10) and the existence of an energetic solution, we refer to the arguments detailed in Francfort and Mielke (2006), Mielke and Roubíček (2015), and Mielke et al. (2008).

Remark 3.2. (a) The consistency of the time incremental minimization problem (3.1) with the differential model of Box 1 can be also inferred directly by finding the first order optimality conditions of (3.1) given by

$$-div\left(\frac{\partial\psi}{\partial\boldsymbol{\varepsilon}}\right)-\boldsymbol{f}(t_{n+1})=0 \tag{3.17a}$$

$$-\frac{\partial\psi}{\partial\beta}+div\left(\frac{\partial\psi}{\partial\nabla\beta}\right)\in\partial_{\beta}\phi(\beta-\beta_n;\,q_n)\,, \tag{3.17b}$$

along with the Neumann-type boundary conditions (2.1) and (2.2). Such conditions represent indeed a time discrete model of the differential model. Eq. (3.17a) is Eq. (2.1) along with Eq. $(2.5)_1$, evaluated at the current time t_{n+1} whereas Eq. (3.17b) is a time discrete model of the evolution law

$$-\frac{\partial\psi}{\partial\beta}+div\left(\frac{\partial\psi}{\partial\nabla\beta}\right)\in\partial_{\dot\beta}\phi(\dot\beta;(\boldsymbol{\varepsilon},\beta)) \tag{3.18}$$

which is derived from the microfield balance Eq. (2.2) and the constitutive Eqs. $(2.5)_{2,\,3}$ and $(2.11)_2$. This is, for instance, the point of view adopted in Miehe (2011).

(b) Under suitable conditions, the a-priori estimate (3.10) along with the bounds (3.8) and (3.9) guarantee that energetic solutions $q(t)$ can be obtained as limit of subsequences of the interpolants $q^{\mathcal{P}}(t)$. We can, therefore, conclude that $q(t)$ will meet the integral form of the evolution law (2.35) as a result of the relationships between the energetic formulation and the gradient constitutive equations displayed in Fig. 1.

(c) Condition (3.7) represents the discrete counterpart of the stability condition (S), which thus ensures the stability of the discrete energetic solution.

(d) In gradient damage models, crack nucleation is defined in Pham et al. (2011), Pham and Marigo (2013), Alessi et al. (2014), and Tamé et al. (2018) for uniaxial traction tests as the localization of the damage within a strip with the damage that grows not uniformly in space in such region until it reaches its ultimate value ($\beta=1$) at some point of the strip. To assess therefore the capability of the formulation to describe crack nucleation, one should verify whether the formulation itself is able to pick up such type of damage profiles. As an application of the stability analysis described in Pham et al. (2011) and Pham and Marigo (2013) for a uniaxial traction test, Luege (2017) analyses the stability of the homogeneous solutions of the optimality conditions of Problem (3.1) for the softening law $E(\beta)=R(\beta)E_0$. In this $1d$ case, we have $V^*=V^{nd}$ (see Remark 2.5(a)), thus $\phi=k\beta$. Homogeneous solutions are those characterized by uniform strain and damage along the bar. Consistent with the findings of Pham et al. (2011), if the bar length L satisfies the inequality (Luege, 2017, Eq. (4.18))

$$\frac{L^2}{D^2}\leq\frac{4\pi^2k(S')^4}{(S'')^3U^2}\,, \tag{3.19}$$

where U is the applied end-free displacement, $S'=dS/d\beta$ and $S''=d^2S/d\beta^2$ with $S=1/E(\beta)$, the homogeneous solutions are stable, for otherwise are unstable. Since for (3.7) the discrete energetic solutions are stable solutions, for being global minima, it follows that when (3.19) is not met, the discrete energetic solutions cannot be homogeneous solutions. Nevertheless, stable solutions of the optimality conditions, which have localization of the damage profile, can be constructed as shown in Pham et al. (2011), Pham and Marigo (2013), and Tamé et al. (2018). These can, therefore, be possible candidates for energetic solutions, which we have not checked and leave for future work.

3.2. Variable splitting and augmented lagrangian formulation

An approach for deriving the finite element equations of the model of Box 1 consists in obtaining first some weak form of the first order optimality conditions (3.17) of the minimization problem (3.1) and then making some assumptions on the shape of the test and trial functions (Miehe, 2011; Miehe et al., 2013). As opposite, an optimization method can be directly applied to the search of the minima (3.1), such as the alternating minimization method suggested in Bourdin et al. (2000, 2008), Mielke and Roubíček (2015), and Mielke et al. (2010) which is a staggered scheme where (3.1) is solved separately and sequentially with respect to each variable, the displacement and the damage field. As shown in Vignollet et al. (2014), the staggered scheme can be very sensitive to the size of the load increments and is not able to capture the snap-back behavior (May, 2016, page 30). As a result, we will opt for solving the full coupled system with a monolithic scheme based on Newton's method. The occurrence of the term $div\left(\frac{\partial\psi}{\partial\nabla\beta}\right)$ in the evolution law (3.17b) makes, on the other hand, cumbersome its numerical treatment. We would need to derive a weak integral formulation of (3.17b) and consequently we would loose one of the appealing features of the finite element method which is the decoupling between the pointwise solution of the constitutive equations (which is in practice carry out only at the Gauss points of each finite element according to the type of element) and the variational problem expressing the global equilibrium equation. Nevertheless, following the method of decomposition-coordination described in Fortin and Glowinski (1983) and applied for instance in Lorentz and Benallal (2005) and Lorentz and Godard (2011), it is possible to retain the above features also for non-local models. The rationale behind such method is, in fact, to transform an eventual weak integral formulation of (3.17b) into a variational equation and local differential inclusions such as the one that occur in a local rate-independent constitutive model (Mielke and Roubíček, 2015; Peric and Owen, 2008). This can be achieved by a variable splitting procedure by which we separate and rename the variable that confers the non-local character to the evolution law and then introduce a linking constraint. For the functional (3.1), since the term $div\left(\frac{\partial\psi}{\partial\nabla\beta}\right)$ comes from $\int_\Omega\frac{c}{2}|\nabla\beta|^2\,d\boldsymbol{x}$, the idea is to treat the variable β, which appears therein, as a new independent variable α and then to enforce the equality $\alpha-\beta=0$.

Hereafter, to be more specific, let us denote by $H^1(\Omega;\mathbb{R}^n)$ and $L^2(\Omega;\mathbb{R})$ the standard Sobolev spaces. We assume then $\mathcal{V}_D=H^1_D(\Omega;\mathbb{R}^n)$ and $\mathcal{B}=L^2(\Omega;\mathbb{R})$ where $H^1_D(\Omega;\mathbb{R}^n)$ is the lifting of the space $H^1_{D,0}(\Omega;\mathbb{R}^n)$ by $\boldsymbol{u}_{D,\boldsymbol{w}}\in H^1(\Omega;\mathbb{R}^n)$, with $H^1_{D,0}(\Omega;\mathbb{R}^n)$ subspace of $H^1(\Omega;\mathbb{R}^n)$ of functions with vanishing trace on $\partial\Omega_D$ (see Quarteroni, 2017 and Section 2.1).

Problem (3.1) is thus transformed into the following variational problem with $\boldsymbol{u}$, α and λ as main variables, $\boldsymbol{\sigma}$ and β as secondary variables, and r a given penalty parameter associated with the weak enforcement of the condition $\alpha-\beta=0$,

$$\begin{aligned}&\text{Let } r\geq 0.\,Find(\boldsymbol{u}_{n+1},\alpha_{n+1},\lambda_{n+1})\in(\boldsymbol{u}_{D,\boldsymbol{w}}+H^1_{D,0})\times L^2\times L^2\\&\int_\Omega\boldsymbol{\sigma}(\boldsymbol{\varepsilon}(\boldsymbol{u}),\beta):\boldsymbol{\varepsilon}(\boldsymbol{v})\,d\boldsymbol{x}=\langle\ell(t_{n+1}),\boldsymbol{v}\rangle+\int_{\partial\Omega_N}\boldsymbol{t}\cdot\boldsymbol{v}\,ds\\&\text{for all }\boldsymbol{v}\in H^1_{D,0}\end{aligned} \tag{3.20a}$$

$$\begin{aligned}&\int_\Omega c\nabla\alpha\cdot\nabla\gamma\,d\boldsymbol{x}+r\int_\Omega(\beta-\alpha)\gamma\,d\boldsymbol{x}+\int_\Omega\lambda\gamma\,dx=0\\&\text{for all }\gamma\in L^2\end{aligned} \tag{3.20b}$$

$$\int_\Omega(\beta-\alpha)q\,d\boldsymbol{x}=0\quad\text{for all } q\in L^2\,, \tag{3.20c}$$

where β is obtained by solving at any point $\boldsymbol{x}\in\Omega$ the following inequality

$$\begin{aligned}&\text{Given } (\boldsymbol{\varepsilon}_n,\ \beta_n) \text{ and } (\boldsymbol{\varepsilon},\ \alpha,\ \lambda)\\&\text{Find } \beta\geq\beta_n \text{ such that}\\&0\leq\beta\leq 1\,,\\&\quad\Big(-V^{nd}(\boldsymbol{\varepsilon},\beta)+V^{nd}(\boldsymbol{\varepsilon}_n,\beta_n)-V^{*}(\boldsymbol{\varepsilon}_n,\beta_n)\\&\qquad -k+\lambda+r\big(\beta-\alpha\big)\Big)(\gamma-\beta)\leq 0\\&\qquad\qquad\qquad\qquad\text{for all } 0\leq\beta_n\leq\gamma\leq 1\,.\end{aligned}\tag{3.21}$$

This is then used to define the mappings that enter (3.20), that is,

$$(\boldsymbol{\varepsilon}(\boldsymbol{x}),\alpha(\boldsymbol{x}),\lambda(\boldsymbol{x}))\to\beta(\boldsymbol{\varepsilon}(\boldsymbol{x}),\alpha(\boldsymbol{x}),\lambda(\boldsymbol{x})) \text{ solution of (3.21)},\tag{3.22}$$

and

$$\boldsymbol{\sigma}(\boldsymbol{\varepsilon}(\boldsymbol{x}),\alpha(\boldsymbol{x}),\lambda(\boldsymbol{x}))=R(\beta(\boldsymbol{x}))\mathbb{E}\boldsymbol{\varepsilon}(\boldsymbol{x})\,.\tag{3.23}$$

The dependence of $\boldsymbol{\sigma}$ also on α and λ is through β which appears as argument of the softening function $R(\beta)$.

Remark 3.3.

(*a*) Inequality (3.21) represents the differential inclusion that defines the evolution law in the optimality conditions of the augmented Lagrangian functional

$$\begin{aligned}\mathcal{L}_r(\boldsymbol{u},\beta,\alpha,\lambda)=&\frac{1}{2}\int_\Omega R(\beta)\mathbb{E}\boldsymbol{\varepsilon}:\boldsymbol{\varepsilon}\,d\boldsymbol{x}-\langle\ell(t_{n+1}),\boldsymbol{u}\rangle\\&+\frac{1}{2}\int_\Omega|\nabla\alpha|^2\,d\boldsymbol{x}+\mathcal{R}(\beta-\beta_n;q_n)\\&+\int_\Omega\lambda(\alpha-\beta)\,d\boldsymbol{x}+\frac{r}{2}\int_\Omega|\alpha-\beta|^2\,d\boldsymbol{x}\end{aligned}\tag{3.24}$$

associated with Problem (3.1).

(*b*) The terms $V^{nd}(\boldsymbol{\varepsilon}_n,\ \beta_n)$ and $V^{*}(\boldsymbol{\varepsilon}_n,\ \beta_n)$ that appear in (3.21) result from the type of dissipation pseudo-potential ϕ (2.9) which we are using and from the type of time-discrete scheme applied to (3.18) which is transformed, by the decomposition-coordination technique into the differential equation

$$-\frac{\partial\psi}{\partial\beta}+r(\beta-\alpha)+\lambda-\partial_\beta\phi(\beta-\beta_n;\,q_n)\ni 0\,.$$

Thus, their effect is to define a system state-dependent damage threshold. As opposite, if ϕ were simply given by $k\dot\beta+I_{\mathbb{R}^+}(\dot\beta)$, then inequality (3.21) would have read

$$\begin{aligned}&0\leq\beta\leq 1\,,\\&\Big(-V^{nd}(\boldsymbol{\varepsilon},\beta)-k+\lambda+r\big(\beta-\alpha\big)\Big)(\gamma-\beta)\leq 0\\&\text{for all } 0\leq\beta_n\leq\gamma\leq 1\,,\end{aligned}\tag{3.25}$$

which is, for instance, the model proposed in Lorentz and Godard (2011), Eq. (18). For the solution of (3.21) we can therefore apply the same algorithm therein given. The difference from the present case would be that the damage threshold is not simply k, but it is given by $k-V^{nd}(\boldsymbol{\varepsilon}_n,\beta_n)+V^{*}(\boldsymbol{\varepsilon}_n,\beta_n)$.

3.3. Finite element discretization

For the variational formulation of the one-single time step (3.20), the fully discrete equations are obtained by replacing the infinite dimensional affine spaces of the trial functions $(\boldsymbol{u},\alpha,\lambda)\in(\boldsymbol{u}_{D,\boldsymbol{w}}+H^1_{D,0})\times L^2\times L^2$ and of the test functions $(\boldsymbol{v},\gamma,q)\in H^1_{D,0}\times L^2\times L^2$ with finite dimensional affine subspaces which are taken here as finite element spaces. Given however the underlying saddle-point structure of (3.20), it is well known that such finite element spaces must meet compatibility conditions in order to avoid locking phenomena and/or the occurrence of spurious modes. In the abstract framework of linear problems, such conditions are the coercivity of the bilinear form dependent on the primary variables, and the inf-sup condition of the biliner form associated with the linear constraint and dependent on the primary and dual variables. However, while in the case of linear problems the coercivity of the augmented lagrangian formulation is guaranteed for a certain range of values of $r>0$ (Boffi et al., 2013), the only concern for the finite element approximation of such formulation is to check the inf-sup condition so to ensure a stable and convergent method. For the analysis of such condition in general, we refer to the specific literature (Fortin and Glowinski, 1983; Boffi and Lovadina, 1997; Boffi et al., 2013).

Let $\mathcal{T}$ be a triangulation of Ω made of simplices. In this paper we will consider continuous piecewise polynomials of degree two for the approximation of the displacement field $\boldsymbol{u}$ and continuous piecewise affine functions for the approximation of the damage field α and of the Lagrange multiplier field λ.

Let us denote by $\boldsymbol{N_u}$, $\boldsymbol{N}_\alpha$ and $\boldsymbol{N}_\lambda$ the shape interpolation functions of $\boldsymbol{u}$, α and λ, respectively; by $\boldsymbol{U}$, $\boldsymbol{U}_D\in\mathbb{R}^{n_{\boldsymbol{u}}}$ the displacement degree of freedom of the test functions $\boldsymbol{u}_{D,0}\in H^1_{D,0}$ and of the lifting function $\boldsymbol{u}_{D,\boldsymbol{w}}\in H^1_D$, respectively, and by $\boldsymbol{A}\in\mathbb{R}^{n_\alpha}$ and $\boldsymbol{L}\in\mathbb{R}^{n_\lambda}$ the degree of freedom of the fields α and λ, respectively. We have then

$$\begin{aligned}\boldsymbol{u}^h(\boldsymbol{x})&=\boldsymbol{u}^h_{D,0}(\boldsymbol{x})+\boldsymbol{u}^h_{D,\boldsymbol{w}}(\boldsymbol{x})\\&=\boldsymbol{N_u}(\boldsymbol{x})(\boldsymbol{U}+\boldsymbol{U}_D),\quad\alpha^h(\boldsymbol{x})=\boldsymbol{N}_\alpha(\boldsymbol{x})\boldsymbol{A},\quad\lambda^h(\boldsymbol{x})=\boldsymbol{N}_\lambda(\boldsymbol{x})\boldsymbol{L}\,,\end{aligned}\tag{3.26}$$

and, consequently,

$$\begin{aligned}\boldsymbol{\varepsilon}^h(\boldsymbol{x})&=\frac{1}{2}\big(\nabla\boldsymbol{u}^h+(\nabla\boldsymbol{u}^h)^T\big)\\&=\boldsymbol{B_u}(\boldsymbol{x})(\boldsymbol{U}+\boldsymbol{U}_D)\qquad\text{and}\qquad\nabla\alpha^h(\boldsymbol{x})=\boldsymbol{B}_\alpha(\boldsymbol{x})\boldsymbol{A}\,,\end{aligned}\tag{3.27}$$

where we have introduced the matrices $\boldsymbol{B_u}$ and $\boldsymbol{B}_\alpha$ which are obtained by appropriately differentiating and combining rows of the matrices $\boldsymbol{N_u}$ and $\boldsymbol{N}_\alpha$, respectively (Bathe, 1996). By using then (3.26) and (3.27) into (3.20), we obtain the following discrete variational formulation

$$\delta\boldsymbol{U}^T\int_\Omega\boldsymbol{B}^T_{\boldsymbol{u}}(\boldsymbol{x})\,{}^h\boldsymbol{\sigma}\big(\boldsymbol{\varepsilon}^h(\boldsymbol{x}),{}^h\beta(\boldsymbol{x})\big)\,d\boldsymbol{x}-\delta\boldsymbol{U}^T\int_\Omega\boldsymbol{N}^T_{\boldsymbol{u}}(\boldsymbol{x})\,\boldsymbol{f}(\boldsymbol{x},t_{n+1})\,d\boldsymbol{x}-\delta\boldsymbol{U}^T\int_{\partial\Omega_N}\boldsymbol{N}^T_{\boldsymbol{u}}(s)\,\boldsymbol{t}(s,t_{n+1})\,ds=0\tag{3.28a}$$

$$\delta\boldsymbol{A}^T\int_\Omega c\boldsymbol{B}^T_\alpha(\boldsymbol{x})\boldsymbol{B}_\alpha(\boldsymbol{x})\boldsymbol{A}\,d\boldsymbol{x}+\delta\boldsymbol{A}^T\int_\Omega r\boldsymbol{N}^T_\alpha(\boldsymbol{x})\Big(\boldsymbol{N}_\alpha(\boldsymbol{x})\boldsymbol{A}-{}^h\beta(\boldsymbol{x})\Big)\,d\boldsymbol{x}+\delta\boldsymbol{A}^T\int_\Omega\boldsymbol{N}^T_\alpha(\boldsymbol{x})\boldsymbol{N}_\lambda(\boldsymbol{x})\boldsymbol{L}\,d\boldsymbol{x}=0\tag{3.28b}$$

$$\delta\boldsymbol{L}^T\int_\Omega\boldsymbol{N}^T_\lambda(\boldsymbol{x})\Big(\boldsymbol{N}_\alpha(\boldsymbol{x})\boldsymbol{A}-{}^h\beta(\boldsymbol{x})\Big)\,d\boldsymbol{x}=0\tag{3.28c}$$

where ${}^h\boldsymbol{\sigma}$ and ${}^h\beta$ are the secondary variables defined, respectively, by (3.23) and (3.22) with $\boldsymbol{\varepsilon}^h=\boldsymbol{B_u}(\boldsymbol{U}+\boldsymbol{U}_D)$. Without loss of generality and for simplifying notation, in the following we drop the work of the traction forces $\boldsymbol{t}$ in (3.28a) and we do not show explicitly the dependence on $\boldsymbol{U}_D$.

Remark 3.4. The symbol ${}^h(\cdot)$ is here used to mean that, in the present formulation, the field $(\cdot)$ is not interpolated but it is computed by solving an equation.

In the actual computation, the integrals that appear in (3.28) are seldom computed exactly. Instead, they are approximated through a process of numerical integration such as Gaussian quadrature formula. If we denote by Ω_e^h a generic element of the triangulation $\mathcal{T}^h$ and by $\boldsymbol{x}_{e,\,i}$ the ith Gauss point of the element Ω_e^h and ngp their number, the discrete variational formulation (3.28) is thus transformed into the following system of nonlinear algebraic equations

$$\boldsymbol{R}_{\boldsymbol{u}}(\boldsymbol{U},\boldsymbol{A},\boldsymbol{L}) := \sum_{\Omega_e^h\in\mathcal{T}^h}\sum_{i=1}^{ngp} w_{e,i}j_{e,i}\Big[\boldsymbol{B}_{\boldsymbol{u}}^T(\boldsymbol{x}_{e,i})\,{}^h\boldsymbol{\sigma}\big(\boldsymbol{\varepsilon}^h(\boldsymbol{x}_{e,i}),{}^h\beta(\boldsymbol{x}_{e,i})\big) - \boldsymbol{N}_{\boldsymbol{u}}^T(\boldsymbol{x}_{e,i})\boldsymbol{f}(\boldsymbol{x}_{e,i},t_{n+1})\Big] = \boldsymbol{0}\,, \tag{3.29a}$$

$$\boldsymbol{R}_{\alpha}(\boldsymbol{U},\boldsymbol{A},\boldsymbol{L}) := \sum_{\Omega_e^h\in\mathcal{T}^h}\sum_{i=1}^{ngp} w_{e,i}j_{e,i}\Big[c\boldsymbol{B}_{\alpha}^T(\boldsymbol{x}_{e,i})\boldsymbol{B}_{\alpha}(\boldsymbol{x}_{e,i})\boldsymbol{A} + r\boldsymbol{N}_{\alpha}^T(\boldsymbol{x}_{e,i})\Big(\boldsymbol{N}_{\alpha}(\boldsymbol{x}_{e,i})\boldsymbol{A} - {}^h\beta(\boldsymbol{x}_{e,i})\Big) + \boldsymbol{N}_{\alpha}^T(\boldsymbol{x}_{e,i})\boldsymbol{N}_{\lambda}(\boldsymbol{x}_{e,i})\boldsymbol{L}\Big] = \boldsymbol{0}\,, \tag{3.29b}$$

$$\boldsymbol{R}_{\lambda}(\boldsymbol{U},\boldsymbol{A},\boldsymbol{L}) := \sum_{\Omega_e^h\in\mathcal{T}^h}\sum_{i=1}^{ngp} w_{e,i}j_{e,i}\Big[\boldsymbol{N}_{\lambda}^T(\boldsymbol{x}_{e,i})\Big(\boldsymbol{N}_{\alpha}(\boldsymbol{x}_{e,i})\boldsymbol{A} - {}^h\beta(\boldsymbol{x}_{e,i})\Big)\Big] = \boldsymbol{0}\,, \tag{3.29c}$$

with $w_{e,i}$ and $j_{e,\,i}$ the weight and the value of the Jacobian determinant at the Gauss point $\boldsymbol{x}_{e,\,i}$ (Bathe, 1996), respectively, whereas ${}^h\boldsymbol{\sigma}(\boldsymbol{\varepsilon}^h(\boldsymbol{x}_{e,\,i}),\,{}^h\beta(\boldsymbol{x}_{e,\,i}))$ and ${}^h\beta(\boldsymbol{x}_{e,\,i})$ are the secondary variables obtained by solving the strain-driven constitutive nonlinear incremental problem (3.21) at such Gauss points.

3.4. Continuation condition based on energy dissipation

Newton's method for the solution of the system (3.29) has a very small domain of convergence. Furthermore, the strain softening characteristic feature of concrete results in unstable global structural responses due to the growth of damage zones which produces a degradation of the elastic material properties, generally caused by redistribution of stresses together with local elastic unloading or elastic energy release higher than the damage zone's dissipation. To understand what are the implications on the actual solution of the system (3.29), in practice one analyses the equilibrium configurations of the system under the variation of generally one parameter which the system depends on. For instance, this can be the load multiplier which defines the current applied load level $\boldsymbol{f}(\boldsymbol{x},\,t)$ or the displacement multiplier which defines the current boundary displacement $\boldsymbol{u}_D(\boldsymbol{x},\,t)$. Hence, if we express the current applied force $\boldsymbol{f}(\boldsymbol{x},\,t)$ in (3.29) as $\boldsymbol{f}(\boldsymbol{x},t)=\zeta(t)\boldsymbol{f}_0(\boldsymbol{x})$, where $\zeta(t)$ is a real parameter that defines the loading history and $\boldsymbol{f}_0(\boldsymbol{x})$ a given loading pattern (or in the case of displacement control, $\boldsymbol{u}_D(\boldsymbol{x},t)=\zeta(t)\boldsymbol{u}_{D,0}(\boldsymbol{x})$ with $\boldsymbol{u}_{D,\,0}(\boldsymbol{x})$ the initial displacement pattern), then the system of nonlinear algebraic Eqs. (3.29) takes on the following form

$$\begin{aligned}&\boldsymbol{R}_{\boldsymbol{u}}(\boldsymbol{U},\boldsymbol{A},\boldsymbol{L},\zeta)=\boldsymbol{0},\\ &\boldsymbol{R}_{\alpha}(\boldsymbol{U},\boldsymbol{A},\boldsymbol{L},\zeta)=\boldsymbol{0}\,,\\ &\boldsymbol{R}_{\lambda}(\boldsymbol{U},\boldsymbol{A},\boldsymbol{L},\zeta)=\boldsymbol{0}\,,\end{aligned} \tag{3.30}$$

where the expression of $\boldsymbol{R}_{\boldsymbol{u}}$ at the time level t_{n+1} is

$$\boldsymbol{R}_{\boldsymbol{u}}(\boldsymbol{U},\boldsymbol{A},\boldsymbol{L},\zeta) := \sum_{\Omega_e^h\in\mathcal{T}^h}\sum_{i=1}^{ngp} w_{e,i}j_{e,i}\Big[\boldsymbol{B}_{\boldsymbol{u}}^T(\boldsymbol{x}_{e,i})\,{}^h\boldsymbol{\sigma}\big(\boldsymbol{\varepsilon}^h(\boldsymbol{x}_{e,i}),{}^h\beta(\boldsymbol{x}_{e,i})\big) - \zeta(t_{n+1})\boldsymbol{N}_{\boldsymbol{u}}^T(\boldsymbol{x}_{e,i})\boldsymbol{f}_0(\boldsymbol{x}_{e,i})\Big]\,, \tag{3.31}$$

whereas the expressions of $\boldsymbol{R}_{\alpha}$ and $\boldsymbol{R}_{\lambda}$ are given by (3.29b) and (3.29c), respectively.

Remark 3.5. The dependence of $\boldsymbol{R}_{\alpha}$ and $\boldsymbol{R}_{\lambda}$ on ζ occurs in the case of displacement control through β, solution of (3.22) with $\boldsymbol{\varepsilon}^h=\boldsymbol{B}_{\boldsymbol{u}}(\boldsymbol{U}+\boldsymbol{U}_D)$.

In this case we are therefore faced with the solution of a parameter dependent system of nonlinear algebraic equations and our interest centers on finding the solutions $(\boldsymbol{U},\,\boldsymbol{A},\,\boldsymbol{L},\,\zeta)$ of (3.30), which form a one-dimensional manifold in the space $\mathbb{R}^{n_{\boldsymbol{u}}}\times\mathbb{R}^{n_{\alpha}}\times\mathbb{R}^{n_{\lambda}}$.

To trace continuous paths of regular solutions of (3.30) with ζ as control parameter, we apply Newton's method. Let us denote by $\mathbb{J}=\mathbb{J}(\boldsymbol{U},\boldsymbol{A},\boldsymbol{L},\zeta)$ the Jacobian of the system (3.30) defined by

$$\mathbb{J}(\boldsymbol{U},\boldsymbol{A},\boldsymbol{L},\zeta)=\begin{bmatrix}\dfrac{D\boldsymbol{R}_{\boldsymbol{u}}}{D\boldsymbol{U}} & \dfrac{D\boldsymbol{R}_{\boldsymbol{u}}}{D\boldsymbol{A}} & \dfrac{D\boldsymbol{R}_{\boldsymbol{u}}}{D\boldsymbol{L}}\\ \dfrac{D\boldsymbol{R}_{\alpha}}{D\boldsymbol{U}} & \dfrac{D\boldsymbol{R}_{\alpha}}{D\boldsymbol{A}} & \dfrac{D\boldsymbol{R}_{\alpha}}{D\boldsymbol{L}}\\ \dfrac{D\boldsymbol{R}_{\lambda}}{D\boldsymbol{U}} & \dfrac{D\boldsymbol{R}_{\lambda}}{D\boldsymbol{A}} & \dfrac{D\boldsymbol{R}_{\lambda}}{D\boldsymbol{L}}\end{bmatrix} \tag{3.32}$$

with $D\boldsymbol{R}_{\boldsymbol{j}}/D\boldsymbol{i}$ derivative of $\boldsymbol{R}_{\boldsymbol{j}}$ with respect to the variable $\boldsymbol{i}$, for $\boldsymbol{i}\in\{\boldsymbol{U},\boldsymbol{A},\boldsymbol{L}\}$, $\boldsymbol{j}\in\{\boldsymbol{u},\alpha,\lambda\}$, and by $(\boldsymbol{U}_n,\,\boldsymbol{A}_n,\,\boldsymbol{L}_n,\,\zeta_n)$ a regular solution of (3.30), that is, a solution of (3.30) such that

$$det\ \mathbb{J}(\boldsymbol{U}_n,\boldsymbol{A}_n,\boldsymbol{L}_n,\zeta_n)\neq 0\,. \tag{3.33}$$

We then take $(\boldsymbol{U}_n,\,\boldsymbol{A}_n,\,\boldsymbol{L}_n,\,\zeta_n)$ as predicted value (starting guess) for the solution $(\boldsymbol{U}_{n+1},\boldsymbol{A}_{n+1},\boldsymbol{L}_{n+1})$ at the given ζ_{n+1}, which is corrected by the Newton's iteration scheme as follows

$$\left|\begin{array}{l}\boldsymbol{U}_{n+1}^0=\boldsymbol{U}_n\\ \boldsymbol{U}_{n+1}^{k+1}=\boldsymbol{U}_{n+1}^k+\Delta\boldsymbol{U}^k\end{array}\right.,\quad \left|\begin{array}{l}\boldsymbol{A}_{n+1}^0=\boldsymbol{A}_n\\ \boldsymbol{A}_{n+1}^{k+1}=\boldsymbol{A}_{n+1}^k+\Delta\boldsymbol{A}^k\end{array}\right.,\quad \left|\begin{array}{l}\boldsymbol{L}_{n+1}^0=\boldsymbol{L}_n\\ \boldsymbol{L}_{n+1}^{k+1}=\boldsymbol{L}_{n+1}^k+\Delta\boldsymbol{L}^k\end{array}\right., \tag{3.34}$$

with the index $k\geq 0$ standing for the iteration step and $(\Delta\boldsymbol{U}^k,\Delta\boldsymbol{A}^k,\Delta\boldsymbol{L}^k)$ solution of the linear system

$$\begin{bmatrix}\Delta\boldsymbol{U}^k\\ \Delta\boldsymbol{A}^k\\ \Delta\boldsymbol{L}^k\end{bmatrix}=-\mathbb{J}^{-1}(\boldsymbol{U}_{n+1}^k,\boldsymbol{A}_{n+1}^k,\boldsymbol{L}_{n+1}^k,\zeta_{n+1})\begin{bmatrix}\boldsymbol{R}_{\boldsymbol{u}}(\boldsymbol{U}_{n+1}^k,\boldsymbol{A}_{n+1}^k,\boldsymbol{L}_{n+1}^k,\zeta_{n+1})\\ \boldsymbol{R}_{\alpha}(\boldsymbol{U}_{n+1}^k,\boldsymbol{A}_{n+1}^k,\boldsymbol{L}_{n+1}^k,\zeta_{n+1})\\ \boldsymbol{R}_{\lambda}(\boldsymbol{U}_{n+1}^k,\boldsymbol{A}_{n+1}^k,\boldsymbol{L}_{n+1}^k,\zeta_{n+1})\end{bmatrix}. \tag{3.35}$$

Algorithm 1 below summarizes the conceptual implementation of Newton's method for solving (3.30).

By the implicit function theorem and under general regularity assumptions on the functions $\boldsymbol{R}_{\boldsymbol{j}}$, $\boldsymbol{j}\in\{\boldsymbol{u},\alpha,\lambda\}$, condition (3.33) guarantees that if for the given value of ζ_{n+1}, the Algorithm 1 does not converge, convergence can still be attained by reducing the value of ζ_{n+1}, for instance by halving the load factor ζ_{n+1} and by applying again Algorithm 1. On the other hand, if condition (3.33) is not met or the Jacobian $\mathbb{J}^{-1}(\boldsymbol{U}_{n+1}^k,\boldsymbol{A}_{n+1}^k,\boldsymbol{L}_{n+1}^k,\zeta_{n+1})$ is ill-conditioned, Algorithm 1 with ζ as continuation parameter fails to converge because of the break down of the Newton's method (3.35). For our model such circumstance occurs when the damaged areas become so influential in the response of the system that there is a change

of the monotonic properties of the equilibrium path. This manifests, for instance, with the occurrence of turning points and decreasing paths. In this case then ζ cannot be used as continuation parameter.

A manner to overcome this problem is to adopt a different parametrization of the solution manifold. This can be realized by introducing an additional equation

$$\varphi(\boldsymbol{U}, \boldsymbol{A}, \boldsymbol{L}, \zeta) = 0\,, \tag{3.36}$$

such that if a solution $(\boldsymbol{U}, \boldsymbol{A}, \boldsymbol{L}, \zeta)$ is singular for $\mathbb{J}$, then the solution $(\boldsymbol{U}, \boldsymbol{A}, \boldsymbol{L}, \zeta)$ is not such for the Jacobian of the augmented system formed by (3.30) and (3.36). Now, given the system (3.30), how do we actually define the additional Eq. (3.36) depends on whether we are able to identify a physical feature of the process, which will be then modeled by (3.36), that varies continuously during the deformation across the turning points. For nonlinear damage models it was observed in Gutierrez (2004) that the configurations past the turning point, which are the one we are interested to, are characterized by monotonically increasing dissipation, thus it came natural to use a dissipation control condition as continuation condition. Such condition was also used effectively in Verhoosel et al. (2009), May et al. (2016), and Vignollet et al. (2014) for plasticity models and geometrically non-linear problems with damage along with the introduction of a criteria for switching the continuation parameter. By assuming such continuation condition, we are practically stating that if, past the turning point, dissipation occurs during the variation of configuration, then we look for the configuration close to the previously converged one such that the dissipation associated to such variation of configuration is equal to a predefined value.

Likewise, in this paper we decide to control the following quantity

$$\frac{1}{2}\left(\zeta(t)\dot{\overline{\boldsymbol{U}}}^T - \dot{\zeta}(t)\overline{\boldsymbol{U}}^T\right)\int_\Omega \boldsymbol{N}_{\boldsymbol{u}}^T \boldsymbol{f}_0(\boldsymbol{x})\, d\boldsymbol{x} - \dot{\boldsymbol{A}}^T \int_\Omega c\boldsymbol{B}_\alpha^T \boldsymbol{B}_\alpha \boldsymbol{A}\, d\boldsymbol{x}\,, \tag{3.37}$$

which represents the Finite Element expression of the total dissipation (2.6) integrated over Ω.

Remark 3.6. Compared with May et al. (2016), Eq. (19) and Verhoosel et al. (2009),Eq. (23), it is of interest to note in (3.37) an additional term that accounts for the part of recoverable energy rate associated with the gradient of the internal variable. This derivation is consistent with the expression of the free Helmholtz energy (2.8) of our model.

By evaluating (3.37) at $t = t_n$ and using therein the difference quotient for the rate quantities, we conclude that the additional constraint $\varphi(\boldsymbol{U}, \boldsymbol{A}, \boldsymbol{L}, \zeta)$ is given by

$$\begin{aligned}\varphi(\boldsymbol{U}, \boldsymbol{A}, \boldsymbol{L}, \zeta) = \frac{1}{2}\left(\zeta_n \dot{\overline{\boldsymbol{U}}}^T - \zeta \overline{\boldsymbol{U}}_n^T\right)\int_\Omega \boldsymbol{N}_{\boldsymbol{u}}^T \boldsymbol{f}_0(\boldsymbol{x})\, d\boldsymbol{x} \\ - \Delta\boldsymbol{A}^T \int_\Omega c\boldsymbol{B}_\alpha^T \boldsymbol{B}_\alpha \boldsymbol{A}_n\, d\boldsymbol{x} - \Delta\tau\end{aligned} \tag{3.38}$$

where $\Delta\boldsymbol{A} = \boldsymbol{A} - \boldsymbol{A}_n$, $\overline{\boldsymbol{U}} = \boldsymbol{U} + \boldsymbol{U}_D$ with known $\boldsymbol{U}_D$, and $\Delta\tau \geq 0$ is the pseudo-arch length that prescribes the amount of energy that is dissipated in each step of the equilibrium path.

The augmented system is thus given, in the case of load control, by

$$\begin{aligned}&\boldsymbol{R}_{\boldsymbol{u}}(\boldsymbol{U}, \boldsymbol{A}, \boldsymbol{L}) - \zeta\hat{\boldsymbol{F}} = 0\\ &\boldsymbol{R}_\alpha(\boldsymbol{U}, \boldsymbol{A}, \boldsymbol{L}) = 0\\ &\boldsymbol{R}_\lambda(\boldsymbol{U}, \boldsymbol{A}, \boldsymbol{L}) = 0\\ &\varphi(\boldsymbol{U}, \boldsymbol{A}, \boldsymbol{L}, \zeta) = 0\end{aligned} \tag{3.39}$$

which can be solved using Newton's method according to the following scheme

$$\left|\begin{array}{l}\boldsymbol{U}_{n+1}^0 = \boldsymbol{U}_n\\ \boldsymbol{U}_{n+1}^{k+1} = \boldsymbol{U}_{n+1}^k + \Delta\boldsymbol{U}^k\end{array}\right|\,,\quad \left|\begin{array}{l}\boldsymbol{A}_{n+1}^0 = \boldsymbol{A}_n\\ \boldsymbol{A}_{n+1}^{k+1} = \boldsymbol{A}_{n+1}^k + \Delta\boldsymbol{A}^k\end{array}\right|\,,$$

$$\left|\begin{array}{l}\boldsymbol{L}_{n+1}^0 = \boldsymbol{L}_n\\ \boldsymbol{L}_{n+1}^{k+1} = \boldsymbol{L}_{n+1}^k + \Delta\boldsymbol{L}^k\end{array}\right|\,,\quad \left|\begin{array}{l}\zeta_{n+1}^0 = \zeta_n\\ \zeta_{n+1}^{k+1} = \zeta_{n+1}^k + \Delta\zeta^k\end{array}\right|\,, \tag{3.40}$$

with $(\Delta\boldsymbol{U}^k, \Delta\boldsymbol{A}^k, \Delta\boldsymbol{L}^k, \Delta\zeta^k)$ solution of the linear system

$$\begin{aligned}&\begin{bmatrix}\Delta\boldsymbol{U}^k\\ \Delta\boldsymbol{A}^k\\ \Delta\boldsymbol{L}^k\\ \Delta\zeta^k\end{bmatrix} = -\mathbb{H}^{-1}(\boldsymbol{U}_{n+1}^k, \boldsymbol{A}_{n+1}^k, \boldsymbol{L}_{n+1}^k, \zeta_{n+1}^k)\\ &\begin{bmatrix}\boldsymbol{R}_{\boldsymbol{u}}(\boldsymbol{U}_{n+1}^k, \boldsymbol{A}_{n+1}^k, \boldsymbol{L}_{n+1}^k, \zeta_{n+1}^k)\\ \boldsymbol{R}_\alpha(\boldsymbol{U}_{n+1}^k, \boldsymbol{A}_{n+1}^k, \boldsymbol{L}_{n+1}^k, \zeta_{n+1}^k)\\ \boldsymbol{R}_\lambda(\boldsymbol{U}_{n+1}^k, \boldsymbol{A}_{n+1}^k, \boldsymbol{L}_{n+1}^k, \zeta_{n+1}^k)\\ \varphi(\boldsymbol{U}_{n+1}^k, \boldsymbol{A}_{n+1}^k, \boldsymbol{L}_{n+1}^k, \zeta_{n+1}^k)\end{bmatrix}\,,\end{aligned} \tag{3.41}$$

where $\mathbb{H}$ is now the Jacobian of the augmented system (3.39) given by

$$\mathbb{H}(\boldsymbol{U}, \boldsymbol{A}, \boldsymbol{L}, \zeta) = \left[\begin{array}{cccc}\frac{D\boldsymbol{R}_{\boldsymbol{u}}}{D\boldsymbol{U}} & \frac{D\boldsymbol{R}_{\boldsymbol{u}}}{D\boldsymbol{A}} & \frac{D\boldsymbol{R}_{\boldsymbol{u}}}{D\boldsymbol{L}} & \frac{D\boldsymbol{R}_{\boldsymbol{u}}}{D\zeta}\\ \frac{D\boldsymbol{R}_\alpha}{D\boldsymbol{U}} & \frac{D\boldsymbol{R}_\alpha}{D\boldsymbol{A}} & \frac{D\boldsymbol{R}_\alpha}{D\boldsymbol{L}} & \frac{D\boldsymbol{R}_\alpha}{D\zeta}\\ \frac{D\boldsymbol{R}_\lambda}{D\boldsymbol{U}} & \frac{D\boldsymbol{R}_\lambda}{D\boldsymbol{A}} & \frac{D\boldsymbol{R}_\lambda}{D\boldsymbol{L}} & \frac{D\boldsymbol{R}_\lambda}{D\zeta}\\ \hline \frac{D\varphi}{D\boldsymbol{U}} & \frac{D\varphi}{D\boldsymbol{A}} & \frac{D\varphi}{D\boldsymbol{L}} & \frac{D\varphi}{D\zeta}\end{array}\right]\,, \tag{3.42}$$

with the detailed expressions of the terms of $\mathbb{H}$ reported in Appendix A.

Remark 3.7. As stopping rule for the iterations of the scheme (3.34) and (3.35) and of the scheme (3.40) and (3.41), depending on the continuation Newton's method we are using, we compare the Euclidean norm of the residuals (3.30) or (3.39) and the Euclidean norm of the increments (3.35) or (3.41) to the respective prescribed error tolerances. These tolerances are taken of the form $tol = \varepsilon|x_n| + \varepsilon$ with x_n denoting the respective previously converged solution, so to control effectively the absolute and relative error (Gautschi, 2012).

The actual realization of the numerical strategy described in this section consists therefore in solving first the Newton's method (3.34) and (3.35) by increasing monotonically the load/displacement parameter ζ until one can achieve convergence. When this is no more possible, that is, the load/displacement based continuation Newton's method (3.34) and (3.35) fails to converge for any value of ζ such that $\zeta_n < \zeta < \zeta_{n+1}$ with ζ_n being the last converged solution with load/displacement control, we switch to the energy dissipation control using now $\Delta\tau$ as continuation parameter. In this case, we therefore prescribe the energy dissipation increment $\Delta\tau$ and solve the Newton's method (3.40) and (3.41) using as starting guess the last converged solution. This scheme will be used until we can achieve convergence for values of $\Delta\tau \geq 0$, for then to switch back to load control. The fail of convergence of (3.40) and (3.41) will occur if there is no close variation of the system configuration which produces dissipation of energy. This means that by this algorithm we actually are able to avoid the artificial unloading described in Pohl et al. (2014), which, on the contrary, might occur in the arc-length continuation method described in Crisfield (1981). By our algorithm, the switch back to

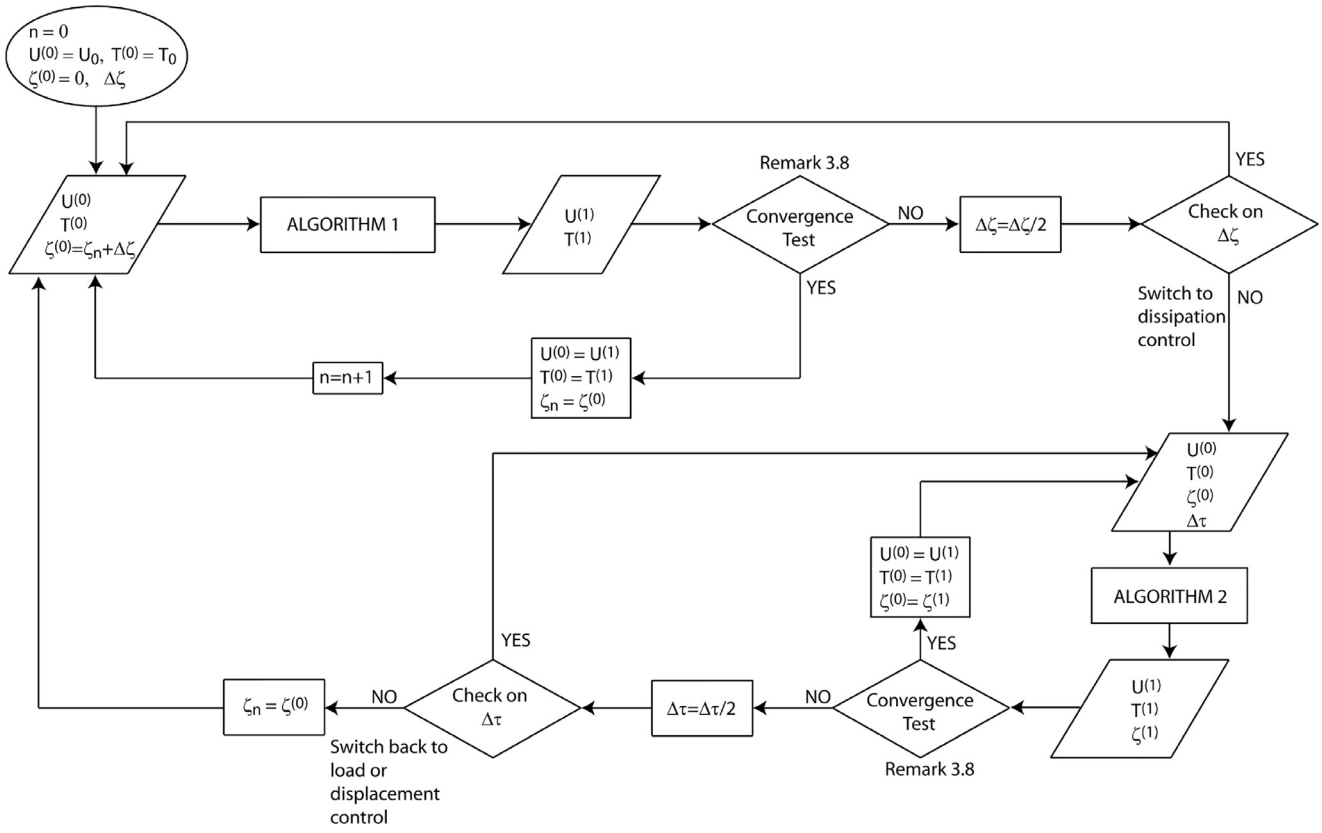

Fig. 2. Flow chart of the complete numerical procedure based on the application of Algorithms 1 and 2. To make notation compact, in the picture we have set $T = (\boldsymbol{A}, \boldsymbol{L}, \beta, \sigma)$.

load/displacement would happen if a global unloading of the system occurs, which is not the case we consider here. A summary of the whole procedure is reported in Algorithm 2 whereas Fig. 2 contains the flow chart of the whole numerical procedure based on the application of Algorithms 1 and 2.

4. Numerical examples

In this Section we study the performance of the energetic formulation and of the proposed numerical algorithms by means of representative numerical examples. The problems that we consider are:

(*i*) A trapezium double cantilever beam to study the properties of stable and rectilinear damage propagation and the sensitivity of the model to mesh size;
(*ii*) A perforated plate with an off-centre hole to study the model's behavior for unstable and multi damage patterns which produce a global snap-back response of the structure;
(*iii*) An asymmetric three point bending test to assess the capability of the numerical model to reproduce curvilinear damage paths.

All the specimens are assumed to be in plane strain conditions. As in Lorentz and Godard (2011), in all the numerical simulations, we take the penalty parameter r that appears in the augmented lagrangian formulation equal to $r = 10^3 \cdot k$, where k is the initial damage threshold that enters (2.9). Numerical experiments of problem (*i*) carried out for different values of r which we do not report here, show that the above choice for r by Lorentz and Godard (2011) gives a good trade-off between the absence of spurious modes on β and the extent to which the constraint $\alpha = \beta$ is met. An improvement of the order of approximation of the finite elements described in Section 3.3 and used in our simulations can, however, be obtained by choosing values of r dependent on the characteristic mesh size h in the damage band as suggested in Boffi and Lovadina (1997). As for the check of convergence of Algorithm 1 we refer to the general observations in Remark 3.7 with $\varepsilon = 10^{-4}$, whereas for the convergence test of Algorithm 2 we consider a tolerance equal to 10^{-3} and $10^{-6}N$ on the values of $\Delta\zeta$ and $\Delta\tau$, respectively.

4.1. Trapezoidal double cantilever beam

We use this first example to highlight the mesh-objective finite element analysis of the energetic formulation of our gradient damage model. We consider therefore the numerical simulation of a structure with softening behavior caused by the stable propagation of a rectilinear damage zone. This problem has already been treated in Lorentz and Godard (2011). It consists of a slight variation of the Double Cantilever Beam (DCB) test which is usually used to determine fracture toughness under pure mode I loading. The geometry of the specimen along with the boundary conditions are displayed in Fig. 3(*a*). The model material parameters of the concrete are given in Table 1. In addition to the elastic constants, Table 1 contains also the parameters that define the softening function $R = R(\beta)$ (2.15) and the equivalent stress σ_{eq} (2.17) which enters the definition of the damage surface and accounts for the asymmetric behavior between tension and compression. The characteristic length D has been set equal to 50 mm. Such value enters the softening function $R = R(\beta)$ and has been taken sufficiently small compared to the characteristic structural length of the specimen shown in Fig. 3(*a*).

Given the symmetry of the mechanical model, only half system was analysed. The unstructured finite element meshes which have been used for the numerical simulations are shown in Fig. 3(*b*). The meshes present different refinement in the zone where we

Data: $(\boldsymbol{U}_n,\, \boldsymbol{A}_n,\, \boldsymbol{L}_n)$, ${}^h\beta_n$, ${}^h\boldsymbol{\sigma}_n$, ζ_{n+1}
Result: $(\boldsymbol{U}_{n+1},\, \boldsymbol{A}_{n+1},\, \boldsymbol{L}_{n+1})$, ${}^h\beta_{n+1}$, ${}^h\boldsymbol{\sigma}_{n+1}$
set
  $k = 0$
  $\boldsymbol{U}^k_{n+1} = \boldsymbol{U}_n$, $\boldsymbol{A}^k_{n+1} = \boldsymbol{A}_n$, $\boldsymbol{L}^k_{n+1} = \boldsymbol{L}_n$, ${}^h\beta^k_{n+1} = {}^h\beta_n$, ${}^h\boldsymbol{\sigma}^k_{n+1} = {}^h\boldsymbol{\sigma}_n$
repeat
  compute
    $\boldsymbol{R}_{\boldsymbol{u}}(\boldsymbol{U}^k_{n+1}, \boldsymbol{A}^k_{n+1}, \boldsymbol{L}^k_{n+1}, \zeta_{n+1})$ by Eq. (3.31)
    $\boldsymbol{R}_{\alpha}(\boldsymbol{U}^k_{n+1}, \boldsymbol{A}^k_{n+1}, \boldsymbol{L}^k_{n+1}, \zeta_{n+1})$ by Eq. (3.29b)
    $\boldsymbol{R}_{\lambda}(\boldsymbol{U}^k_{n+1}, \boldsymbol{A}^k_{n+1}, \boldsymbol{L}^k_{n+1}, \zeta_{n+1})$ by Eq. (3.29c)
    $\mathbb{J}(\boldsymbol{U}^k_{n+1}, \boldsymbol{A}^k_{n+1}, \boldsymbol{L}^k_{n+1}, \zeta_{n+1})$ by Eq. (3.32) with the derivatives given in Appendix A
  solve
    Eq. (3.35) for $\Delta\boldsymbol{U}^k$, $\Delta\boldsymbol{A}^k$, $\Delta\boldsymbol{L}^k$
  update
    $\boldsymbol{U}^{k+1}_{n+1} = \boldsymbol{U}^k_{n+1} + \Delta\boldsymbol{U}^k$, $\boldsymbol{A}^{k+1}_{n+1} = \boldsymbol{A}^k_{n+1} + \Delta\boldsymbol{A}^k$, $\boldsymbol{L}^{k+1}_{n+1} = \boldsymbol{L}^k_{n+1} + \Delta\boldsymbol{L}^k$
  compute at each Gauss point $\boldsymbol{x}_{e,i}$, $i = 1, \ldots, ngp$, of each element $\Omega^h_e \in \mathcal{T}^h$
    $\boldsymbol{\varepsilon}^{k+1}_{n+1} = \boldsymbol{B}_{\boldsymbol{u}}\boldsymbol{U}^{k+1}_{n+1}$, $\alpha^{k+1}_{n+1} = \boldsymbol{N}_{\alpha}\boldsymbol{A}^{k+1}_{n+1}$, $\lambda^{k+1}_{n+1} = \boldsymbol{N}_{\lambda}\boldsymbol{L}^{k+1}_{n+1}$
    ${}^h\beta^{k+1}_{n+1}$ by Eq. (3.22) with data $(\boldsymbol{\varepsilon}_n,\, {}^h\beta_n)$ and $(\boldsymbol{\varepsilon}^{k+1}_{n+1},\, \alpha^{k+1}_{n+1},\, \lambda^{k+1}_{n+1})$
    ${}^h\boldsymbol{\sigma}^{k+1}_{n+1}$ by Eq. (3.23)
  $k = k + 1$
until *converge test is met (see Remark 3.7)*

Algorithm 1. Newton's method for the incremental problem with load or displacement control.

Data: $(\boldsymbol{U}_n,\, \boldsymbol{A}_n,\, \boldsymbol{L}_n)$, ${}^h\beta_n$, ${}^h\boldsymbol{\sigma}_n$, ζ_n, $\Delta\tau$
Result: $(\boldsymbol{U}_{n+1},\, \boldsymbol{A}_{n+1},\, \boldsymbol{L}_{n+1})$, ${}^h\beta_{n+1}$, ${}^h\boldsymbol{\sigma}_{n+1}$, ζ_{n+1}
set
  $k = 0$
  $\boldsymbol{U}^k_{n+1} = \boldsymbol{U}_n$, $\boldsymbol{A}^k_{n+1} = \boldsymbol{A}_n$, $\boldsymbol{L}^k_{n+1} = \boldsymbol{L}_n$, ${}^h\beta^k_{n+1} = {}^h\beta_n$, ${}^h\boldsymbol{\sigma}^k_{n+1} = {}^h\boldsymbol{\sigma}_n$, $\zeta^k_{n+1} = \zeta_n$
repeat
  compute
    $\boldsymbol{R}_{\boldsymbol{u}}(\boldsymbol{U}^k_{n+1}, \boldsymbol{A}^k_{n+1}, \boldsymbol{L}^k_{n+1}, \zeta_{n+1})$ by Eq. (3.31)
    $\boldsymbol{R}_{\alpha}(\boldsymbol{U}^k_{n+1}, \boldsymbol{A}^k_{n+1}, \boldsymbol{L}^k_{n+1})$ by Eq. (3.29b)
    $\boldsymbol{R}_{\lambda}(\boldsymbol{U}^k_{n+1}, \boldsymbol{A}^k_{n+1}, \boldsymbol{L}^k_{n+1})$ by Eq. (3.29c)
    $\varphi(\boldsymbol{U}^k_{n+1}, \boldsymbol{A}^k_{n+1}, \boldsymbol{L}^k_{n+1}, \zeta^k_{n+1})$ by Eq. (3.38)
    $\mathbb{H}(\boldsymbol{U}^k_{n+1}, \boldsymbol{A}^k_{n+1}, \boldsymbol{L}^k_{n+1}, \zeta^k_{n+1})$ by Eq. (3.42) with the derivatives given in Appendix A
  solve
    Eq. (3.41) for $\Delta\boldsymbol{U}^k$, $\Delta\boldsymbol{A}^k$, $\Delta\boldsymbol{L}^k$, $\Delta\zeta^k$,
  update
    $\boldsymbol{U}^{k+1}_{n+1} = \boldsymbol{U}^k_{n+1} + \Delta\boldsymbol{U}^k$, $\boldsymbol{A}^{k+1}_{n+1} = \boldsymbol{A}^k_{n+1} + \Delta\boldsymbol{A}^k$, $\boldsymbol{L}^{k+1}_{n+1} = \boldsymbol{L}^k_{n+1} + \Delta\boldsymbol{L}^k$,
    $\zeta^{k+1}_{n+1} = \zeta^k_{n+1} + \Delta\zeta^k$
  compute at each Gauss point $\boldsymbol{x}_{e,i}$, $i = 1, \ldots, ngp$, of each element $\Omega^h_e \in \mathcal{T}^h$
    $\boldsymbol{\varepsilon}^{k+1}_{n+1} = \boldsymbol{B}_{\boldsymbol{u}}\boldsymbol{U}^{k+1}_{n+1}$, $\alpha^{k+1}_{n+1} = \boldsymbol{N}_{\alpha}\boldsymbol{A}^{k+1}_{n+1}$, $\lambda^{k+1}_{n+1} = \boldsymbol{N}_{\lambda}\boldsymbol{L}^{k+1}_{n+1}$
    ${}^h\beta^{k+1}_{n+1}$ by Eq. (3.22) with data $(\boldsymbol{\varepsilon}_n,\, {}^h\beta_n)$ and $(\boldsymbol{\varepsilon}^{k+1}_{n+1},\, \alpha^{k+1}_{n+1},\, \lambda^{k+1}_{n+1})$
    ${}^h\boldsymbol{\sigma}^{k+1}_{n+1}$ by Eq. (3.23)
  $k = k + 1$
until *converge test is met (see Remark 3.7)*

Algorithm 2. Continuation Newton's method with energy dissipation control.

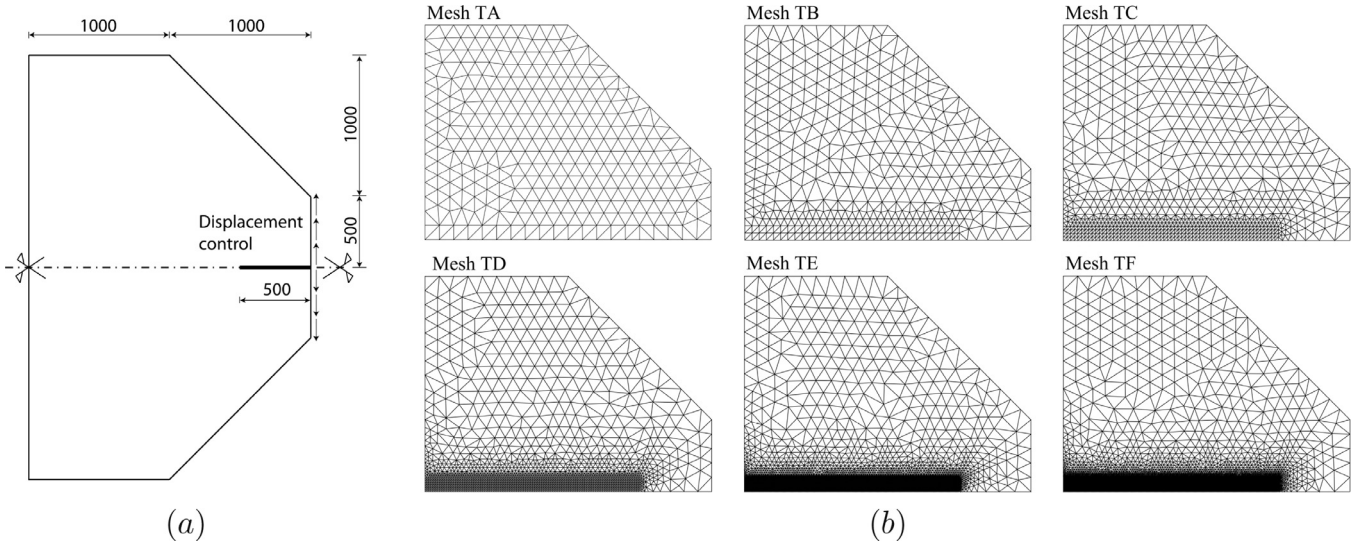

Fig. 3. Example 4.1. (*a*) Mechanical model. Geometry and boundary conditions. Displacement control is applied on one edge of the specimen. (*b*) Finite element meshes used in the simulations. The mesh has especially been refined across the area where the damage pattern is anticipated to develop.

Table 1
Concrete model material properties. The parameter ℓ_1 accounts for the different values between the initial uniaxial compressive and tensile strength.

Elastic material properties	
E_0	$3 \cdot 10^4$MPa
ν	$2 \cdot 10^{-1}$
Softening function (2.15)	
D	$5 \cdot 10^{-2}$m
G_f	$1 \cdot 10^{-4}$MPa $\cdot$ m
f_{t0}	3 MPa
p	2
q	0
Damage surface (2.17)	
ℓ_1	10
ℓ_2	0.1
ℓ_3	7.66
ℓ_4	3.5

Table 2
Example 4.1. Number of nodes and elements of each finite element mesh. The mesh density is determined by the number of elements used across the expected damage band width. Such area is marked in the picture with a rectangle.

	Number of:		
	Nodes	Elements	Elements in D
Mesh TA	200	1118	1/2
Mesh TB	543	2896	1
Mesh TC	1417	7380	2
Mesh TD	3812	19574	4
Mesh TE	7603	38910	8
Mesh TF	22792	115626	16

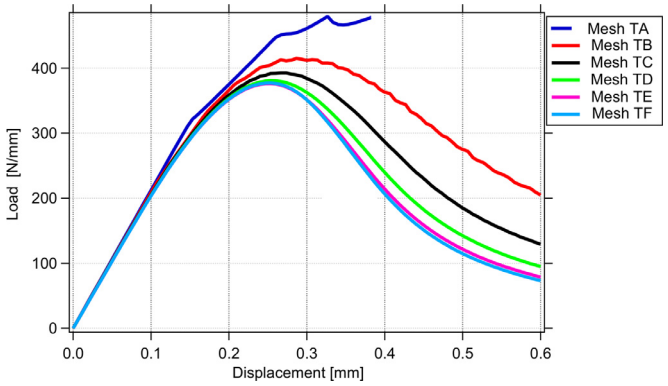

Fig. 4. Example 4.1. Diagram of the reaction force on the restrained edge versus the uniform prescribed displacement of such edge.

expect damage to develop. Therein, the mesh density is determined by the number of elements present within the distance D, the material internal length scale. The total number of nodes and elements corresponding to each type of finite element mesh are given in Table 2. All the numerical simulations could be carried out by applying only Algorithm 1 with displacement control. That is, it has never been necessary to switch to energy dissipation control. The failure of convergence of Algorithm 1 was, in fact, always caused by the development of complete damage in a meaningful number of elements which provoked the formation of a rigid body mechanism.

Fig. 4 compares the curves reaction force versus displacement of the restrained edge obtained with the different finite element meshes. Apart from the response corresponding to the coarse mesh, which shows a poor approximation of the numerical results, all the other curves, on the contrary, approximate a fixed curve as the refinement increases. In particular, the reaction-displacement curve corresponding to the finite element mesh *TE* with 7603 elements almost coincides with the one relative to the finite element mesh *TF* with 22792 elements, which can therefore be taken as response of the experiment set-up of Fig. 3(*a*). We note that all the curves present the typical global softening behavior of a mode I loading, which is induced by the damage growth at the local level. Fig. 5 displays a zoom of the damage field obtained at the end of each simulation. We observe that, by refining the mesh, the width of the damage band does not shrink to zero. In contrast, it attains a stable value of about 50 mm which is comparable with the value of the material internal length scale of the model. We confirm in this manner the regularization of the formulation due to the presence of the damage gradient. Finally, we also note that we are able to reproduce such behavior just by using finite element meshes with at least two elements across the zone where the damage pattern develops.

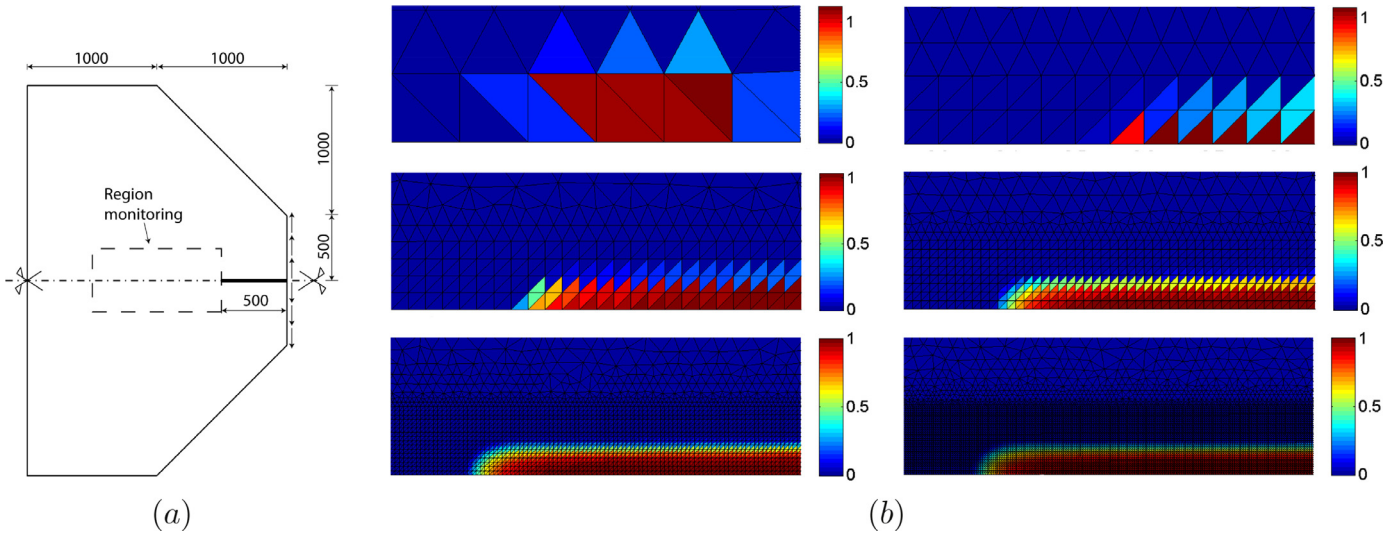

Fig. 5. Example 4.1. (*a*) Region monitoring for damage evolution. (*b*) Map of the damage field for the different meshes at the end of the simulation in the area depicted in (*a*). The damage spreads across the finite elements in the damage band of width *D*. Such width is constant along the damage path.

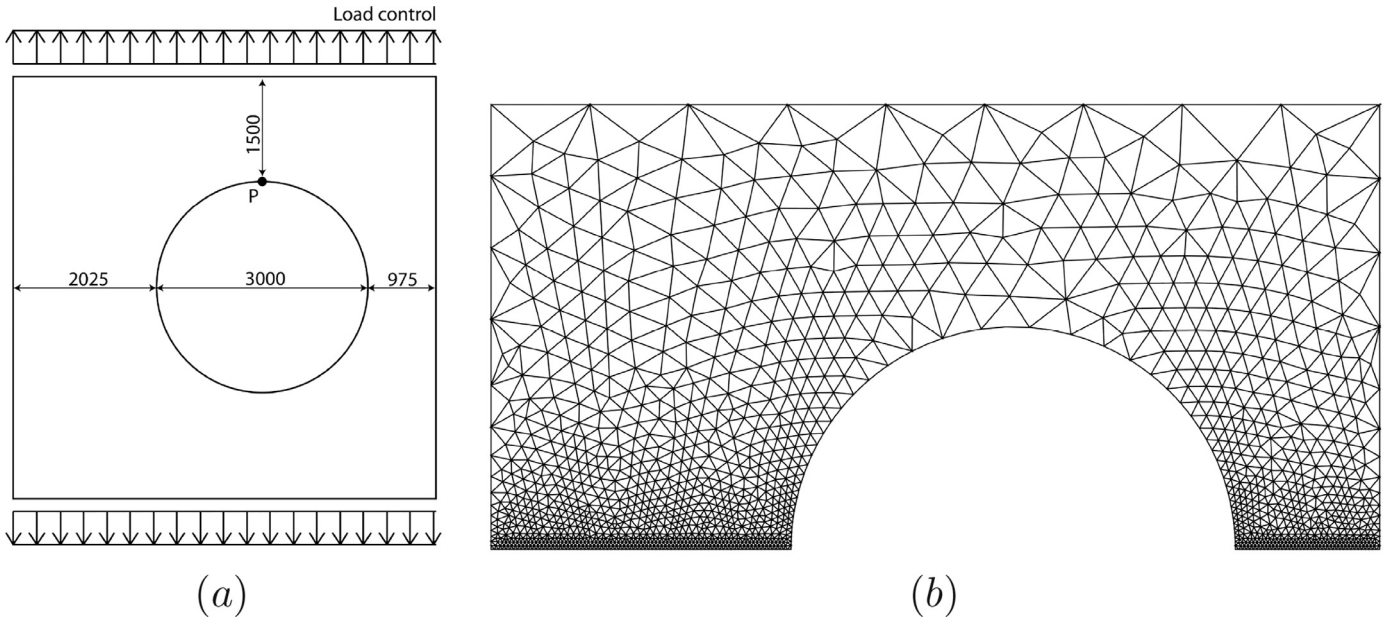

Fig. 6. Example 4.2. Mechanical and computational model. (*a*) Geometry and boundary conditions for the whole plate. (*b*) Finite element mesh for only half plate.

4.2. Plate with off-centre hole

In this second example we test the continuation Newton's method for the numerical simulation of a system with sharp snap-back equilibrium branches caused by the formation of multiple damage paths. This problem has also been examined in Lorentz and Godard (2011), Lorentz and Badel (2004), and Pohl et al. (2014). It consists of a square plate with an off-centre hole loaded with uniform tension on two opposite sides whereas the other two sides are set free. The setting up of the model is displayed in Fig. 6(*a*). Given the presence of the hole, damage will clearly start where stress concentrations are expected to occur. We designed, therefore, the unstructured finite element mesh of 2767 linear elements shown in Fig. 6(*b*) with mesh refinement of the weakened region for a width *D*, with $D = 50\,\text{mm}$. The minimal element size in this region was set equal to $h = 20\,\text{mm}$. The model material properties are the same as the one used for the Example 4.1 and are given in Table 1.

As for the computation, this was performed by applying first Algorithm 1 with load control. This was possible until damage started to propagate towards left and right from the hole. At this instant, the procedure switched to energy dissipation control using Algorithm 2 and keeping this continuation condition active until the end of the simulation, though with different values of $\Delta\tau$. These were varying between $10^{-4}N$ and $10^{-3}N$, according to the branch of the equilibrium path which was being described.

Fig. 7 contains the curve representing the total load (in equilibrium with the configuration) versus the opening displacement. The latter was computed as twice the displacement of the point *P* shown in Fig. 6(*a*). On this curve we have highlighted some representative points of the deformation process. In fact, we can distinguish a first phase which is the elastic one followed by the occurrence of damage first on the right side of the hole and soon after on the left. At this stage, we get to the peak of the response represented by the point *A*. After passing point *A*, we enter a second phase. During such phase, the damage stops to advance on the left

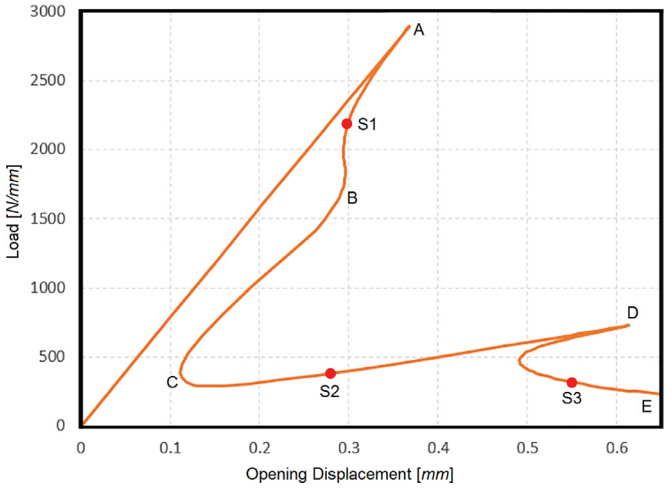

Fig. 7. Example 4.2. Equilibrium curve of the system in terms of the total load versus the opening displacement given by twice the displacement of the point P shown in Fig. 6(a).

side of the hole and it propagates only on the right side until we reach the point B. From this instant on, the damage band tends to stabilize resulting in a sharp snap-back from B to C. From point C to point D, the opening displacement of the hole starts to increase caused by the re-activation of the damage on the left side of the hole. After passing D, the damage continues to propagate and grow until we reach the free left boundary. In this moment, convergence could not be anymore achieved, because we have complete damage in all the elements at the left and right side of the hole. As a result, the structure was cut in to half with the formation of a rigid body mechanism. Similar behaviors have been reported also in the experiments by Lorentz and Badel (2004) and Pohl et al. (2014). Finally, Fig. 8 displays the damage distribution on the initial configuration at some significant stages of the deformation process, identified as stage $S1$, $S2$ and $S3$ on the load-displacement curve shown in Fig. 7.

4.3. Asymmetric three-point-bending test

Aim of this example is to show the model energetic formulation's capability of reproducing curved damage patterns with different band widths. We consider the finite element analysis of the three-point beam test with an eccentric notch reported in Galvez et al. (1998) and treated numerically also in Nedjar (2001) and Miehe et al. (2010). The test is designed to study the mixed mode concrete fracture which is known to be a challenging problem, beyond the capability of many models (Caner and Bazant, 2013; Galvez et al., 1998). The geometry and the boundary conditions of the test specimen are shown in Fig. 9 where the notch presents a width of 5 mm and reaches a depth of 20 mm in a beam with

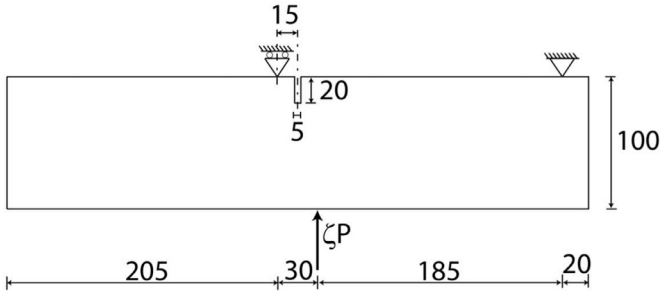

Fig. 9. Example 4.3. Mechanical model. Geometry and boundary conditions. Loading conditions.

Table 3
Example 4.3. Concrete model material properties.

Elastic material properties	
E_0	$3.3 \cdot 10^4$ MPa
ν	0.18
Softening function (2.15)	
D_1	$5 \cdot 10^{-3}$ m
D_2	$2.5 \cdot 10^{-3}$ m
D_3	$1.25 \cdot 10^{-3}$ m
G_f	$5 \cdot 10^{-5}$ MPa · m
f_{t0}	2.8 MPa
p	2
q	0
Damage surface (2.17)	
ℓ_1	20
ℓ_2	0
ℓ_3	7.66
ℓ_4	3.5

height equal to 100 mm. The applied load is eccentric with respect to the notch which is placed at 15 mm from it. We consider, moreover, the simplified setting of proportional loading. In this case, the damage pattern, and thus what is to be the crack pattern, can be guessed from kinematic considerations. The loading produces combined normal and shear stress in the vertical crack-tip cross section, and the crack starts at the right corner of the notch and ends where the load is applied. This behavior is quite well documented in the literature on the three point bend testing of notched beams with eccentric notch (Jenq and Shah, 1988; Galvez et al., 1998). The model material parameters are given in Table 3 along with different values of the parameter D which, as shown in the previous two examples, are related to the internal length-scale and control the damage band width. Correspondingly to each value of D, we carried out our simulations using unstructured finite element meshes that are refined in the region where damage is expected to occur. The characteristic element size in such region was chosen as function of D so to obtain an objective response. As a result, for the mesh RA, we set $h = 2.5$ mm, for the mesh RB $h = 1.25$ mm, and

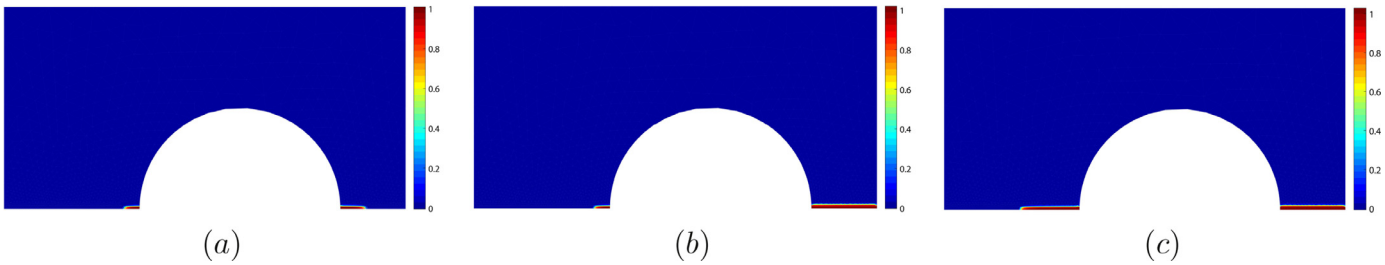

Fig. 8. Example 4.2. Damage distribution on the initial configuration at different stages of the equilibrium path. (a) Stage $S1$; (b) Stage $S2$ and (c) Stage $S3$ shown on the load-displacement curve in Fig. 7.

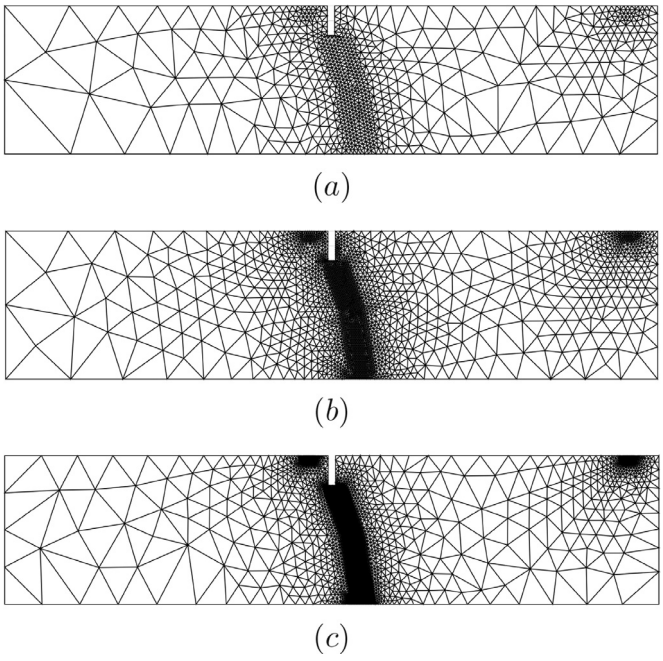

Fig. 10. Example 4.3. Unstructured finite element meshes used in the simulations, with different refinement density in the region where damage is expected to develop. The refinement was designed so to have at least two elements in the D-wide damage band. (a) Mesh *RA* presents a characteristic mesh size in the refined zone equal to $h = 2.5$ mm. (b) Mesh *RB* with $h = 1.25$ mm. (c) Mesh *RC* with $h = 0.625$ mm.

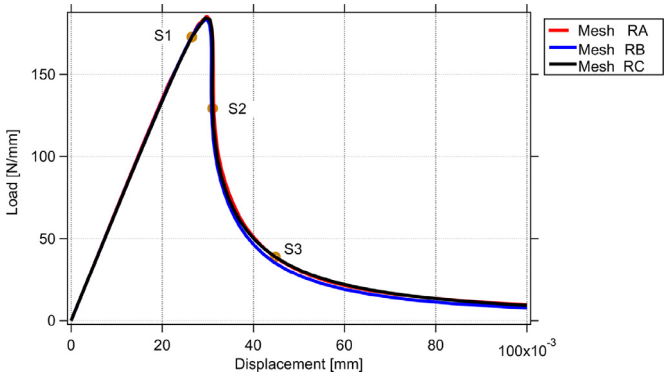

Fig. 11. Example 4.3. Total reaction force versus point-applied load displacement for different finite element meshes.

Table 4
Example 4.3. General data of the unstructured finite element meshes used in the simulations. The symbol h denotes the minimal characteristic element size in the refined region.

	Minimal mesh size	Number of elements	Number of nodes
Mesh *RA*	$h_1 = 2.5$ mm	1449	7588
Mesh *RB*	$h_2 = 1.25$ mm	4533	23170
Mesh *RC*	$h_3 = 0.625$ mm	7594	38616

finally for the mesh *RC*, it was taken $h = 0.625$ mm. Fig. 10 displays the three different meshes whereas Table 4 contains general data about the number of nodes and elements of each mesh, and the minimal characteristic element size h in the refined region.

In order to ascertain the dependence of the damage pattern on the internal length scale D in the case of curvilinear paths, for each value of D we first carried out our simulations using the three above meshes. The results, which however are not displayed here and in conformity also with the results of the two previous examples, showed that by just having two elements in the expected damage band width, we were able to obtain an objective response of the system independent on the mesh, with a stable localization of the damage in a region of width D. That is, the damage does not shrinks on one element but remains localized with finite size. Taking thus as representative of the response of the system, the coarsest mesh for each value of D which yields stable results (the mesh *RA* for the simulations of the model with $D = 2.5$ mm, the mesh *RB* for the simulations of the model with $D = 1.25$ mm and the mesh *RC* for the simulations of the model with $D = 2.5$ mm), Fig. 11 displays the total reaction force versus the displacement of the point-applied load for each model. Each curve presents its characteristic shape with softening and snap-back of the global response. Although the response of the three models appear to be close to each other, apart from differentiating slightly at the late stage of the simulation, the map of the damage field in the refined zone at the end of the simulation, which is displayed in Fig. 12, reveals clearly the different width of the damage band, ultimately related to the value of D. Fig. 13 shows the map of the damage field at some meaningful stages of the deformation process for the model with $D = 1.25$ mm simulated with the mesh *RB*. These stages were identified as the ones before getting to the peak of the response, after the peak on the branch with sharp slope, and finally on the tail of the reaction force-displacement curve. By inspecting these pictures, we can appreciate the evolution of the damage pattern as predicted by experiments, i.e., the damage pattern starts at the right corner of the notch and then propagates up to the location of the applied point load.

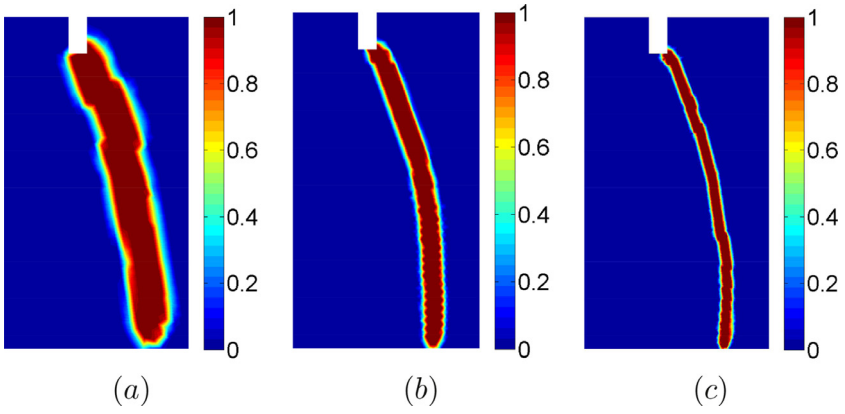

Fig. 12. Example 4.3. Map of the damage field in the refined zone at the end of the simulation run with: (a) Mesh *RA*; (b) Mesh *RB* and (c) Mesh *RC*. Influence of the internal length scale D.

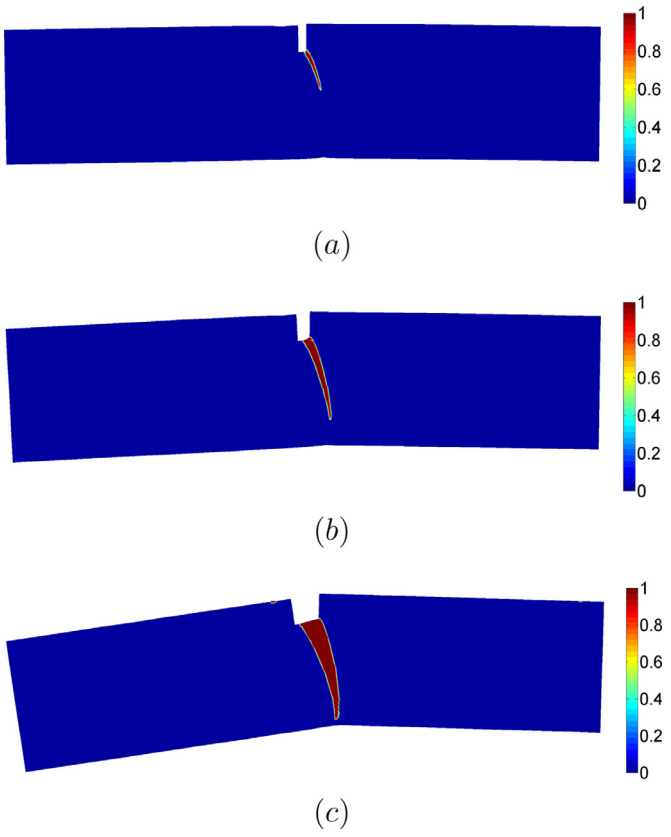

Fig. 13. Example 4.3. Map of the Damage field in the case of Mesh *RC* at the stages: (*a*) *S*1, (*b*) *S*2 and (*c*) *S*3. The displayed deformed configuration has been amplified by the factor $1 \cdot 10^2$.

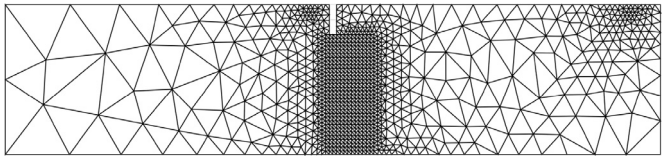

Fig. 14. Example 4.3. Finite element mesh with uniform refinement in the region where damage is expected to develop.

Table 5
Example 4.3. Data for the finite element mesh with uniform refinement in the region where the damage pattern is expected to develop.

	Minimal mesh size	Number of elements	Number of nodes
Mesh *RA*1	$h_1 = 2.5\,\text{mm}$	2005	10416

For the model with $D = 5\,\text{mm}$, we compared furthermore the response of the test specimen for different types of refinement in the region where damage was expected to develop. We considered therefore the mesh displayed in Fig. 14 with uniform refinement $h = 2.5\,\text{mm}$ and general data given in Table 5. Fig. 15 compares the reaction force-displacement curves obtained with the mesh *RA* and the mesh *RA*1, whereas Fig. 16 compares the damage field in such region at the end of the simulation together with the respective damage profile across the crack taken at the middle height of the beam. For both simulations, we find two elements ($h = 2.5\,\text{mm}$) in the transition zone ($D = 5\,\text{mm}$) with no practical difference both in the response and in the damage field.

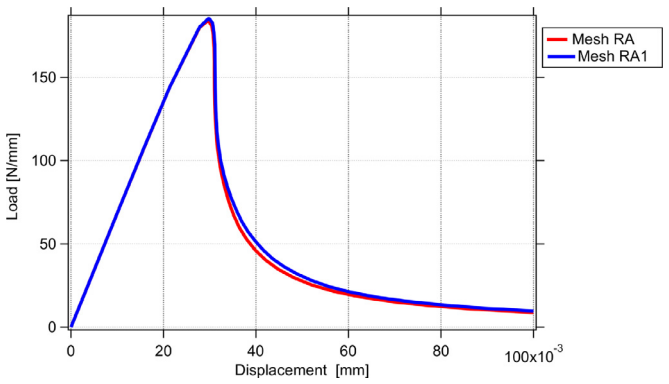

Fig. 15. Example 4.3. Total reaction force versus point-applied load displacement for uniform and unstructured refinement of the region where damage is expected to develop.

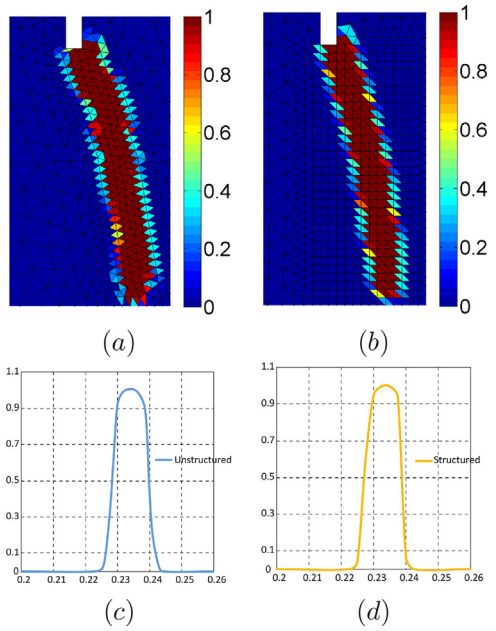

Fig. 16. Example 4.3. Map of the damage field at the end of the simulation for (*a*) unstructured and (*b*) uniform refinement of the region where damage is expected to develop with the correspondent damage profile across the crack taken at the middle height of the beam. In these simulations, $D = 5\,\text{mm}$ and $h = 2.5\,\text{mm}$.

To describe the whole deformation process, the numerical procedure of Fig. 2 was applied in all the simulations first with load control until reaching the peak response. At this instant, the procedure switched to energy dissipation control with steps $\Delta\tau = 5 \cdot 10^{-4} N$ until the end of the simulation. As in the previous examples, the simulation was terminated when we had complete damage in all the elements of the damage band with consequent formation of a rigid body mechanism.

5. Conclusions

In this paper we have presented the energetic formulation of a rate-independent gradient damage model for concrete where damage evolution does not meet the normality rule. This has been possible at the expense of defining a state variable-dependent dissipation potential by which we restore the variational structure.

By applying a semi-implicit Euler method for the time discretization, we have derived the incremental problem consistent

with the continuous formulation and found some interesting properties met by the discrete energetic solution. Starting then from the variational structure of the incremental problem, we have developed a numerical procedure based on variable splitting and constrained optimization to deal with the constraint enforced by the gradient of the damage field.

The nonlinear algebraic equations obtained by applying the finite element method for the spatial discretization have been solved by applying a path following Newton's method which uses the energy dissipation as continuation condition.

The modeling framework and the numerical procedure have been successfully verified by the numerical simulation of basic engineering benchmark problems, which represent standard testing procedures for crack propagation in concrete.

We can therefore conclude that for its sound mathematical, numerical and mechanical basis, the energetic formulation proves to be an attractive paradigma also for the modeling and simulation of standard materials with non-associated flow rule, provided that the evolution law of the internal variables can be eventually obtained by a state-variable dependent-dissipation potential. In this manner, the field of applications of the energetic formulation can be extended to more realistic constitutive models for describing material deterioration effects.

There are however some aspects of this formulation that deserve further investigation. These are how to ensure the global optimality of the discrete energetic solution and the relevance of the global optimization as modeling paradigma. Both are being analyzed in an ongoing work.

Acknowledgments

The authors are extremely grateful to the anonymous referees, whose constructive comments on earlier versions of the manuscript have contributed to produce a better version of the paper and make the authors appreciate subtleties of this fascinating topic. ML, AO and MA wish to thank the partial financial support of the Argentinian Research Council (CONICET), the National University of Tucumán, Argentina for the financial support through the Project PIUNT CX-E625 and the FonCyT through the Project PICT-201-0105 2016, whereas EP acknowledges partial financial support through the Project PIP CONICET 11220150100500CO, PUE CONICET 22920160100134CO and SECyT UNC 05 B/392.

Appendix A. Consistent stiffness matrix

We give hereafter the expression of all the terms of the linearization of the augmented system (3.39) which also includes the continuation condition

$$\begin{aligned}
&\boldsymbol{R_u}(\boldsymbol{U},\boldsymbol{A},\boldsymbol{L},\zeta)=\boldsymbol{0}\\
&\boldsymbol{R}_\alpha(\boldsymbol{U},\boldsymbol{A},\boldsymbol{L},\zeta)=\boldsymbol{0}\\
&\boldsymbol{R}_\lambda(\boldsymbol{U},\boldsymbol{A},\boldsymbol{L},\zeta)=\boldsymbol{0}\\
&\varphi(\boldsymbol{U},\boldsymbol{A},\boldsymbol{L},\zeta)=0\,,
\end{aligned}\tag{A.1}$$

with $\boldsymbol{R_u}$, $\boldsymbol{R}_\alpha$, $\boldsymbol{R}_\lambda$ and φ given by (3.31), (3.29b), (3.29c) and (3.38), respectively. Let

$$\begin{aligned}
&\Delta\boldsymbol{U}=\boldsymbol{U}^{k+1}-\boldsymbol{U}^k\,,\quad \Delta\boldsymbol{A}=\boldsymbol{A}^{k+1}-\boldsymbol{A}^k\,,\quad \Delta\boldsymbol{L}=\boldsymbol{L}^{k+1}-\boldsymbol{L}^k\\
&\qquad\text{and}\quad \Delta\zeta=\zeta^{k+1}-\zeta^k\,,
\end{aligned}\tag{A.2}$$

the first order expansion of (A.1) then reads as follows

$$\begin{aligned}
&\boldsymbol{R_u}(\boldsymbol{U}^i,\boldsymbol{A}^i,\boldsymbol{L}^i,\zeta^i)+\frac{D\boldsymbol{R_u}}{D\boldsymbol{U}}\Delta\boldsymbol{U}+\frac{D\boldsymbol{R_u}}{D\boldsymbol{A}}\Delta\boldsymbol{A}+\frac{D\boldsymbol{R_u}}{D\boldsymbol{L}}\Delta\boldsymbol{L}+\frac{D\boldsymbol{R_u}}{D\zeta}\Delta\zeta=\boldsymbol{0}\,,\\
&\boldsymbol{R}_\alpha(\boldsymbol{U}^i,\boldsymbol{A}^i,\boldsymbol{L}^i,\zeta^i)+\frac{D\boldsymbol{R}_\alpha}{D\boldsymbol{U}}\Delta\boldsymbol{U}+\frac{D\boldsymbol{R}_\alpha}{D\boldsymbol{A}}\Delta\boldsymbol{A}+\frac{D\boldsymbol{R}_\alpha}{D\boldsymbol{L}}\Delta\boldsymbol{L}+\frac{D\boldsymbol{R}_\alpha}{D\zeta}\Delta\zeta=\boldsymbol{0}\,,\\
&\boldsymbol{R}_\lambda(\boldsymbol{U}^i,\boldsymbol{A}^i,\boldsymbol{L}^i,\zeta^i)+\frac{D\boldsymbol{R}_\lambda}{D\boldsymbol{U}}\Delta\boldsymbol{U}+\frac{D\boldsymbol{R}_\lambda}{D\boldsymbol{A}}\Delta\boldsymbol{A}+\frac{D\boldsymbol{R}_\lambda}{D\boldsymbol{L}}\Delta\boldsymbol{L}+\frac{D\boldsymbol{R}_\lambda}{D\zeta}\Delta\zeta=\boldsymbol{0}\,,\\
&\varphi(\boldsymbol{U}^i,\boldsymbol{A}^i,\boldsymbol{L}^i,\zeta^i)+\frac{D\varphi}{D\boldsymbol{U}}\Delta\boldsymbol{U}+\frac{D\varphi}{D\boldsymbol{A}}\Delta\boldsymbol{A}+\frac{D\varphi}{D\boldsymbol{L}}\Delta\boldsymbol{L}+\frac{D\varphi}{D\zeta}\Delta\zeta=0\,.
\end{aligned}\tag{A.3}$$

Given the expression (3.31) of $\boldsymbol{R_u}$, we find that

$$\boxed{\frac{D\boldsymbol{R_u}}{D\boldsymbol{U}}=\sum_{\Omega_e^h\in\mathcal{T}^h}\sum_{i=1}^{ngp}w_{e,i}j_{e,i}\boldsymbol{B}_{\boldsymbol{u}}^T(\boldsymbol{x}_{e,i})\,\frac{D^h\boldsymbol{\sigma}}{D\boldsymbol{U}}(\boldsymbol{x}_{e,i})\,.}\tag{A.4}$$

To simplify notation, from now on we will leave as understood that the terms of the sum are evaluated at the Gauss points $\boldsymbol{x}_{e,i}$.

Since the dependence of $\boldsymbol{\sigma}$ on $\boldsymbol{U}$ is through $\boldsymbol{\varepsilon}$ and through β, with the latter that depends as well on $\boldsymbol{U}$ through $\boldsymbol{\varepsilon}$, the application of the chain rule gives

$$\frac{D^h\boldsymbol{\sigma}}{D\boldsymbol{U}}=\frac{D^h\boldsymbol{\sigma}}{D\boldsymbol{\varepsilon}}\boldsymbol{B_u}+\frac{D^h\boldsymbol{\sigma}}{D\beta}\frac{D\beta}{D\boldsymbol{\varepsilon}}\boldsymbol{B_u}\,.\tag{A.5}$$

From (2.10), we have therefore that

$$\frac{D\boldsymbol{\sigma}}{D\boldsymbol{\varepsilon}}=R(\beta)\mathbb{E}\quad\text{and}\quad\frac{D\boldsymbol{\sigma}}{D\beta}=R'\mathbb{E}\boldsymbol{\varepsilon}\,,\tag{A.6}$$

whereas by differentiating (3.22) with β defined implicitly by (3.21), we can show that there holds

$$\frac{D\beta}{D\boldsymbol{\varepsilon}}=-\frac{R'}{R''\omega^*+r}\frac{D\omega^*}{D\boldsymbol{\varepsilon}}\tag{A.7}$$

with $\omega^*=\sigma_{eq}^2/2E$, r the penalty parameter and

$$\frac{D\omega^*}{D\boldsymbol{\varepsilon}}=\frac{\sigma_{eq}}{E}\mathbb{E}\frac{D\sigma_{eq}}{D\boldsymbol{\sigma}^0}\,.\tag{A.8}$$

Moreover, from (2.17) it is

$$\frac{D\sigma_{eq}}{D\boldsymbol{\sigma}_0}=\frac{1}{1-\alpha}\left(\sqrt{\frac{3}{4J_2}}\boldsymbol{\sigma}_{0,D}+\alpha\boldsymbol{\delta}+\beta\frac{D\langle\sigma_{0,max}\rangle}{D\boldsymbol{\sigma}_0}\right)\tag{A.9}$$

with $\boldsymbol{\sigma}_{0,D}$ the deviatoric part of the undamaged stress $\boldsymbol{\sigma}_0=\mathbb{E}\boldsymbol{\varepsilon}$, $\boldsymbol{\delta}$ the identity tensor and

$$\frac{D\langle\sigma_{0,max}\rangle}{D\boldsymbol{\sigma}_0}=\begin{cases}\boldsymbol{v}\otimes\boldsymbol{v} & \text{if } \sigma_{0,max}>0\\ \boldsymbol{0} & \text{if } \sigma_{0,max}\le 0\,,\end{cases}\tag{A.10}$$

where $\boldsymbol{v}$ is the normalized eigenvector of $\boldsymbol{\sigma}_0$ associated with the maximum eigenvalue $\sigma_{0,max}$ and $\boldsymbol{v}\otimes\boldsymbol{v}$ is the tensor product between $\boldsymbol{v}$ and itself.

Given the expression (3.31) of $\boldsymbol{R_u}$, we find that

$$\boxed{\frac{D\boldsymbol{R_u}}{D\boldsymbol{A}}=\sum_{\Omega_e^h\in\mathcal{T}^h}\sum_{i=1}^{ngp}w_{e,i}j_{e,i}\boldsymbol{B}_{\boldsymbol{u}}^T\,\frac{D^h\boldsymbol{\sigma}}{D\boldsymbol{A}}\,.}\tag{A.11}$$

Noting then that the dependence of $\boldsymbol{\sigma}$ on $\boldsymbol{A}$ is through β which in turn depends on $\boldsymbol{A}$ through α, using the chain rule gives

$$\frac{D^h\boldsymbol{\sigma}}{D\boldsymbol{A}}=\frac{D^h\boldsymbol{\sigma}}{D\beta}\frac{D\beta}{D\alpha}\boldsymbol{N}_\alpha\,,\tag{A.12}$$

with $D\beta/D\alpha$ obtained by differentiating (3.22), so that

$$\frac{D\beta}{D\alpha}=\frac{r}{R''\omega^*+r}\tag{A.13}$$

where $R''=d^2R/d\beta^2$.

Given the expression (3.31) of $\boldsymbol{R_u}$, we find that

$$\boxed{\frac{D\boldsymbol{R_u}}{D\boldsymbol{L}}=\sum_{\Omega_e^h\in\mathcal{T}^h}\sum_{i=1}^{ngp}w_{e,i}j_{e,i}\boldsymbol{B}_{\boldsymbol{u}}^T\,\frac{D^h\boldsymbol{\sigma}}{D\boldsymbol{L}}\,.}\tag{A.14}$$

However, since the dependence of $\boldsymbol{\sigma}$ on $\boldsymbol{L}$ is through β which in turn depends on $\boldsymbol{L}$ through λ, by applying the chain rule, we obtain

$$\frac{D^h\boldsymbol{\sigma}}{D\boldsymbol{L}} = \frac{D^h\boldsymbol{\sigma}}{D\beta}\frac{D\beta}{D\lambda}\boldsymbol{N}_\lambda\,, \tag{A.15}$$

with $D\beta/D\alpha$ still obtained by differentiating (3.22) and given by

$$\frac{D\beta}{D\lambda} = \frac{1}{R''\omega^* + r}\,. \tag{A.16}$$

Given the expression (3.31) of $\boldsymbol{R_u}$, we find that, in the case of load control, it is

$$\boxed{\frac{D\boldsymbol{R_u}}{D\zeta} = -\sum_{\Omega_e^h\in\mathcal{T}^h}\sum_{i=1}^{ngp} w_{e,i}j_{e,i}\boldsymbol{N_u}^T\boldsymbol{f}_0\,,} \tag{A.17}$$

whereas, in the case of displacement control, by applying the chain rule, we have

$$\boxed{\frac{D\boldsymbol{R_u}}{D\zeta} = -\sum_{\Omega_e^h\in\mathcal{T}^h}\sum_{i=1}^{ngp} w_{e,i}j_{e,i}\boldsymbol{B_u}^T\left[\frac{D^h\boldsymbol{\sigma}}{D\boldsymbol{\varepsilon}}\frac{D\boldsymbol{\varepsilon}}{D\zeta} + \frac{D^h\boldsymbol{\sigma}}{D\beta}\frac{D\beta}{D\boldsymbol{\varepsilon}}\frac{D\boldsymbol{\varepsilon}}{D\zeta}\right],} \tag{A.18}$$

where $D\boldsymbol{\sigma}/D\boldsymbol{\varepsilon}$ and $D\boldsymbol{\sigma}/D\beta$ are given by (A.6), $D\beta/D\boldsymbol{\varepsilon}$ by (A.7) and $D\boldsymbol{\varepsilon}/D\zeta = \boldsymbol{B_u}\boldsymbol{U}_{D,0}$.

Given the expression (3.29b) of $\boldsymbol{R}_\alpha$, we find that

$$\boxed{\frac{D\boldsymbol{R}_\alpha}{D\boldsymbol{U}} = -r\sum_{\Omega_e^h\in\mathcal{T}^h}\sum_{i=1}^{ngp} w_{e,i}j_{e,i}\boldsymbol{N}_\alpha^T\frac{D\beta}{D\boldsymbol{\varepsilon}}\boldsymbol{B_u}\,.} \tag{A.19}$$

Given the expression (3.29b) of $\boldsymbol{R}_\alpha$, we find that

$$\boxed{\frac{D\boldsymbol{R}_\alpha}{D\boldsymbol{A}} = \sum_{\Omega_e^h\in\mathcal{T}^h}\sum_{i=1}^{ngp} w_{e,i}j_{e,i}\left[c\boldsymbol{B}_\alpha^T\boldsymbol{B}_\alpha + r\boldsymbol{N}_\alpha^T\left(\boldsymbol{N}_\alpha - \frac{D\beta}{D\alpha}\boldsymbol{N}_\alpha\right)\right].} \tag{A.20}$$

Given the expression (3.29b) of $\boldsymbol{R}_\alpha$, we find that

$$\boxed{\frac{D\boldsymbol{R}_\alpha}{D\boldsymbol{L}} = \sum_{\Omega_e^h\in\mathcal{T}^h}\sum_{i=1}^{ngp} w_{e,i}j_{e,i}\left[-r\boldsymbol{N}_\alpha^T\frac{D\beta}{D\lambda}\boldsymbol{N}_\lambda + \boldsymbol{N}_\alpha^T\boldsymbol{N}_\lambda\right].} \tag{A.21}$$

Given the expression (3.29b) of $\boldsymbol{R}_\alpha$, we find that, in the case of load control, it is

$$\boxed{\frac{D\boldsymbol{R}_\alpha}{D\zeta} = \boldsymbol{0}} \tag{A.22}$$

whereas, in the case of displacement control, by applying the chain rule, we have

$$\boxed{\frac{D\boldsymbol{R}_\alpha}{D\zeta} = \frac{D\boldsymbol{R}_\alpha}{D\beta}\frac{D\beta}{D\boldsymbol{\varepsilon}}\frac{D\boldsymbol{\varepsilon}}{D\zeta}} \tag{A.23}$$

where

$$\frac{D\boldsymbol{R}_\alpha}{D\beta} = -r\sum_{\Omega_e^h\in\mathcal{T}^h}\sum_{i=1}^{ngp} w_{e,i}j_{e,i}\boldsymbol{N}_\alpha^T\,, \tag{A.24}$$

$D\beta/D\boldsymbol{\varepsilon}$ is given by (A.7) and $D\boldsymbol{\varepsilon}/D\zeta = \boldsymbol{B_u}\boldsymbol{U}_{D,0}$.

Given the expression (3.29c) of $\boldsymbol{R}_\lambda$, we find that

$$\boxed{\frac{D\boldsymbol{R}_\lambda}{D\boldsymbol{U}} = -\sum_{\Omega_e^h\in\mathcal{T}^h}\sum_{i=1}^{ngp} w_{e,i}j_{e,i}\boldsymbol{N}_\lambda^T\frac{D\beta}{D\boldsymbol{\varepsilon}}\boldsymbol{B_u}\,.} \tag{A.25}$$

Given the expression (3.29c) of $\boldsymbol{R}_\lambda$, we find that

$$\boxed{\frac{D\boldsymbol{R}_\lambda}{D\boldsymbol{A}} = \sum_{\Omega_e^h\in\mathcal{T}^h}\sum_{i=1}^{ngp} w_{e,i}j_{e,i}\boldsymbol{N}_\lambda^T\left(\boldsymbol{N}_\alpha - \frac{D\beta}{D\alpha}\boldsymbol{N}_\alpha\right).} \tag{A.26}$$

Given the expression (3.29c) of $\boldsymbol{R}_\lambda$, we find that

$$\boxed{\frac{D\boldsymbol{R}_\lambda}{D\boldsymbol{L}} = -\sum_{\Omega_e^h\in\mathcal{T}^h}\sum_{i=1}^{ngp} w_{e,i}j_{e,i}\boldsymbol{N}_\lambda^T\frac{D\beta}{D\lambda}\boldsymbol{N}_\lambda\,.} \tag{A.27}$$

Given the expression (3.29c) of $\boldsymbol{R}_\lambda$, we find that, in the case of load control, it is

$$\boxed{\frac{D\boldsymbol{R}_\lambda}{D\zeta} = \boldsymbol{0}} \tag{A.28}$$

whereas, in the case of displacement control, by applying the chain rule, we have

$$\boxed{\frac{D\boldsymbol{R}_\lambda}{D\zeta} = \frac{D\boldsymbol{R}_\lambda}{D\beta}\frac{D\beta}{D\boldsymbol{\varepsilon}}\frac{D\boldsymbol{\varepsilon}}{D\zeta}} \tag{A.29}$$

where

$$\frac{D\boldsymbol{R}_\lambda}{D\beta} = -\sum_{\Omega_e^h\in\mathcal{T}^h}\sum_{i=1}^{ngp} w_{e,i}j_{e,i}\boldsymbol{N}_\lambda^T\,, \tag{A.30}$$

$D\beta/D\boldsymbol{\varepsilon}$ is given by (A.7) and $D\boldsymbol{\varepsilon}/D\zeta = \boldsymbol{B_u}\boldsymbol{U}_{D,0}$.

Given the expression (3.38) of φ, we find that

$$\boxed{\frac{D\varphi}{D\boldsymbol{U}} = \frac{1}{2}\zeta_n\sum_{\Omega_e^h\in\mathcal{T}^h}\sum_{i=1}^{ngp} w_{e,i}j_{e,i}\boldsymbol{N_u}^T\boldsymbol{f}_0\,.} \tag{A.31}$$

Given the expression (3.38) of φ, we find that

$$\boxed{\frac{D\varphi}{D\boldsymbol{A}} = -c\sum_{\Omega_e^h\in\mathcal{T}^h}\sum_{i=1}^{ngp} w_{e,i}j_{e,i}\boldsymbol{B}_\alpha^T\boldsymbol{B}_\alpha\boldsymbol{A}_n\,.} \tag{A.32}$$

Given the expression (3.38) of φ, we find that

$$\boxed{\frac{D\varphi}{D\boldsymbol{L}} = \boldsymbol{0}\,.} \tag{A.33}$$

Given the expression (3.38) of φ, we find that

$$\boxed{\frac{D\varphi}{D\zeta} = -\frac{1}{2}\boldsymbol{U}^T\sum_{\Omega_e^h\in\mathcal{T}^h}\sum_{i=1}^{ngp} w_{e,i}j_{e,i}\boldsymbol{N_u}^T\boldsymbol{f}_0\,.} \tag{A.34}$$

References

Alessi, R., Marigo, J.J., Vidoli, S., 2014. Gradient damage models coupled with plasticity and nucleation of cohesive cracks. Arch. Ration Mech. Anal. 214, 575–615.
Amor, H., Marigo, J.J., Maurini, C., 2009. Regularized formulation of the variational brittle fracture with unilateral contact: numerical experiments. J. Mech. Phys. Solids 57, 1209–1229.
Bathe, K., 1996. Finite Element Procedures. Prentice Hall.

Bazant, Z.P., 1976. Instability, ductility, and size effect in strain-softening concrete. J. Eng. Mech. Div. 102, 331–344.

Bazant, Z.P., 1991. Why continuum damage is nonlocal: micromechanics arguments. J. Eng. Mech. 117, 1070–1087.

Bazant, Z.P., Planas, J., 1997. Fracture and Size Effect in Concrete and Other Quasibrittle Materials. CRC Press Boca Raton.

Belytschko, T., Bazant, Z.P., Hyun, Y.-W., Chang, T.-P., 1986. Strain-softening materials and finite-element solutions. Comput. Struct. 23, 163–180.

Benallal, A., Billardon, R., Geymonat, G., 1993. Bifurcation and Localization in Rate-independent Materials. In: Nguyen, Q.S. (Ed.), CISM Lecture Notes on Bifurcation and Stability of Dissipative Systems. Springer-Verlag.

Benesova, B., 2011. Global optimization numerical strategies for rate–independent processes. J. Global Optim. 50, 197–220.

Besson, J., Cailletaud, G., Chaboche, J.L., Forest, S., Blétry, M., 2010. Non-Linear Mechanics of Materials. Springer, Dordrecht.

Boffi, D., Brezzi, F., Fortin, M., 2013. Mixed Finite Element Methods and Applications. Springer-Verlag Berlin Heidelberg.

Boffi, D., Lovadina, C., 1997. Analysis of new augmented lagrangian formulations for mixed finite element schemes. Numer. Math. 75, 405–419.

Bouchitté, G., Mielke, A., Roubicek, T., 2009. A complete-damage problem at small strains. ZAMP Zeitschrift fur angewandte Mathematik und Physik 60, 205–236.

Bourdin, B., 2007. Numerical implementation of the variational formulation for quasi-static brittle fracture. Interf. Free Bound. 9, 411–430.

Bourdin, B., Francfort, G.A., Marigo, J.J., 2000. Numerical experiments in revisited brittle fracture. J. Mech. Phys. Solids 48, 797–826.

Bourdin, B., Francfort, G.A., Marigo, J.J., 2008. The Variational Approach to Fracture. Springer, USA.

Caner, F.C., Bazant, Z.P., 2013. Microplane model m7 for plain concrete. II: calibration and verification. ASCE J. Eng. Mech. 139, 1724–1735.

Comi, C., 1999. Computational modelling of gradient-enhanced damage in quasi-brittle materials. Mech. Cohesive Frict. Mater. 4, 17–36.

Conti, S., Focardi, M., Iurlano, F., 2016. Phase field approximation of cohesive fracture models. Annal. Inst. Henri Poincare Linear Anal. 33, 1033–1067.

Conti, S., Lenz, M., Rumpf, M., 2016. Hysteresis in magetic shape memory composites: modeling and simulation. J. Mech. Phys. Solids 89, 272–286.

Crisfield, M.A., 1981. A fast incremental/iterative solution procedure that handles 'snap-through'. Comput. Struct. 13, 55–62.

Fortin, M., Glowinski, R., 1983. Augmented lagrangian methods: Application to the numerical solution of boundary-value problems. studies in mathematics and its applications, north-holland.

Francfort, G., Garroni, A., 2006. A variational view of partial brittle damage evolution. Arch. Ration. Mech. Anal. 182, 125–152.

Francfort, G., Mielke, A., 2006. Existence results for a class of rate-independent material models with nonconvex elastic energies. J. für die reine und angewandte Math. 595, 55–91.

Francfort, G.A., 2018. Recovering convexity in non-associated plasticity. C.R. Mec. 346, 198–205.

Freddi, F., Royer-Carfagni, G., 2010. Regularized variational theories of fracture: a unified approach. J. Mech. Phys. Solids 58, 1154–1174.

Frémond, M., 2002. Non-smooth Thermomechanics. Springer-Verlag Berlin.

Frémond, M., Nedjar, B., 1995. Damage in concrete: the unilaterla phenomenon. Nucl. Eng. Des. 156, 323–335.

Frémond, M., Nedjar, B., 1996. Damage, gradient of damage and principle of virtual power. Int. J. Solids Struct. 33, 1083–1103.

Galvez, J.C., Elices, M., Guinea, G.V., Planas, J., 1998. Mixed mode fracture of concrete under proportional and nonproportional loading. Int. J. Fract. 94, 267–284.

Gautschi, W., 2012. Numerical Analysis, second ed. Birkhäuser, New York.

Germain, P., Nguyen, Q.S., Suquet, P., 1983. Continuum thermodynamics. J. Appl. Mech. 50, 1010–1020.

Giry, C., Dufour, F., Mazars, J., 2011. Stress-based nonlocal damage model. Int. J. Solids Struct. 48, 3431–3443.

Gutierrez, M.A., 2004. Energy release control for strain–softening finite element simulations. Int. J. Numer. Methods Eng. 60, 499–526.

Halphen, B., Nguyen, Q.S., 1975. Sur les materiaux standards généralisés. J. Mécanique 14, 39–63.

Hiriart-Urruty, J.B., Lemaréchal, C., 2001. Fundamentals of Convex Analysis. Springer-Verlag, Berlin.

Jenq, Y., Shah, S.P., 1988. Mixed-mode fracture of concrete. Int. J. Fract. 38, 123–142.

Kachanov, L.M., 1958. Time of the rupture process under creep conditions. Izvestiia Akademii Nauk SSSR 8, 26–31.

Krajcinovic, D., 1996. Damage Mechanics. Elsevier, Amsterdam.

Lemaitre, J., 1996. A Course on Damage Mechanics. Springer-Verlag Berlin Heidelberg.

Lorentz, E., 2017. A nonlocal damage model for plain concrete consistent with cohesive fracture. Int. J. Fract. 207, 123–159.

Lorentz, E., Andrieux, S., 1999. A variational formulation for nonlocal damage models. Int. J. Plast. 15, 119–138.

Lorentz, E., Andrieux, S., 2003. Analysis of non-local models through energetic formulations. Int. J. Solids Struct. 40, 2905–2936.

Lorentz, E., Badel, P., 2004. A new path-following constraint for strain-softening finite element simulations. Int. J. Numer. Methods Eng. 60, 499–526.

Lorentz, E., Benallal, A., 2005. Gradient constitutive relations: numerical aspects and application to gradient damage. Comput. Methods Appl. Mech. Eng. 194, 5191–5220.

Lorentz, E., Cuvilliez, S., Kazymyrenko, K., 2011. Convergence of a gradient damage model toward a cohesive zone model. Comptes Rendus Mécanique 339, 20–26.

Lorentz, E., Cuvilliez, S., Kazymyrenko, K., 2012. Modelling large crack-propagation: from gradient damage to cohesive zone models. Int. J. Fract. 178, 85–95.

Lorentz, E., Godard, V., 2011. Gradient damage models: toward full-scale computations. Comput. Methods Appl. Mech. Eng. 200, 1927–1944.

Lubliner, J., Oliver, J., Oller, S., Oñate, E.O., 1989. A plastic–damage model for concrete. Int. J. Solids Struct. 25, 299–326.

Luege, M.,. Análisis de unicidad y estabilidad de la respuesta homogénea de una barra de hormigón modelada con un modelo gradiente de daño. In: Scarabino, A., Idiart, M. (Eds.), Mecánica Computacional XXIII, ENIEF 2017, La Plata, Argentina. Available at https://cimec.org.ar/ojs/index.php/mc/article/view/5411/5375. Accessed: 2018-06-06.

Marigo, J.J., 2002. From Clausius-duhem and Drucker-ilyushin inequalities to standard materials. In: Maugin, G.A., Drouot, R., Sidoroff, F. (Eds.), Continuum Thermomechanics: The Art and Science of Modelling Material Behaviour. Springer, pp. 289–300.

Marigo, J.J., Maurini, C., Pham, K., 2016. An overview of the modelling of fracture by gradient damage models. Meccanica 51, 3107–3128.

Maugin, G., 2017. Non-Classical Continuum Mechanics: A Dictionary. Springer, Singapore.

May, S., 2016. Splines for Damage and Fracture in Solids. University of Glasgow, UK Ph.d. dissertation.

May, S., Vignollet, J., de Borst, R., 2016. A new arc-length control method based on the rates of the internal and the dissipated energy. Eng. Comput. Swansea 33, 100–115.

Miehe, C., 2011. A multi-field incremental variational framework for gradient-extended standard dissipative solids. J. Mech. Phys. Solids 59, 898–923.

Miehe, C., Aldakheel, F., Mauthe, S., 2013. Mixed variational principles and robust finite element implementations of gradient plasticity at small strains. Int. J. Numer. Methods Eng. 94, 1037–1074.

Miehe, C., Welschinger, F., Hofacker, M., 2010. Thermodynamically consistent phase–field models of fracture: variational principles and multi–field FE implementations. Int. J. Numer. Methods Eng. 83, 1273–1311.

Mielke, A., 2005. Evolution of Rate-independent Systems. In: Dafermos, C.M., Feireisl, E. (Eds.), Handbook of Differential Equations, Evolutionary Equations, vol. 2. Elsevier, Amsterdam, pp. 461–559.

Mielke, A., Roubíček, T., 2006. Rate-independent damage processes in nonlinear elasticity. Math. Models Methods Appl. Sci. 16, 177–209.

Mielke, A., Roubíček, T., 2009. Numerical approaches to rate-independent processes and applications in inelasticity. ESAIM Math. Modell. Numer. Anal. 43, 399–428.

Mielke, A., Roubíček, T., 2015. Rate-Independent Systems: Theory and Application. Springer–Verlag, Berlin.

Mielke, A., Roubíček, T., Stefanelli, U., 2008. γ-Limits and relaxations for rate-independent evolutionary problems. Calc. Var. Partial Differ. Equ. 31, 387–416.

Mielke, A., Roubíček, T., Zeman, J., 2010. Complete damage in elastic and viscoelastic media and its energetics. Comput. Methods Appl. Mech. Eng. 199, 1242–1253.

Mielke, A., Theil, F., Levitas, V.I., 2002. A variational formulation of rate-independent phase transformations using an extremum principle. Arch. Ration. Mech. Anal. 162, 137–177.

Nedjar, B., 2001. Elastoplastic-damage modelling including the gradient of damage: formulation and computational aspects. Int. J. Solids Struct. 38, 5421–5451.

Nguyen, Q.S., 2010. On standard dissipative gradient models. Ann. Solid Struct. Mech. 1, 79–86.

Nguyen, Q.S., 2014. Some remarks on standard gradient models and gradient plasticity. Math. Mech. Solids 1, 1–10.

Nguyen, Q.S., 2016. Quasi-static responses and variational principles in gradient plasticity. J. Mech. Phys. Solids 97, 156–167.

Oller, S., Onate, E., Oliver, J., Lubliner, J., 1990. Finite element nonlinear analysis of concrete structures using a plastic-damage model. Eng. Fract. Mech. 35, 219–231.

de Souza Neto, E.A., Peric, D., Owen, D.R.J., 2008. Computational Methods for Plasticity: Theory and Applications. John Wiley & Sons, Singapore.

Pham, K., Amor, H., Marigo, J.J., Maurini, C., 2011. Gradient damage models and their use to approximate brittle fracture. Int. J. Damage Mech. 20, 618–652.

Pham, K., Marigo, J.J., 2010. Approche variationnelle de l'endommagement: i. les concepts fondamentaux. Comptes Rendus Mécanique 338, 191–198.

Pham, K., Marigo, J.J., 2010. Approche variationnelle de l'endommagement: II. les modéles á gradient. Comptes Rendus Mécanique 338, 199–206.

Pham, K., Marigo, J.J., 2013. From the onset of damage to rupture: construction of responses with damage localization for a general class of gradient damage model. Continuum Mech. Thermodyn. 25, 147–171.

Pham, K., Marigo, J.J., Maurini, C., 2011. The issues of the uniqueness and the stability of the homogeneous response in uniaxial tests with gradient damage models. J. Mech. Phys. Solids 59 (6), 1163–1190.

Pijaudier-Cabot, G., Bazant, Z.P., 1987. Nonlocal damage theory. J. Eng. Mech. 113, 1512–1533.

Pohl, T., Ramm, E., Bischoff, M., 2014. Adaptive path following schemes for problems with softening. Finite Elem. Anal. Des. 86, 12–22.

Quarteroni, A., 2017. Numerical Models for Differential Problems. Springer Verlag, Milan.

Tamé, E., Li, T., Bourdin, B., Marigo, J.J., Maurini, C., 2018. Crack nucleation in variational phase-field models of brittle fracture. J. Mech. Phys. Solids 110, 80–99.

Verhoosel, C.V., Remmers, J.J.C., Gutiérrez, M.A., 2009. A dissipation–based arc–length method for robust simulation of brittle and ductile failure. Int. J. Numer. Methods Eng. 77, 1290–1321.
Vermeer, P.A., de Borst, R., 1984. Non-associated Plasticity for Soils, Concrete and Rock, 29. Heron, pp. 1–64.
Vignollet, J., May, S., de Borst, R., Verhoosel, C.V., 2014. Phase-field models for brittle and cohesive fracture. Meccanica 49, 2587–2601.
Zhang, J., Li, J., 2012. Investigation into lubliner yield criterion of concrete for 3d simulation. Eng. Struct. 44, 122–127.